Ph.D. Thesis

Biological effects of cerium oxide nanoparticles. Implications at the Bio-Nano interface

Gerardo Pulido Reyes

June, 2017

Thesis submitted to the Universidad Autónoma de Madrid for the degree of International Doctor of Philosophy (Microbiology Program 1393/2007)

Biological effects of cerium oxide nanoparticles. Implications at the Bio-Nano interface

Doctoral Thesis presented by:

Gerardo Pulido Reyes

Dpto. de Biología, Facultad de Ciencias

UNIVERSIDAD AUTÓNOMA DE MADRID

June, 2017

Supervisors:

Dr. Francisca Fernández Piñas
Dpto. de Biología
Facultad de Ciencias
Universidad Autónoma de Madrid

Dr. Roberto Rosal García
Dpto. Química Analítica, Química Física e Ingeniería Química
Universidad de Alcalá

A mis padres y a mi querida hermana

TABLE OF CONTENTS

Fundings		1
Summary		3
Resumen		7
Chapter 1	**General Introduction**	11
	1.1 Nanotechnology: nanoscale implications, definitions and types of nanomaterials Nanoscale implications	13
	1.2 Cerium Oxide Nanoparticles: unique chemistry and huge potentialities	20
	1.3 The interactions of Cerium oxide nanoparticles with a/biotic entities and the environment	23
	1.4 References	27
Objectives		37
Chapter 2	**Bio-Nano interface and environment: a critical review**	41
	2.1 Abstract	43
	2.2 Introduction	44
	2.3 Understanding the Bio-Nano interface	45
	2.4 Transformation of ENM in the environment and consequences for the Bio-Nano interface	51
	2.5 Biological identity of ENM	58
	2.6 Studying and characterizing the Bio-Nano interface	65

2.7 Critical opinion & research needed in the Bio-Nano interface field 71
2.8 References 75

Chapter 3 **Untangling the biological effects of cerium oxide nanoparticles: the role of surface valence states** 93

3.1 Abstract 95
3.2 Introduction 96
3.3 Results 98
3.4 Discussion 115
3.5 Methods 118
3.6 References 123
3.7 Supplementary information 131

Chapter 4 **Internalization and toxicological mechanisms of uncoated and PVP-coated cerium oxide nanoparticles in the freshwater alga *Chlamydomonas reinhardtii*** 137

4.1 Abstract 139
4.2 Introduction 141
4.3 Methods 142
4.4 Results 146
4.5 Discussion 154
4.6 Conclusions 156
4.7 References 157
4.8 Supplementary information 165

Chapter 5 **Hypochlorite scavenging activity of cerium oxide nanoparticles** 167

5.1 Abstract 169
5.2 Introduction 169
5.3 Results and Discussion 171

	5.4 Conclusions	179
	5.5 References	180
	5.6 Supplementary information	182
Chapter 6	**Physicochemical and biological interactions between cerium oxide nanoparticles and a 1,8-naphthalimide derivative**	189
	6.1 Abstract	191
	6.2 Introduction	193
	6.3 Material and Methods	194
	6.4 Results and discussion	198
	6.5 Conclusions	214
	6.6 References	214
	6.7 Supplementary information	223
Chapter 7	**General Discussion**	227
General conclusions/		237
Conclusiones Generales		241
Acknowledgments/ Agradecimientos		243
Appendix I	Abbreviations	247
Appendix II	Scientific divulgation	251

FUNDINGS

This work has been possible due to the “Formación de Profesorado Universitario” fellowship (FPU 2012 program) of Ministerio de Educación, Gobierno de España (Ref: FPU12/01796), the research projects: CTM2013-45775-C2-1-R and CTM2013-45775-C2-2-R grants from MINECO and the Dirección General de Universidades e Investigación de la Comunidad de Madrid Research Network S2013/MAE-2716.

SUMMARY

The nanotechnology and nanoscience fields have evolved sharply during last years. Many different nanomaterials have been synthesized and used in numerous products and consumer goods and many more will come shortly into the market. This revolutionary technology brings plenty of advantages in many sectors and, at the same time, it generates several uncertainties that need to be tackled regarding the unintended risks and potential harmful effects to human health and the environment. The pathways of entry into the environment, the biological effect to the whole food chain and the potential fate of nanomaterials in specific environmental compartments are just some of the open questions that need to be answered before nanotechnology continues growing. Recently, cerium oxide nanoparticles (CNPs) have received considerable attention due to their wide range of applications, their unique surface chemistry and their antioxidant/oxidant duality. However, a deep characterization of their bioactivity and interrelationship with other molecules has not been fully undertaken yet. The overall aim of this Thesis was to address the biological effects of cerium oxide nanoparticles (CNPs), emphasizing the role played by the Bio-Nano interface.

Chapter 1 constitutes a general introduction, which includes the description of some basic concepts such as nanotechnology, nanomaterials and their implications. The particularities of CNPs derived of their physicochemical properties are described: It also contains a section dedicated to examine their interactions with different molecules and environmentally relevant organisms.

Within Chapter 2, the state of the art of the Bio-Nano interface field is presented from an environmental point of view. Nanomaterials, once in the

environment, are prone to suffer alterations (chemical, physical and biological transformations) which affect the Bio-Nano interface, so a full description of those transformations is included. Moreover, the importance and impact of the formation of an environmental identity or eco-corona onto the surface of nanomaterials is discussed and highlighted. The Research Needs section discusses the problems and knowledge gaps that need to be resolved in the near future regarding the environmental Bio-Nano interface.

The biological effects and toxicological mechanisms of different types of CNPs (varying morphologies, sizes, coatings and methods of synthesis) towards two environmentally relevant microorganisms (the microalgae *Pseudokirchneriella subcapitata* and *Chlamydomonas reinhardtii*) are presented and discussed in Chapters 3 and 4. Chapter 3 evaluates the importance of several particle properties such as nominal size, effective diameter, % surface Ce^{3+}, nanoparticle ζ-potential and shape as explanatory variables for the observed bioactivity. The results show that only one driver, the percent (ratio) of surface Ce^{3+}, explains the toxic response. The toxicological mechanisms of CNPs are the formation of abiotic Reactive Oxygen Species (ROS) and the attachment of particles to the cell envelopes. A totally different mechanism is observed when the CNPs are coated with an organic molecule (Chapter 4). Polyvinylpyrrolidone(PVP)-CNPs increased the formation of intracellular ROS, which impaired some physiological parameters without direct damage to cell envelopes. Different degrees of toxicity are found depending on the PVP chain length: The higher the molecular weight, the lower the toxicity observed.

Little is known about the internalization process of CNPs in algae. There is evidence of CNP-internalization by some organisms, but the internalization mechanism and route of uptake are not fully understood. In Chapter 4, it is

described that all CNPs are able to internalize in the microalgal cells and that the process follows a time dependent relationship. Besides, using various endocytosis inhibitors, it is determined that the clathrin-dependent endocytosis is the main pathway for nanoparticle entry.

Due to the coexistence of oxidant and antioxidant properties in CNPs, the results presented in Chapters 3 and 4 shed light regarding the contradictory biological effects of CNPs that have been reported in the scientific literature. The reported discrepancies on the effects of CNPs could be attributed to the fact that the surface content of $Ce^{3+/4+}$ has not been measured in all cases and also that, the biological effect of coated-CNPs has been disregarded.

Chapters 5 and 6 are dedicated to study the interaction between CNPs and two different molecules. Firstly, the antioxidant properties of CNPs are expanded by proving that CNPs are able to scavenge *in vitro* hypochlorite anions (a strong oxidant compound) (Chapter 5). Surface interaction and the reduction of Ce^{4+} to Ce^{3+} revealed as the scavenging mechanisms. Secondly, the interactions of several CNPs with a 1,8-naphthalimide derivative are also studied (Chapter 6). CNPs could modulate the photophysical properties of the molecule as their spectroscopic properties varied depending on the complex formed. The bioluminescent model bacterium (*Anabaena sp.* PCC7120 CPB4337) allowed assessing the effect of CNPs and the complex they form with the organic molecule (nahthalimide derivative). The complex between the organic molecule and CNP with the higher content of surface Ce^{3+} acted additively towards the used model organism. Conversely, when the complex was formed by CNPs with higher content of surface Ce^{4+}, an antagonistic effect was observed, highlighting the importance of CNPs surface chemistry.

Altogether, this Thesis shows that CNPs are a versatile kind of nanomaterial whose biological effects could be extremely different depending on the physicochemical characteristics derived from their synthesis. The adsorption of molecules on their surface could modulate their Bio-Nano interface resulting in reduced toxicity. The surface content of Ce^{3+}/Ce^{4+} and the type of coating must be taken into account by safer-by-design strategies, in the Environmental Health and Safety assessment of CNPs, but also in specific applications where a precise content should be presented to display their intended function. As CNPs have shown solid harmful effects towards several environmentally relevant microorganisms, this Thesis aimed at improving our understanding of the toxicity of this type of nanomaterial and by these means to contribute to the sustainable and reasonable development of nanotechnology.

RESUMEN

Los campos de la nanociencia y la nanotecnología han evolucionado rápidamente en los últimos años. Se ha sintetizado una gran cantidad de nanomateriales para su incorporación en numerosos productos y artículos de consumo. Esta tecnología revolucionaria trae consigo numerosas ventajas en diferentes sectores, pero, al mismo tiempo, genera una serie de incertidumbres respecto a los riesgos colaterales y efectos dañinos que pudieran tener tanto en la salud humana como en el medio ambiente. Las vías de entrada al medio, los efectos biológicos en la cadena trófica y la distribución potencial de los nanomateriales en los distintos compartimentos ambientales son sólo algunas de las preguntas que necesitan ser respondidas antes de que la nanotecnología siga creciendo. Recientemente, las nanopartículas de óxido de cerio han despertado bastante expectación debido a su amplio rango de aplicaciones, su química superficial única y su dualidad oxidante/antioxidante. Sin embargo, todavía no se ha realizado una caracterización exhaustiva de su bio-actividad ni de su interrelación con otras moléculas. El objetivo general de esta tesis ha sido abordar los efectos biológicos de las nanopartículas de óxido de cerio (CNPs), enfatizando el papel de la Bio-Nano interfaz.

El Capítulo 1 constituye una introducción general, en la que se incluye la descripción de algunos conceptos básicos tales como nanotecnología, nanomateriales y sus implicaciones. Asimismo, se describen las particularidades de las CNPs derivadas de sus propiedades fisicoquímicas y se incluye una sección dedicada a examinar sus interacciones con diferentes moléculas y organismos de especial relevancia ecológica.

En el Capítulo 2 se detalla los conocimientos actuales acerca de la Bio-Nano interfaz desde un punto de vista medioambiental. Los nanomateriales, una vez llegan al medio, pueden sufrir alteraciones química, físicas o biológicas que afectan directamente a la Bio-Nano interfaz, por lo que se ha incluido una descripción completa de dichas transformaciones. Además, se ha resaltado y discutido la importancia y el impacto de la formación de una identidad ambiental o eco-corona en la superficie de los nanomateriales. La sección denominada 'Research Needs' discute los problemas y lagunas de conocimiento existentes que necesitan ser abordados en el futuro próximo acerca de la Bio-Nano interfaz medioambiental.

Los Capítulos 3 y 4 están dedicados a discutir los efectos biológicos y mecanismos de acción tóxica de diferentes tipos de CNPs (en los que se ha variado la morfología, el tamaño, el recubrimiento y el método de síntesis) en dos microorganismos de especial relevancia ecológica (las microalgas *Pseudokirchneriella subcapitata* y *Chlamydomonas reinhardtii*). Específicamente, el Capítulo 3 evalúa la importancia de varias propiedades de las nanopartículas tales como el tamaño nominal, el diámetro efectivo, el % de Ce^{3+} superficial, el potencial ζ (carga superficial) y la forma de la partícula como variables explicativas de su bioactividad. Los resultados muestran la existencia de un único factor que explica la respuesta tóxica, el % de Ce^{3+} superficial. Los mecanismos toxicológicos de las CNPs son: la formación abiótica de especies reactivas de oxígeno y la adsorción de nanopartículas en las envueltas celulares. No obstante, cuando las CNPs se recubrieron con una molécula orgánica (polivinilpirrolidona (PVP)) se observó un mecanismo de acción distinto (Capítulo 4). Las CNPs recubiertas con PVP incrementaron la formación de especies reactivas intracelulares, alterando diversos parámetros fisiológicos sin dañar directamente a las envueltas celulares. Se observó

diferente grado de toxicidad dependiendo del peso molecular de la molécula de PVP: a mayor peso molecular, menor toxicidad.

Poco se sabe acerca de los procesos de internalización de las CNPs en algas. Existen ciertas evidencias en algunos organismos, pero los mecanismos de internalización y las rutas de endocitosis no se conocen con precisión. En el Capítulo 4, se describe cómo todas las CNPs utilizadas son capaces de internalizarse/penetrar en las células de *Chlamydomonas reinhardtii* y que el proceso sigue una relación dependiente del tiempo. Además, usando varios inhibidores de endocitosis, se ha podido demostrar que la principal vía de entrada es la endocitosis dependiente de la proteína clatrina.

En definitiva, debido a la coexistencia de propiedades oxidantes y antioxidantes atribuidas a las CNPs, los resultados presentados en los Capítulos 3 y 4 permiten esclarecer la confusión existente en la literatura científica referente a los efectos biológicos de estas nanopartículas. Las discrepancias observadas en cuanto a los efectos de las CNPs se pueden atribuir a la diferente relación de Ce^{3+}/Ce^{4+} superficial, un parámetro que no se mide habitualmente. A la vista de los resultados, los efectos de los recubrimientos pueden haber pasado desapercibidos de igual manera.

Los Capítulos 5 y 6 están dedicados a estudiar la interacción entre las CNPs y dos moléculas muy diferentes. Primeramente, las propiedades antioxidantes de las CNPs se han puesto de manifiesto mediante su capacidad para neutralizar *in vitro* al anión hipoclorito (un fuerte agente oxidante) (Capítulo 5). La interacción superficial y la reducción de Ce^{4+} to Ce^{3+} mostraron ser los mecanismos de neutralización. En segundo lugar, el Capítulo 6 se dedica al estudio de las interacciones de varias CNPs con una molécula derivada de la naftalimida. Se pudo demostrar que las CNPs modulan las propiedades

fotofísicas del derivado natalimídico, puesto que se observó un cambio en las propiedades espectroscópicas de la molécula una vez que ésta se adsorbió a la superficie de las nanopartículas. Cabe reseñar que las alteraciones fueron diferentes, dependiendo del complejo CNP-naftalimida formado. La bacteria modelo *Anabaena sp.* PCC7120 CPB4337 permitió evaluar el efecto biológico de las CNPs y los complejos formados con la molécula orgánica. El complejo entre el derivado de la naftalimida con las CNPs con alto contenido en Ce^{4+} superficial dio lugar a menor efecto biológico (antagonismo) que las mismas concentraciones de naftalmida y CNP por separado. En cambio, cuando se trató de CNPs con mayor contenido de Ce^{3+} la respuesta biológica fue aditiva. Los resultados destacan de nuevo la importancia de la química superficial de las CNPs.

En conjunto, esta Tesis muestra la versatilidad de las nanopartículas de óxido de cerio, cuyos efectos biológicos pueden ser distintos dependiendo de las características fisicoquímicas derivadas de su síntesis. La adsorción de moléculas en su superficie puede modular la Bio-Nano interfaz reduciendo la toxicidad exhibida. El contenido superficial de Ce^{3+}/Ce^{4+} y el tipo de recubrimiento deben de ser tomados en consideración al abordar el diseño seguro de nanomateriales, durante la evaluación de la contaminación ambiental y los riesgos potenciales para la salud humana, pero también en aplicaciones específicas donde es preciso conocer en exactitud su química superficial. Dado que las CNPs han exhibido efectos perjudiciales en una variedad de organismos medioambientalmente relevantes, esta Tesis tiene como objetivo global mejorar nuestro conocimiento de la toxicidad de este tipo de nanomaterial y al mismo tiempo, contribuir al desarrollo sostenible y razonable de la nanotecnología.

CHAPTER 1

GENERAL INTRODUCTION

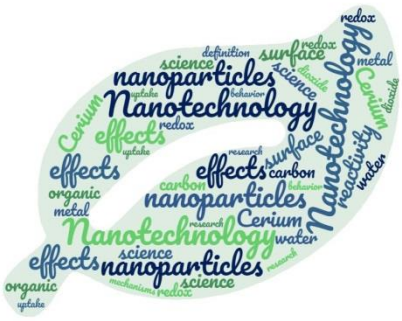

CHAPTER 1. GENERAL INTRODUCTION

1.1 Nanotechnology: nanoscale implications, definitions and types of nanomaterials

Nanotechnology is a new technology that will significantly improve, or even revolutionize, many areas and industrial sectors [1]. The fields of nanoscience and nanotechnology have gained considerable global visibility during the last 15 years and this new technology has resulted in an explosion in both public funding and private investments. The forecast for nanotechnology estimates that the global value of nano-enabled products, nano-intermediates, and engineered nanomaterials will reach $4.4 trillion by 2018 [4].

With extremely varied applications, nanotechnology has already taken its place in our everyday lives. According to the last Nanotechnology Consumer Products Inventory (CPI) developed by The Woodrow Wilson Institute in its project on emergent nanotechnologies [5], there has been a thirty-fold increase in

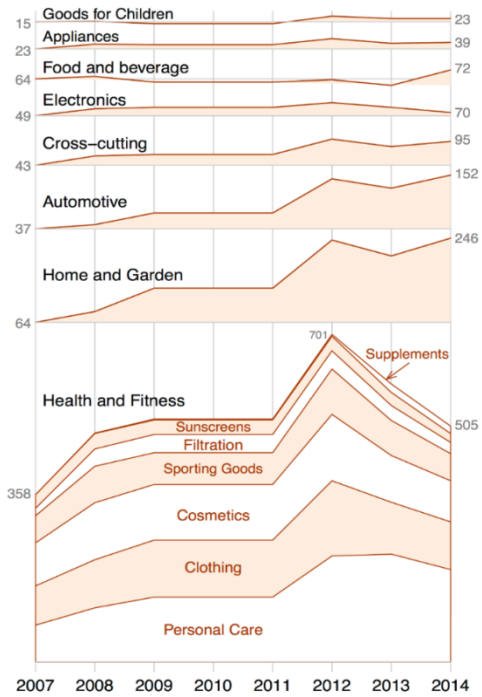

Figure 1.1.- Number of available products over time (since 2007) in each major category and in the Health and Fitness subcategories. Taken from [2].

the number of nanoproducts in the market over the 54 originally listed in 2005 to the 1814 registered in 2014 [2] (at present, the total amount is expected to be higher). Interestingly, all those products can be readily purchased by consumers in a number of goods for a variety of applications. Grouping all goods into eight categories, the Health and Fitness category included the largest listing of products in the CPI, comprising 42% of listed products (excluding archived products), being Personal Care Products (e.g., toothbrushes, lotions, and hairstyling tools and products) the largest subcategory with 39% of products (see Figure 1.1). All those products and applications have the potential to create major technological breakthroughs, and therefore nanomaterials have been identified as a key enabling technology by the European Commission together with micro and nanoelectronics, industrial biotechnology, advanced materials, photonics, and advanced manufacturing technologies [6, 7].

In the scientific field, nanotechnology has also become a vibrant area of research over the past 15 years. The number of publications and patents related to the 'nano-world' has always had an ascending trend, reaching the 130623 international scientific indexed nano-articles in 2015 [5]. Ranking by countries, United States is the top country in the publication of total indexed articles while China, Germany, and UK possess the next ranks. A number of 10003 nanotechnology granted patents have been published just in 2015 if we combine the registers from the European Patent Office and United States Patent and Trademark Office [5].

There is no internationally harmonized definition of nanotechnology that would fulfill the requirements for use in legislation, either at European or international level. However, in a broader sense, nanotechnology can be

defined as the study, design, synthesis, control, manipulation, and application of functional materials, devices, and systems through control of matter at the nanometer scale (1–100 nanometers) by exploiting the distinct properties and phenomena at that scale as compared to those associated with single atoms or molecules or bulk behavior [8-10]. In the International System of Units, the prefix "nano" means one-billionth, or 10^{-9}, of a meter and, just for a scale comparison, a human hair is approximately 80,000-100,000 nanometers wide.

Working at this scale has several implications. Firstly, nanoscale materials have considerable larger surface areas than similar masses of larger-scale objects (Figure 2.1). As surface area per mass of a material increases, a greater amount of the material can come into contact with the surrounding medium, thus affecting reactivity. Secondly, the nanomaterials are subject to quantum effects. This means they can behave in different ways as they can manifest the laws governing microscopic objects, which are usually hidden for larger scale objects. Nanoscale gold illustrates the unique properties that occur at the nanoscale (Figure 2.1). Gold nanoparticles are not the yellow color with which we are familiar; they can appear red or purple. At the nanoscale, the motion of the gold's electrons is confined and due to that the movement is restricted, gold nanoparticles react differently with light compared to larger-scale gold particles [11].

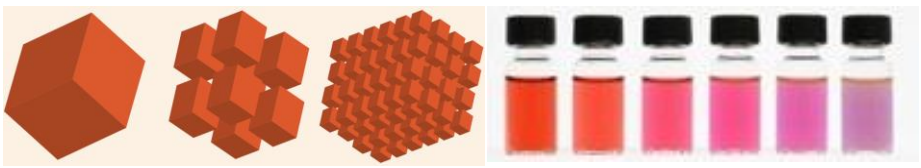

Figure 1.2.- The implications of working at the nanoscale. Increase in the ratio of surface area to volume in the transition from a homogeneous solid to a set of nanoparticles (left image). Different suspensions of gold nanoparticles with increasing particle sizes (right image). Adapted from [1].

According to the European Commission which released a 'Recommendation on the definition of a nanomaterial in 2011 (2011/696/EU))' [12], a nanomaterial means: *a natural, incidental or manufactured material containing particles, in an unbound state or as an aggregate or as an agglomerate and where, for 50 % or more of the particles in the number size distribution, one or more external dimensions is in the size range 1 nm - 100 nm.* A review on that definition was expected to have concluded in 2016 after extensive consultation with the stakeholders. It has not been launched yet, but from the information available the revision is only focusing technical details. For example, whether the number size distribution threshold of 50 % should be increased or decreased. No major amendments are expected to take place. Although there is still controversy regarding a definition that might fit in all cases, the definition proposed by the European Commission could be used primarily to identify materials for which special provisions might apply (e.g. for risk assessment or ingredient labelling).

Under the definition stated above, there are three different sources of nanomaterials: nanomaterials which are deliberately synthesized to exploit unique properties exhibited only at nanoscale dimensions (engineered nanomaterials (ENM)); nanomaterials which are of human origin; and nanomaterials which are of natural origin (Table 1.1; [13]). Nanomaterials of natural or human origin are composed mainly of undesirable products, known as ultrafine particles, that come from mechanical operations (e.g., metal machining), thermal operations (e.g., diesel engine emissions), or natural phenomenon (volcanic smoke, sea air, forest fires, etc.).

Table 1.1 gives some examples of natural substances that contain nanoparticles. There are several mechanisms that create nanoparticles in the

environment and these can be either geological or biological. Geological mechanisms include [13]:

- Physicochemical weathering: the result of physical (abrasion) and decomposition of rock material, to produce a powder,

- Neoformation: when chemical degradation eventually results in high enough concentrations of certain dissolved species to exceed the saturation in solution of a phase, leading to its nucleation and growth; and

- Volcanic activity, including also geysers and other geothermal/hydrothermal activities produce a variety of particle sizes, which include nanoparticles.

There are also several intracellular or extracellular biological mechanisms through which organisms may produce nanoparticles. In this regards, many bacteria, fungi and plants have shown the ability to synthesize metallic nanoparticles [14, 15].

Table 1.1.- Some examples of naturally occurring nanoparticles. Adapted from [13].

Location of NPs	Particle types and ecotoxicological potential
Volcanic dust	Bismuth oxide nanoparticles were found in the stratosphere in 1985, and the presence of these materials was linked to volcanic eruptions in the 1980s
Volcanic ash	Cristobalite (crystalline silica) extracted from volcanic ash from the Montserrat eruption causes lung inflammation and lymph node granuloma in laboratory rats
Soil	A complex matrix containing mineral particles, colloids in pore water, and there are concerns about adsorption and binding of pollutants within the matrix
Freshwater	Natural freshwater contain very complex colloid material which includes inorganic minerals and organic matter such as humic substances. Concerns exist over the accumulation and transportation of NPs in the

	colloid fraction
Other natural waters	Nanoparticles were found in many types of natural water including the oceans, surface waters, groundwater, atmospheric water, and even treated drinking water. These include a wide variety of nanoscale mineral particles, and demonstrates the ubiquitous nature of nanoparticles in the natural environment.
Ice cores	Carbon nanotubes, carbon fullerenes and silicon dioxide nanocrystals have been found in 10,000 year old ice cores. The carbon nanoparticles are assumed to be derived from natural combustion processes and deposited into the ice core via atmospheric deposition
Historic sediments	Examination of the Cretaceous-Tertiary (K-T) boundary layer at Gubbio, Italy showed iron particles (hematite) and silicates. The average particle size of the hematite was 16–27 nm. There is speculation that meteorite impacts could alter NP formation in sediments.

ENM can be classified into carbon-based nanomaterials [16] such as carbon spheres (e.g., fullerenes; [17]) or carbon single/multiwalled nanotubes [18, 19]; dendrimers and other polymeric nanomaterials [20], metal-based nanoparticles [21-23], composite nanomaterials [24] or multi-metallic nanoparticles [25], and also coated ENM with an external coating or capping agent (e.g., functionalized zinc oxide nanoparticles [26]). Various prominent features and applications of different types of ENM are mentioned in Table 1.2 [27].

Table 1.2.- Various characteristics and brief applications of different ENM. Adapted from [27].

Nanomaterial	Properties	Applications
Fullerenes (C60)	High electron affinity	Improved magnetic properties, catalysts, pyrolysis, lubricants, solar cells, electrolyte membranes, ion-exchange membranes, oxygen and methane storage, drug delivery
Carbon	High electrical	Nanoelectronics and quantum computers,

Nanotubes	conductivity, exceptional mechanical strength	ultra-strong materials, electrostatic dissipators, hydrogen storage, biosensors, chemical sensors, super condensers, reinforced polymer composites, super-strong cable, ultra-light parts for land, air and space vehicles, additives.
TiO_2 NP	Anti-UV and UV-visible optical properties, photocatalytic effect	Solar cells, UV sunblock creams, anti-UV paint, environmental treatments, transparent wood coatings, self-cleaning materials, antimicrobial agent, cancer treatment
Ag NP	Antimicrobial agent	Medical equipment, consumer products, food packaging, anti-odor textiles, electronic and household appliances, cosmetics, disinfectants
Metal oxides NP (e.g.: Zn, Ce, Zr)	Large surface area, optical properties	Ceramics, anti-scratch coatings for lenses, cosmetics, sun screens.
Dendrimers	Hydrophilic/hydrophobic	Medical and biomedical applications

NP: nanoparticle.

With advances in nanotechnology and the development of different ENM being incorporated into consumer and industrial products, it is important to understand the impact that these products may have on human and environmental health. Many efforts have been focused on the biological effect of ENM in the human system through the use of different *in vitro* cell lines [28, 29]. However, much less attention has been paid to the biological consequences of ENM in the environment. Several authors have shown that environmentally relevant microorganisms might be affected by ENM if they are released into the environment [30, 31]. However, a direct link between nanoparticle properties and biological effects is not well established yet and represents one of the most important questions on 'nanoecotoxicology'. This

knowledge could help to design and to synthesize materials in which those properties are modified to be less toxic (safer-by-design ENM; Table 1.3) or to nanosafety regulators in order to make general guidelines on nanosafety key issues.

Table 1.3.- Summary of toxic mechanisms associated with various ENM and proposed variations of their physicochemical properties. Adapted from [32].

Material examined	Mechanism of toxicity	Possible design features to mitigate toxicity
Carbon nanotubes (MWCNT)	frustrated phagocytosis leads to inflammation and oxidative DNA damage	modify structure to reduce stiffness; reduce aspect ratio
Al_2O_3 NP	ROS generation	coat or functionalize surface
Au (NP and nanorods)	disruption of protein formation	modify charge, size, hydrophilicity
CdSe QD	dissolution of toxic Cd and Se ions	cpolymers or inorganic shells
SiO_2 NP	ROS generation; protein unfolding; Membrane disruption	induce particle aggregation; modify size and/or surface charge

MWCNT: multiwalled carbon nanotubes; NP: nanoparticles; QD: quatum dots.

1.2 Cerium Oxide Nanoparticles: unique chemistry and huge potentialities

Metal and metal oxide-based nanoparticles are gaining much attention due to their enormous variety and multiple applications [33, 34]. They have semi-

conductive and catalytic properties and are being manufactured in large quantities for industrial purposes [35]. In 2008, the OECD launched a list of representative ENM (where several metal ENM were included) based on different factors: current or potential existence into market, world production volume or the existing information that is likely to be available on such materials, among others [36]. Between them, CeO_2 nanoparticles were included on the list due to their catalytic properties, the high variety of applications and uncertainties regarding their possible effects in human and environmental health safety.

The element cerium (atomic number 58; the second member of the lanthanide series or rare earth elements) is, paradoxically, not particularly rare in abundance in the earth's crust. It is the most abundant element of the rare earth family, approaching levels of the major industrial metals Ni, Cu and Zn [37]. Cerium (electron configuration $[Xe]4f^15d^16s^2$) is unique in that it can exist in both the +3 (Ce^{3+} = $[Xe]4f^1$) and +4 (Ce^{4+} = [Xe]) oxidation states, unlike most of the other rare earth metals which mainly exist in the trivalent state [38].

Cerium itself has no biological significance in mammalian physiology, but soluble Ce^{3+} salts (nitrate, acetate, chloride, *etc.*) have been traditionally used by humans for biomedical purposes due to their antiemetic, bacteriostatic and bactericidal properties [39]. The insoluble oxide form of Ce (cerium oxide, CeO_2) is not only naturally occurring, but is also manufactured both as a bulk material and as an ENM. One of the reasons by which Cerium Oxide Nanoparticles (CNPs) are being widely studied and used derives by the great and unique chemistry of their surfaces. Karakoti et al [40] showed that CNPs have a large number of surface defects which are associated with oxygen vacancies at the surface of the nanoparticle lattice [41]. The outstanding

catalytic properties of CNPs are explained by these surface defects, where Ce^{3+} atoms occupy the center of the oxygen vacancies surrounded by Ce^{4+} atoms [42]. This dual oxidation state of cerium at the nanoparticle surface (see Figure 1.3) enables them to act as both oxidizing and reducing agents. Changes in both oxidation states (switching between Ce^{3+} and Ce^{4+}) has been identified as major contributing parameter to the reactivity behavior of these particles [43].

CNPs are used in a variety of applications including chemical/mechanical polishing, catalysis, environmental remediation or sensing [44]. CNPs are also used as a combustion catalyst in diesel fuel where they act by increasing the combustion efficiency and consequently decreasing the emission of soot [45]. Due to CNPs having the ability to absorb UV radiation, while being transparent to visible light, they have been considered to be used in sunscreens [46] and as anti-corrosion agent [47].

Apart from the industrial applications, CNPS have also gained a lot of interest for biomedical applications which are mainly driven by the broad range of antioxidant properties. It has been found that CNPs display superoxide-dismutase mimetic activity [48], catalase mimetic activity [49] or the capacity to scavenge nitric oxide radicals [50], among others. Moreover, CNPs have shown several benefits in a range of diseases where

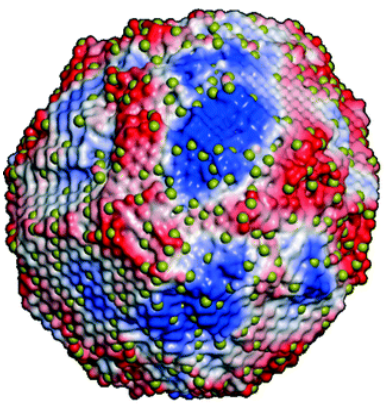

Figure 1.3.- Surface reactivity of CNPs. Regions colored red indicate high reactivity and regions colored blue indicate low reactivity. The green spheres indicate the positions of Ce^{3+} species. Adapted from [3].

oxidative stress plays a key role: ischemic brain injury, autoimmune diseases, heart failure or light-induced damage of the retina [51].

1.3 The interactions of Cerium oxide nanoparticles with a/biotic entities and the environment

There are two principal impacts of nanotechnology on the environment. The first one is immediate and direct, the second long-term and indirect. The first is concerned with the use of nanoparticles for environmental remediation. In particular, some ENM are being used as alternative to existing remediation procedures for groundwater contaminated with chlorinated organic compounds, nitroaromatic compounds, arsenic or heavy metals [52]. The second, the long-term and indirect effects, are derived by the release of ENM into the environment. They can be released by discharges of consumer products or accidental release during transport or production. Therefore, a major research effort is underway around the world to quantify and understand the impacts of ENM on the environment and, specifically, on the living organisms and trophic chain.

The release of ENM, including CNPs, into the environment has been barely studied. Nowadays, environmental concentrations are unknown and can only be estimated. Environmental concentrations of CNPs in different environmental compartments (surface waters and soil) have been predicted derived from the commercial information on the use of these nanoparticles as fuel additive in the UK [53]. For soils within 20 m of a road the highest predicted contamination level was 0.02 mg/kg and a concentration of 0.02

ng/L was predicted for river water contamination, considering direct aerial deposition and soil drainage water. A higher predicted water concentration of 300 ng/L was reported for surface run off water from roads [53]. Liu et al [54] developed a compartmental multimedia model to predict the dynamic environmental multimedia mass distribution and concentrations of CNPs in the Los Angeles region at the end of 1-year simulation. Concentrations of 5 ng/L, 0.05 μg/kg and 100 μg/kg were predicted for the water, soil and sediment compartment, respectively.

Once in the environment, the potential behavior of CNPs in aquatic systems includes agglomeration, aggregation, sedimentation, dispersion and/or interaction with biological entities. These processed depend on the physicochemical properties of CNPs and are, as well, influenced by environmental parameters such as pH, the presence of anions and cations and natural organic matter (NOM) [55]. The fate of CNPs in the aquatic environment is currently unclear and only little data is available, so a potential risk for the environment through harmful interactions with organisms has to be carefully evaluated and the assessment of ecotoxicological effects of CNP is required. The biological effects of CNPs on both Gram-positive and Gram-negative bacteria have been widely studied [56, 57]. Pelletier et al [56] showed that CNPs exhibited size-dependent and concentration-dependent growth inhibition of both *Escherichia coli* (*E. coli*) and *Bacillus subtilis*, but no adverse effects were found for *Shewanella oneidensis*. Direct contact between CNPs with the cellular envelopes and increase of the intracellular oxidative stress have been postulated as the main mechanisms of toxicity in different organisms such as *E. coli*, the cyanobacterium *Synechocystis* PCC6803 or *Anabaena* CPB4337 and the microalga *Pseudokirchneriella subcapitata* [58-60]. However, several studies have demonstrated no harmful effects of CNPs

to algae [56, 61], so much research is needed to completely understand the toxicological mechanisms of CNPs. It remains still unclear whether CNPs toxicity can be directly attributed solely to cellular adsorption or whether CNPs uptake leads to intracellular effects, especially because negatively charged particles should be repelled by the large negatively charged domains of cell membranes and the presence of biological barriers like cell wall would avoid the entry of CNPs higher than 20 nm [62].

The effects of CNPs in higher organisms such as crustaceans, earthworms or plants have also been assessed [43, 63, 64]. Some recent studies showed toxicological effects of CNPs to *Daphnia* [65, 66]. Artells et al [67] evaluated the effects of CNPs on the survival and the swimming performance of *Daphnia similis* and *Daphnia pulex*. *D. similis* was 350 times more sensitive than *D. pulex*, indicating a specie-specific effect for CNPs. *Caenorhabditis elegans* (*C. elegans*), a well-known model organism, has been also exposed to CNPs. Collin et al [68] used CNPs with differently charged surface coatings and observed particle uptake, but positively charged particles had significantly higher bioaccumulation than neutral or negatively charged particles [68]. The authors also showed that the bioaccumulation of CNPs decreased in the presence of excess humic acid, revealing the complexity of assessing the uptake of CNPs in realistic scenarios. In fact, the reduce toxicity was related with the adsorption of organic matter to the surface of CNPs.

Studies of the transport characteristics in biological environments pose different challenges due to the presence of high concentrations of biomolecules that have been shown to attach to particles forming a corona [69] and affecting their transport characteristics within *in vivo* and *in vitro* systems, accumulation and uptake. Lately, how CNPs interact with

biomolecules or other compounds is being extensively studied. CNPs in a natural aquatic system may interact with natural colloids, affecting their behavior and fate. Due to the high amount of natural colloids in the aquatic system, process of agglomeration between CNPs and natural colloids, following CNPs-sedimentation, are likely to occur [70]. Conversely, the NOM fraction of natural colloids, which consists of relatively small organic compounds such as humic and fulvic acids, may increase the stability of CNPs by a steric or electrostatic repulsion. It has been shown that NOM stabilized CNPs over 12 days by decreasing the surface charge [71]. Moreover, Patil et al [72] reported that positively charged CNPs adsorbed more bovine serum albumin than negatively charged particles, which showed little or no protein adsorption and consequently preferential cellular uptake.

With the exception of H_2O_2 or O_2^-, little is known about the interaction of CNPs with other redox active components of the environmental and biological systems. Species such as ascorbic acid and citric acid as well as a variety of phenolic compounds can act as reducing agents of Ce^{4+} on the particle surface converting it to Ce^{3+}. These species can form strong chemical bonds with the surface exposed hydroxyl species and with the Ce^{3+} generating surface complexes [73]. Interaction of CNPs with these compounds, many of which have physiological relevance and are widely present in living organisms, is important as their oxidation or complexation by CNPs might affect metabolic and oxidative processes. These findings indicate the need for a more comprehensive assessment of the interaction of CNPs with redox active components that are present in biological and environmental systems.

As concluding remark, current nanotechnology can substantially improve the properties of a wide range of products in all sectors of activity, from the

manufacture of materials with ground-breaking performance to medical diagnostics and treatment, however, numerous uncertainties are still unclear regarding the interaction of CNPs with different compounds which definitively will affect the transport, fate and behavior of CNPs in the environment.

1.4 References

[1] Lyle SN, Lourtioz J-M, Lahmani M, Dupas-Haeberlin C, Hesto P. 2015. Nanosciences and nanotechnology: evolution or revolution? Springer.

[2] Vance ME, Kuiken T, Vejerano EP, McGinnis SP, Hochella Jr MF, Rejeski D, Hull MS. 2015. Nanotechnology in the real world: Redeveloping the nanomaterial consumer products inventory. Beilstein journal of nanotechnology 6:1769-1780.

[3] Sayle TX, Molinari M, Das S, Bhatta UM, Möbus G, Parker SC, Seal S, Sayle DC. 2013. Environment-mediated structure, surface redox activity and reactivity of ceria nanoparticles. Nanoscale 5:6063-6073.

[4] Flynn H. 2014. Nanotechnology update: corporations up their spending as revenues for nano-enabled products increase. Lux research.

[5] StatNano. 2015. Status of NanoScience, Technology and Innovation. http://statnanocom.

[6] Jesus de la Maza SG, Markus Wilkens, Bart van Caenegem. 2015. Key enabling technologies for regional growth. Synergies between Horizon 2020 and European Structural and Investment Funds (ESIF) : proceedings from the EC workshop Brussels, 6 May 2015

[7] Compañó R, Hullmann A. 2002. Forecasting the development of nanotechnology with the help of science and technology indicators. Nanotechnology 13:243.

[8] Roco MC. 2011. The long view of nanotechnology development: the National Nanotechnology Initiative at 10 years. Springer.

[9] Salamanca-Buentello F, Persad DL, Martin DK, Daar AS, Singer PA. 2005. Nanotechnology and the developing world. PLoS Med 2:e97.

[10] Williams D, Amman M, Autrup H, Bridges J, Cassee F, Donaldson K, Fattal E, Janssen C, De Jong W, Jung T. 2005. The appropriateness of existing methodologies to assess the potential risks associated with engineered and adventitious products of nanotechnologies. Report for the European Commission Health and Consumer Protection Directorate General by the Scientific Committee on Emerging and Newly Identified Health Risks Brussels.

[11] Ramsden J. 2016. Nanotechnology: an introduction. William Andrew.

[12] Commission E. 2011. Recommendation on the definition of nanomaterial (2011/696/EU).

[13] Handy RD, Owen R, Valsami-Jones E. 2008. The ecotoxicology of nanoparticles and nanomaterials: current status, knowledge gaps, challenges, and future needs. Ecotoxicology 17:315-325.

[14] Pantidos N, Horsfall LE. 2014. Biological synthesis of metallic nanoparticles by bacteria, fungi and plants. Journal of Nanomedicine & Nanotechnology 5:1.

[15] Castro L, Blázquez ML, Muñoz JA, González F, Ballester A. 2013. Biological synthesis of metallic nanoparticles using algae. IET nanobiotechnology 7:109-116.

[16] Georgakilas V, Perman JA, Tucek J, Zboril R. 2015. Broad family of carbon nanoallotropes: classification, chemistry, and applications of fullerenes, carbon dots, nanotubes, graphene, nanodiamonds, and combined superstructures. Chemical reviews 115:4744-4822.

[17] Guldi DM, Martin N. 2013. Fullerenes: from synthesis to optoelectronic properties. Springer Science & Business Media.

[18] Yang F, Wang X, Zhang D, Yang J, Luo D, Xu Z, Wei J, Wang J-Q, Xu Z, Peng F. 2014. Chirality-specific growth of single-walled carbon nanotubes on solid alloy catalysts. Nature 510:522-524.

[19] Lin Y-A, Cheetham AG, Zhang P, Ou Y-C, Li Y, Liu G, Hermida-Merino D, Hamley IW, Cui H. 2014. Multiwalled nanotubes formed by catanionic mixtures of drug amphiphiles. ACS nano 8:12690-12700.

[20] Caminade A-M, Yan D, Smith DK. 2015. Dendrimers and hyperbranched polymers. Chemical Society reviews 44:3870-3873.

[21] Abbasi E, Milani M, Fekri Aval S, Kouhi M, Akbarzadeh A, Tayefi Nasrabadi H, Nikasa P, Joo SW, Hanifehpour Y, Nejati-Koshki K. 2016. Silver nanoparticles: synthesis methods, bio-applications and properties. Critical reviews in microbiology 42:173-180.

[22] Shah M, Badwaik VD, Dakshinamurthy R. 2014. Biological applications of gold nanoparticles. Journal of nanoscience and nanotechnology 14:344-362.

[23] Das S, Dowding JM, Klump KE, McGinnis JF, Self W, Seal S. 2013. Cerium oxide nanoparticles: applications and prospects in nanomedicine. Nanomedicine (London, England) 8:1483-1508.

[24] Engelbrekt C, Law M, Zhang J. 2016. Composite nanomaterials of semiconductors and noble metals as plasmonic photocatalysts. International Conference on Advances in Semiconductors and Catalysts for Photoelectrochemical Fuel Production (SolarFuel16).

[25] Chen P-C, Liu X, Hedrick JL, Xie Z, Wang S, Lin Q-Y, Hersam MC, Dravid VP, Mirkin CA. 2016. Polyelemental nanoparticle libraries. Science 352:1565-1569.

[26] Punnoose A, Dodge K, Rasmussen JW, Chess J, Wingett D, Anders C. 2014. Cytotoxicity of ZnO nanoparticles can be tailored by modifying their surface structure: a green chemistry approach for safer nanomaterials. ACS sustainable chemistry & engineering 2:1666-1673.

[27] Claude Ostiguy MD, Brigitte Roberge, André Dufresne. 2015. Best Practices Guidance for Nanomaterial Risk Management in the Workplace. 2nd Edition.

[28] Elsaesser A, Howard CV. 2012. Toxicology of nanoparticles. Advanced drug delivery reviews 64:129-137.

[29] Arora S, Rajwade JM, Paknikar KM. 2012. Nanotoxicology and in vitro studies: the need of the hour. Toxicology and applied pharmacology 258:151-165.

[30] von Moos N, Slaveykova VI. 2014. Oxidative stress induced by inorganic nanoparticles in bacteria and aquatic microalgae--state of the art and knowledge gaps. Nanotoxicology 8:605-630.

[31] Ivask A, Juganson K, Bondarenko O, Mortimer M, Aruoja V, Kasemets K, Blinova I, Heinlaan M, Slaveykova V, Kahru A. 2014. Mechanisms of toxic action of Ag, ZnO and CuO nanoparticles to selected ecotoxicological test organisms and mammalian cells in vitro: a comparative review. Nanotoxicology 8:57-71.

[32] Nel AE, Madler L, Velegol D, Xia T, Hoek EM, Somasundaran P, Klaessig F, Castranova V, Thompson M. 2009. Understanding biophysicochemical interactions at the nano-bio interface. Nature materials 8:543-557.

[33] Su X-Y, Liu P-D, Wu H, Gu N. 2014. Enhancement of radiosensitization by metal-based nanoparticles in cancer radiation therapy. Cancer biology & medicine 11:86-91.

[34] Zhang W, Saliba M, Stranks SD, Sun Y, Shi X, Wiesner U, Snaith HJ. 2013. Enhancement of perovskite-based solar cells employing core–shell metal nanoparticles. Nano letters 13:4505-4510.

[35] Zhang H, Ji Z, Xia T, Meng H, Low-Kam C, Liu R, Pokhrel S, Lin S, Wang X, Liao Y. 2013. Use of metal oxide nanoparticle band gap to develop a predictive paradigm for oxidative stress and acute pulmonary inflammation. ACS Nano 6 (5), 4349e4368.

[36] List of Manufactured Nanomaterials and List of Endpoints for Phase One of the OECD Testing Programme. Series on the Safety of Manufactured Nanomaterials No. 6; Organization for Economic Cooperation and Development: Paris, rance, 2008; http://www.olis.oecd.org/olis/2008doc.nsf/LinkTo/NT000034C6/$FILE/JT03248749.PDF.

[37] Reed K, Cormack A, Kulkarni A, Mayton M, Sayle D, Klaessig F, Stadler B. 2014. Exploring the properties and applications of nanoceria: is there still plenty of room at the bottom? Environmental Science: Nano 1:390-405.

[38] Dahle JT, Arai Y. 2015. Environmental geochemistry of cerium: applications and toxicology of cerium oxide nanoparticles. International journal of environmental research and public health 12:1253-1278.

[39] Jakupec M, Unfried P, Keppler B. 2005. Pharmacological properties of cerium compunds. Reviews of physiology, biochemistry and pharmacology:101-111.

[40] Karakoti AS, Monteiro-Riviere NA, Aggarwal R, Davis JP, Narayan RJ, Self WT, McGinnis J, Seal S. 2008. Nanoceria as Antioxidant: Synthesis and Biomedical Applications. JOM (Warrendale, Pa : 1989) 60:33-37.

[41] Campbell CT, Peden CHF. 2005. Oxygen Vacancies and Catalysis on Ceria Surfaces. Science 309:713-714.

[42] Esch F, Fabris S, Zhou L, Montini T, Africh C, Fornasiero P, Comelli G, Rosei R. 2005. Electron Localization Determines Defect Formation on Ceria Substrates. Science 309:752-755.

[43] Zhang H, He X, Zhang Z, Zhang P, Li Y, Ma Y, Kuang Y, Zhao Y, Chai Z. 2011. Nano-CeO2 exhibits adverse effects at environmental relevant concentrations. Environmental science & technology 45:3725-3730.

[44] Andreescu D, Bulbul G, Özel RE, Hayat A, Sardesai N, Andreescu S. 2014. Applications and implications of nanoceria reactivity: measurement tools and environmental impact. Environmental Science: Nano 1:445-458.

[45] Cassee FR, van Balen EC, Singh C, Green D, Muijser H, Weinstein J, Dreher K. 2011. Exposure, Health and Ecological Effects Review of Engineered Nanoscale Cerium and Cerium Oxide Associated with its Use as a Fuel Additive. Critical Reviews in Toxicology 41:213-229.

[46] Caputo F, De Nicola M, Sienkiewicz A, Giovanetti A, Bejarano I, Licoccia S, Traversa E, Ghibelli L. 2015. Cerium oxide nanoparticles, combining antioxidant and UV shielding properties, prevent UV-induced cell damage and mutagenesis. Nanoscale 7:15643-15656.

[47] Sharmila R, Selvakumar N, Jeyasubramanian K. 2013. Evaluation of corrosion inhibition in mild steel using cerium oxide nanoparticles. Materials Letters 91:78-80.

[48] Heckert EG, Karakoti AS, Seal S, Self WT. 2008. The role of cerium redox state in the SOD mimetic activity of nanoceria. Biomaterials 29:2705-2709.

[49] Pirmohamed T, Dowding JM, Singh S, Wasserman B, Heckert E, Karakoti AS, King JE, Seal S, Self WT. 2010. Nanoceria exhibit redox state-dependent catalase mimetic activity. Chemical communications 46:2736-2738.

[50] Dowding JM, Dosani T, Kumar A, Seal S, Self WT. 2012. Cerium oxide nanoparticles scavenge nitric oxide radical (NO). Chemical communications 48:4896-4898.

[51] DeCoteau W, Heckman KL, Estevez AY, Reed KJ, Costanzo W, Sandford D, Studlack P, Clauss J, Nichols E, Lipps J. 2016. Cerium oxide nanoparticles with antioxidant properties ameliorate strength and prolong life in mouse model of amyotrophic lateral sclerosis. Nanomedicine: Nanotechnology, Biology and Medicine 12:2311-2320.

[52] Fu F, Dionysiou DD, Liu H. 2014. The use of zero-valent iron for groundwater remediation and wastewater treatment: a review. Journal of hazardous materials 267:194-205.

[53] Johnson AC, Park B. 2012. Predicting contamination by the fuel additive cerium oxide engineered nanoparticles within the United Kingdom and the associated risks. Environmental Toxicology and Chemistry 31:2582-2587.

[54] Liu HH, Cohen Y. 2014. Multimedia environmental distribution of engineered nanomaterials. Environmental science & technology 48:3281-3292.

[55] Handy RD, Von der Kammer F, Lead JR, Hassellöv M, Owen R, Crane M. 2008. The ecotoxicology and chemistry of manufactured nanoparticles. Ecotoxicology 17:287-314.

[56] Pelletier DA, Suresh AK, Holton GA, McKeown CK, Wang W, Gu B, Mortensen NP, Allison DP, Joy DC, Allison MR. 2010. Effects of engineered cerium oxide nanoparticles on bacterial growth and viability. Applied and environmental microbiology 76:7981-7989.

[57] García A, Delgado L, Torà JA, Casals E, González E, Puntes V, Font X, Carrera J, Sánchez A. 2012. Effect of cerium dioxide, titanium dioxide, silver, and gold nanoparticles on the activity of microbial communities intended in wastewater treatment. Journal of hazardous materials 199:64-72.

[58] Thill A, Zeyons O, Spalla O, Chauvat F, Rose J, Auffan M, Flank AM. 2006. Cytotoxicity of CeO2 Nanoparticles for Escherichia coli. Physico-Chemical Insight of the Cytotoxicity Mechanism. Environmental science & technology 40:6151-6156.

[59] Zeyons O, Thill A, Chauvat F, Menguy N, Cassier-Chauvat C, Oréar C, Daraspe J, Auffan M, Rose J, Spalla O. 2009. Direct and indirect CeO2nanoparticles toxicity forEscherichia coliandSynechocystis. Nanotoxicology 3:284-295.

[60] Rodea-Palomares I, Gonzalo S, Santiago-Morales J, Leganes F, Garcia-Calvo E, Rosal R, Fernandez-Pinas F. 2012. An insight into the mechanisms of nanoceria toxicity in aquatic photosynthetic organisms. Aquatic toxicology 122-123:133-143.

[61] Velzeboer I, Hendriks AJ, Ragas AM, Van de Meent D. 2008. Aquatic ecotoxicity tests of some nanomaterials. Environmental toxicology and chemistry / SETAC 27:1942-1947.

[62] Navarro E, Baun A, Behra R, Hartmann NB, Filser J, Miao A-J, Quigg A, Santschi PH, Sigg L. 2008. Environmental behavior and ecotoxicity of engineered nanoparticles to algae, plants, and fungi. Ecotoxicology 17:372-386.

[63] Hernandez-Viezcas JA, Castillo-Michel H, Andrews JC, Cotte M, Rico C, Peralta-Videa JR, Ge Y, Priester JH, Holden PA, Gardea-Torresdey JL. 2013. In situ synchrotron X-ray fluorescence mapping and speciation of CeO2 and ZnO nanoparticles in soil cultivated soybean (Glycine max). ACS nano 7:1415-1423.

[64] Zhao L, Peng B, Hernandez-Viezcas JA, Rico C, Sun Y, Peralta-Videa JR, Tang X, Niu G, Jin L, Varela-Ramirez A, Zhang J-y, Gardea-Torresdey JL. 2012. Stress Response and Tolerance of Zea mays to CeO2 Nanoparticles: Cross Talk among H2O2, Heat Shock Protein, and Lipid Peroxidation. ACS nano 6:9615-9622.

[65] Auffan M, Bertin D, Chaurand P, Pailles C, Dominici C, Rose J, Bottero JY, Thiery A. 2013. Role of molting on the biodistribution of CeO2 nanoparticles within Daphnia pulex. Water research 47:3921-3930.

[66] Gaiser BK, Biswas A, Rosenkranz P, Jepson MA, Lead JR, Stone V, Tyler CR, Fernandes TF. 2011. Effects of silver and cerium dioxide micro- and nano-sized particles on Daphnia magna. Journal of Environmental Monitoring 13:1227.

[67] Artells E, Issartel J, Auffan M, Borschneck D, Thill A, Tella M, Brousset L, Rose J, Bottero J-Y, Thiéry A. 2013. Exposure to cerium dioxide nanoparticles differently affect swimming performance and survival in two daphnid species. PloS one 8:e71260.

[68] Collin B, Oostveen E, Tsyusko OV, Unrine JM. 2014. Influence of natural organic matter and surface charge on the toxicity and bioaccumulation of functionalized ceria nanoparticles in Caenorhabditis elegans. Environmental science & technology 48:1280-1289.

[69] Gunawan C, Teoh WY, Marquis CP, Amal R. 2011. Cytotoxic origin of copper (II) oxide nanoparticles: comparative studies with micron-sized particles, leachate, and metal salts. ACS nano 5:7214-7225.

[70] Klaine SJ, Alvarez PJJ, Batley GE, Fernandes TF, Handy RD, Lyon DY, Mahendra S, McLaughlin MJ, Lead JR. 2008. Nanomaterials in the environment: Behavior, fate, bioavailability, and effects. Environmental Toxicology and Chemistry 27:1825-1851.

[71] Quik JTK, Lynch I, Hoecke KV, Miermans CJH, Schamphelaere KACD, Janssen CR, Dawson KA, Stuart MAC, Meent DVD. 2010. Effect of natural organic matter on cerium dioxide nanoparticles settling in model fresh water. Chemosphere 81:711-715.

[72] Patil S, Sandberg A, Heckert E, Self W, Seal S. 2007. Protein adsorption and cellular uptake of cerium oxide nanoparticles as a function of zeta potential. Biomaterials 28:4600-4607.

[73] Sharpe E, Frasco T, Andreescu D, Andreescu S. 2013. Portable ceria nanoparticle-based assay for rapid detection of food antioxidants (NanoCerac). The Analyst 138:249-262.

OBJECTIVES

OBJECTIVES

Due to the wide and vast number of applications, cerium oxide nanoparticles need to be studied deeply to unravel their potential effects in the environment. Besides, the main nanoparticle properties which could drive their toxicity are being examined intensively during the last years. All that information will be useful for nanosafety research and regulation purposes where general outlines could be drawn. The overall aim of this thesis is to address the biological effects of cerium oxide nanoparticles with special emphasis on the study of the Bio-Nano interface. Firstly, the mechanisms and physicochemical properties which underlie the biological activity of cerium oxide nanoparticle will be assessed. Secondly, the effects of coatings and possible internalization process of cerium oxide nanoparticles will also be considered as potential factors on their toxicity for nanosafety considerations. Last but not least, the physicochemical properties of the nanoparticle surface and how they affect the interaction with several compounds of interest will be evaluated as well as the biological consequences of the interaction.

Specific objectives:

1. To review the state of the art of the Bio-Nano interface and how the environment may alter the pristine nanoparticles into transformed particles with a biological or environmental identity.

2. To untangle the main physicochemical descriptors which drive the biological activity of different cerium oxide nanoparticles using the microalgae *Pseudokirchneriella subcapitata* and *Chlamydomonas reinhardtii* as model of study, paying attention to the nanoparticle colloidal stability and redox chemistry.
3. To determine the role of coatings and internalization processes on the toxicity of cerium oxide nanoparticles.
4. To unravel the implication of the surface redox chemistry of cerium oxide nanoparticles in the interaction with compounds of interest in the industrial and medicine field.

CHAPTER 2

BIO-NANO INTERFACE AND ENVIRONMENT: A CRITICAL REVIEW

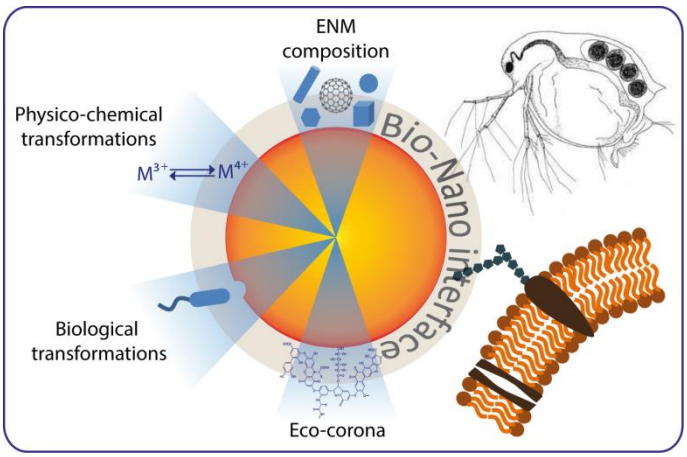

CHAPTER 2. BIO-NANO INTERFACE AND ENVIRONMENT: A CRITICAL REVIEW

2.1 Abstract

The Bio-Nano interface is the boundary where the Engineered NanoMaterials (ENM) meet the biological system, exerting the biological function for what they have been designed or inducing adverse effects to other cells or organisms when they reach non-target scenarios, i.e: the natural environment. Research has been performed to determine the fate, transport, and toxic properties of ENM, but much of it focused on pristine or "as manufactured" ENM or where modifications of the materials were not assessed. This article reviews the most recent progresses regarding the Bio-Nano interface and the transformations that ENM suffer in the environment, paying special attention to the adsorption of environmental biomolecules on the surface of ENM. Whereas the protein corona (PC) has received considerable attention in biomedical field and human toxicology, its environmental analogue (the eco-corona) has been much less studied. A section dedicated to the analytical methods for studying and characterizing the eco-corona is also presented. We conclude with a Research Needs section where the key problems and knowledge gaps that need to be resolved in the near future regarding the Bio-Nano interface and eco-corona are presented and discussed.

2.2 Introduction

Nanotechnology is considered as a new technology that will significantly improve, or even revolutionize, many areas and industrial sectors. The forecast for nanotechnology estimates that the global value of nano-enabled products, nano-intermediates, and ENM will reach $4.4 trillion by 2018 [1] [see also [2, 3]]. Nanotechnology has become a vibrant area of research over the past 15 years. This enthusiasm derives from two main factors: (1) the industrial interest in ENM, leading to their increased use in consumer products (ENM are used as chemically inert or active additives that impart desired qualities, such as increased hardness or surface area, antimicrobial behavior, UV protection, and coloring, among others[4] and (2) the increased possibility of human and environmental exposure, which emerged concerns about the harmful effects that these new objects could have in human and environmental safety.

The more money is expected that the technology generates, the more money is funded by international agencies to deal with nanotechnology risk-related research: In Europe, the expense was €261M between 2006 and 2013, with a further €71M injection through Horizon 2020. Between 2006 and 2015, the US federal government invested US$830M in nanotechnology environment, health and safety research [5]. In 2008, in particular, the US federal government published its first comprehensive research plan for nano-safety research [6] and, in 2012, the US National Academy of Sciences published an independent nanotechnology safety research strategy [7]. In Europe, the 7th Framework Programme included continuing thematic calls on nano-safety topics as an integral part of its Nanotechnologies, Materials and Production Technologies (NMP) programme. Additionally, since 2007, the Organization

for Economic Cooperation and Development (OECD) also headed international efforts on validating toxicity test methods for ENM [8].

The potential benefits of nanotechnology depend on mastering a specific fraction, the ENM surface and its interaction with the surrounding environment. A complete understanding of the Physical Chemistry of ENM when its surface approaches macromolecular entities will help to improve the development of these materials. This interface, known as the Bio-Nano interface, hosts "the dynamic physicochemical interactions, kinetics and thermodynamic exchanges between nanomaterial surfaces and the surfaces of biological components" [9].

The aim of this critical review is to summarize the more recent research contributions to the Bio-Nano interface field from the last 5 years, although previous relevant bibliography is also included. The literature from January 2011 to December 2016 (and part of 2017) was searched using Scopus for studies related with the Bio-Nano-Eco interface field, focusing on how environmental variables and non-target organisms influence it. A description of the current techniques that are being used to study this fraction is included. Finally, a critical point of view and a summary of research needs are included as well.

2.3 Understanding the Bio-Nano interface

To fully understand the processes that happen at this interface, it is necessary to describe several elements: a) the nanomaterial surface; b) the medium where the ENM is suspended; and c) the properties and influence of the

biological entities. The first factor influencing the Bio-Nano interface is the nanomaterial surface itself (Figure 2.1). Prominently, its characteristics are determined by its physicochemical composition, e.g.: elemental composition, size, shape, surface area, porosity, functional groups, ligands, etc., [10, 11]. Recently, it has been shown that size and surface structure have a crucial effect on the interaction with biological components like proteins. In this sense, silica particles of 200 nm (and bigger) induced conformational changes in myoglobin and Bovine Serum Albumin protein (BSA) upon adsorption [12]. Huang et al. [13] also showed that the NP surface characteristics are key parameters during the protein adsorption, since they might be able to module the protein conformation on NP surface. Surface oxidation state is a key factor that modulates the toxicity of cerium oxide nanoparticle. It has been determined that only the NP with high surface % of Ce^{3+} exerted toxicity in a study with an ecologically relevant aquatic organism [14].

The second factor, external to the ENM, but with a deep influence on nanoparticle fate and properties, is the characteristics of the surrounding medium (Figure 2.1). Not dependent, nevertheless, does not mean that they do not have important implications on the ENM. This parameter has a great impact on several measurable properties of ENM such as hydrodynamic size, state of aggregation, effective charge, dissolution or surface valences, which are all influenced by basic factors like ionic strength, pH and temperature, among others. Over the last years, it has been extendedly reported how the NP aggregation state and colloidal stability strongly depend on the medium where they are suspended [15-18]. Moreover, the dissolution of metal oxide nanoparticles extremely varies depending on the characteristics of the surrounding media. For example, it has been shown for CuO NP that the presence of amino acid rich environment can lead to nearly complete NP

dissolution, while the presence of NaCl did not have any significant effects on the solubility of these nanoparticles [19].

The third main factor is derived from the biological entities themselves and determined by their surface composition and their ability of influencing their surrounding environment. This factor is greatly mediated by the presence of large organic molecules, which include natural organic matter (NOM), proteins and other biomolecules. For instance, it is established that the presence of NOM can control the nanoparticles aggregation state by creating an adsorbed layer on nanoparticle surface. The interaction may improve the steric stability of the system and its colloidal stability, hence letting the ENM remain suspended in the media [20, 21]. Alternatively, NOM can destabilize ENM, inducing aggregation by charge neutralization [16]. Louie et al. [22] have recently pointed out that NOM-weight-averaged molecular weight was the best indicator of ENM aggregation in the presence of NOM. The authors used Suwannee River NOM and five additional NOM isolates covering a range of sources (terrestrial, freshwater, and marine) and preparations (fulvic and humic acids) and showed that there was a trend in how the ENM and NOM interact as biomolecules with molecular weight higher than 100 kg/mol provided better stability than lower molecular weight components for each type of NOM [22].

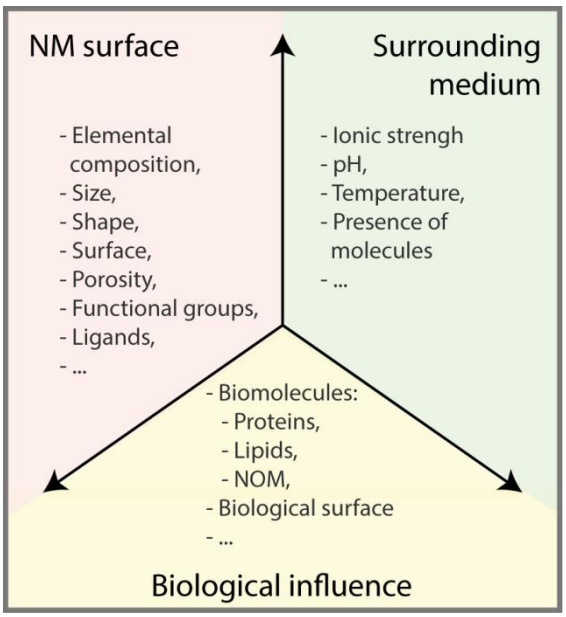

Figure 2.1.- The three sides of the Bio-Nano interface triangle. The main parameters governing the interface are surface, medium characteristics and biological factors.

These three general parameters are important in the fate, transport, behavior and bioavailability of ENM in the environment, but the last one, the adsorption of organic molecules on their surfaces, is critical when ENM approach biological surfaces. The formation of an external 'biolayer' in the extracellular environment has been shown to alter nanoparticle size, shape, and surface properties, creating a "biological identity" that is distinct from its initial "synthetic identity" [23].

Therefore, how ENM interact with different cells and organisms depends on the substances attached to their surface. Recently, the interaction between ENM and biomolecules has been extensively studied in biomedicine [24, 25], due to the enormous applications of nanotechnology in this field [26-29]. The

conclusions created a know-how about the behavior of ENM in complex matrices where they are surrounded by multiples 'bioelements' like proteins. The phenomenon describing the assembly of ENM and adsorbed proteins is called the ENM-protein corona (PC). The PC has been recognized as a dynamic entity that "evolves" as proteins continuously adsorb on the nanoparticle surface, desorb, and are replaced by other proteins. It is well-known that the surface of ENM is covered by a layer of tightly adsorbed proteins, the so-called hard corona (Figure 2.2) [30]. Strong biding affinity, long residence time, slow exchange time and high conformational changes are some of the most important characteristics of this layer. Some models suggest that on top of this 'hard corona' a 'soft corona' may exist, which consists of a more loosely associated and rapidly exchanging layer of biomolecules with low degree of conformational changes (Figure 2.2) [31].

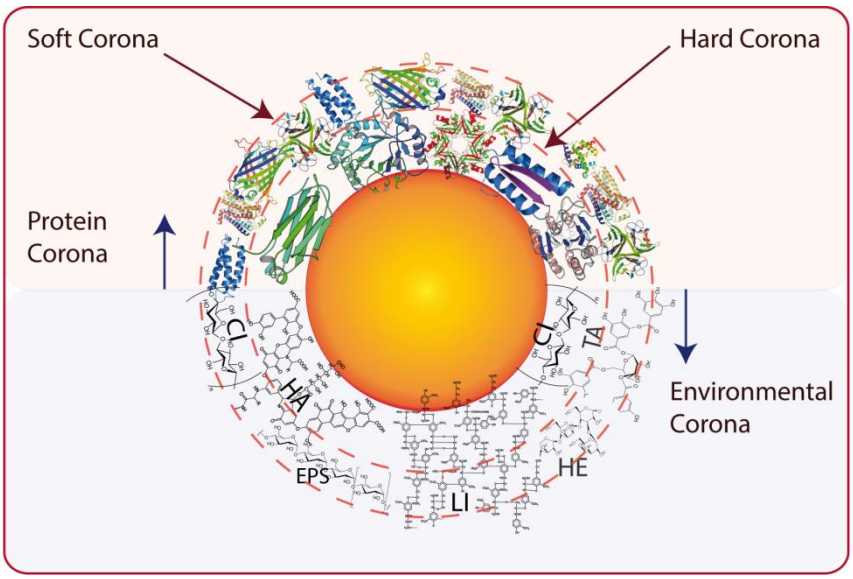

Figure 2.2.- ENM–protein (top) and environmental (down) corona. HE: hemicellulose; Cl: cellulose; TA: tannic acid; LI: lignin; EPS: exopolymeric substances; HA: humic acid

Similarly, a NP-adsorbate association might also exist when ENM enter to the environment, ending up in the formation of an eco-corona. Lynch et al. [32] described that ENM could adsorb 'ecomolecules', which are macromolecules acquired by the ENM from the environment (Figure 2.2), mostly the already mentioned NOM or secreted biomolecules like Extracellular Polymeric Substances (EPS), among others. EPS are complex mixtures composed of proteins, polysaccharides, fats, nucleic acids, and inorganic substances released from different microorganisms [33]. Grunér et al. [34] have recently shown that hydrophobins, highly adhesive proteins secreted in large quantities by fungi, could strongly bind to polystyrene NP of different sizes and surface groups, increasing their stability when exposed to complex medium compared to pristine NP. Therefore, the adsorption of environmental molecules onto the ENM surface may strongly modify NP behavior with respect to uncoated particles. In this regard, a number of studies address the effect of EPS interaction on the toxicity of ENM. Generally, EPS have protective effects for bacteria [35] and algae [36]. Su et al. [35] found that EPS-poor *Escherichia coli* cells were more vulnerable to Ag-doped multi-walled carbon nanotubes than EPS-rich cells. Recently, Zhou et al. [36] discovered that the amino and aromatic carboxylic groups in the EPS were involved in the interaction between EPS and different capped Ag nanoparticles (AgNPs). The authors showed that EPS could alleviate the algal toxicity of AgNPs not only by reducing the concentration of released free Ag^+ in the culture medium and inhibiting the cell internalization of Ag^+, but also by restraining the toxic pathway of "Trojan-horse" mechanism by limiting the internalization of AgNPs. All those works highlight the importance of the formation of an eco-corona onto the ENM surface. However, much research is still needed to fully understand which types of environmental biomolecules are potentially able to

adsorb on ENM surface and to determine the toxicological consequences of the formation of Bio-Nano interfaces.

2.4 Transformation of ENM in the environment and consequences for the Bio-Nano interface

There are several routes by which ENM can enter the environment. They can be released by direct discharges of consumer products, accidental release during transport or production or by the intentional distribution of ENM for remediation purposes. Due to the high surface to volume ratio and reactivity of ENM, they are prone to suffer alterations in the highly dynamic environmental compartments. These changes can modify the original material yielding a different one. The resulting transformations of the ENM may affect the Bio-Nano interface as well as their fate, transport and toxic properties. These transformations include chemical, physical and biological transformations.

Natural oxidation-reduction reactions, photooxidation/photoreduction, dissolution, sulfidation and aggregation are amongst the most studied physicochemical transformations (Figure 2.3). Depending on the particle redox potential and the prevailing conditions in an environmental compartment, ENM may be susceptible to oxidation or reduction. Zero-valent iron nanoparticles (nZVI) are being used for groundwater remediation [37], however, nZVI are easily oxidizable and could rapidly transform into particles without redox chemistry. It is known that nZVI will oxidize once into the environment, either completely or partially from Fe^0 to various Fe oxides and hydroxides. Aged/oxidized nZVI particles have lower redox activity and

presumably lower reaction potential to remediate contaminants in groundwater. Reinsch et al. [38] examined the aging of commercially nZVI in solutions containing common groundwater anions (Cl^-, NO_3^-, HCO_3^-, SO_4^{2-}, and HPO_4^{2-}). The authors showed that inorganic anions do not inhibit the oxidation of nZVI with the exception of nitrate, which passivates the surface, thereby encapsulating the Fe^0 and decreasing particle reactivity. The decrease of redox activity also correlates with a decrease in the cytotoxicity of nZVI to *Escherichia coli* as demonstrated by Auffan et al. [39].

In other cases, the oxidation of metal ENM leads to the dissolution and release of the ENM elemental ions [40]. In this context, silver NPs (AgNP) are the most studied case among the metal NPs [41], due to the toxic effect of Ag^+ ions through various environmentally relevant species [40]. Mitrano et al. [42] elegantly studied the dissolution of AgNP at environmentally relevant concentrations (ng L^{-1}) in laboratory, natural, and processed waters using single particle ICP-MS (spICP-MS), proving that while the available techniques currently used are generally not capable of measuring AgNP-transformation at these concentrations, spICP-MS can measure it even in complex matrices. One interesting result is that the effect of AgNP coating may be irrelevant in natural waters, as the authors did not find differences in the dissolution rates among coatings either in the 60 or 100 nm AgNP.

Moreover, nanoparticles and their ligands could undertake light-induced transformations via direct light absorption and reaction. Yin et al. [43] have shown that sunlight could accelerate the morphology change, aggregation, and further sedimentation of AgNPs in eight typical environmental water samples. Similarly, Cheng et al. [44] found that AgNPs undergo aggregation under sunlight irradiation, but they also evaluated the biological effect of

these phototransformed nanoparticles towards the wetland plant *Lolium multiflorum* and observed that the toxicity of the AgNPs was significantly reduced by sunlight in comparison with non-irradiated samples. It is important to note that light reactions are also present in carbon based ENM where aggregation, Reactive Oxygen Species (ROS) generation and surface modification have been observed [45, 46]. In addition to these transformations, it has been shown that under ambient environmental light conditions, Ag ions bound to NOM can be reduced to form AgNP in river water or synthetic natural water samples [47], showing a new route for AgNP synthesis in the environment. Interestingly, Glover et al. [48] showed that, under environmental relevant conditions (relative humidity greater than 50%), new silver and copper NP could form in the vicinity of the parent particles or even in the proximity of metallic-non-nanoscale objects.

Another important environmental process which could affect ENM is sulfidation (Figure 2.3). This phenomenon may take place during waste water treatment [49] or in freshwater wetland [50]. It is already well-known that the sulfidation of metallic ENM in the environment reduces the release of ions and, thus, their toxicity to diverse organisms such as *Caenorhabditis elegans* (*C. elegans* hereinafter, a model soil organism; [51]), *Danio rerio* (*D. rerio*, a model fish; [52]) and the aquatic plant *Lemna minuta* (duckweed; [53]), among other [53]. Interestingly, Starnes et al. [54] analyzed the transcriptomic profiling of nematodes which were exposed to pristine AgNP or sulfidized AgNP and found that their toxicological mechanisms were completely different. The toxicity of AgNP was explained by dissolution, release of Ag ions and particle specific effects, while the processes most affected by sulfidized AgNP was related to molting and the cuticle envelope.

Apart from the chemical transformations that have been described previously, there are several physical transformations involving ENM. Mitrano et al. [55] classified these alterations in two main categories: abrasion/mechanical erosion and aggregation. The authors focused on how mechanical or abrasion processes could end up in the formation of a nano-object and its subsequent release from the original material. However, the most important physical process affecting ENM is agglomeration/aggregation (including homoagglomeration and homoaggregation and their hetero-forms), as this is something that can change the high reactivity of ENM, due to the increase of the overall size. As described by Gonzalo et al. [18], the aggregation state of nZVI resulted in a non-linear dose-response toxicological curve due to the different colloidal stability, which was identified as the main driver for nZVI bioactivity. nZVI resulted in adverse biological effects towards a model microalga when destabilized (higher sizes), but not when it was forming a stable suspension. Altogether, agglomeration relies on a myriad of physicochemical interactions between the particles and water chemistry and this is the reason why, here, both ENM-transformation factors (chemical and physical factors) are shown together in Figure 2.3, instead of illustrating both parameters independently like Lowry et al. [50] and Mitrano et al. [55] did.

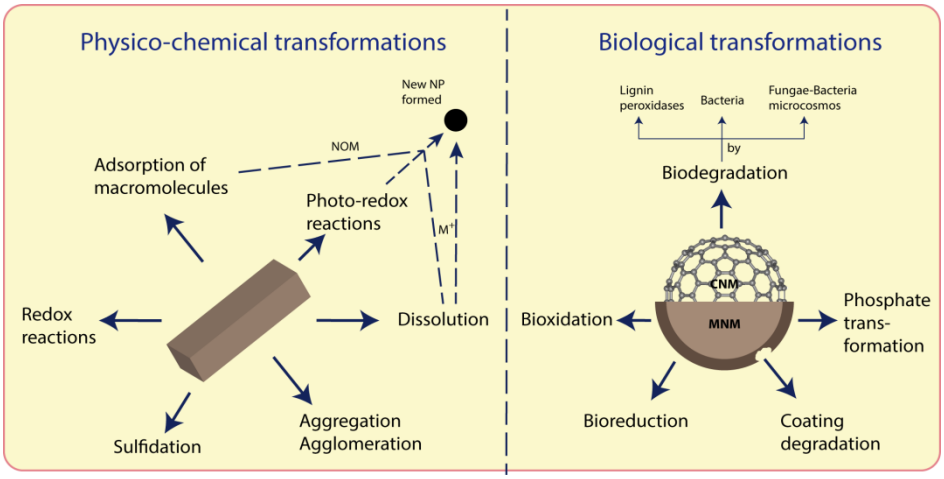

Figure 2.3.- Scheme of representative physicochemical (left panel) and biological (right panel) transformations of ENM in the environment. MNM: metallic ENM, CNM: carbon-based ENM, NOM: natural organic matter, M^+: metallic ion, NP: nanoparticle.

Biological entities, such as bacteria, fungi, microalgae, plants and other organisms, or their secreted enzymatic components could also have an effect on the coating and on the ENM itself. The process is known as biotransformation (Figure 2.3). Kirschling et al. [56] have demonstrated that polymer coatings covalently bound to nanomaterials are bioavailable and can be degraded by a community of different bacteria. Significant advances in ENM-biotransformation have been done with different plant organisms [57-63]. Parsons et al. [57] reported for the first time the biotransformation of NPs by a plant system where, from nickel NPs, a Ni(II)-organic acid complex was found in shoots and leaves. Furthermore, different processes of NP oxidation [58] and reduction [59] have been observed for plants exposed to Ag or CuO NPs, respectively. Recently, more studies have focused on Rare Earth Oxide NPs, due to their great potential in a wide range of applications. The

biotransformation of La_2O_3, Yb_2O_3 and CeO_2 NPs was reported to follow a common transformation route with dissolution promoted by reducing substances and re-precipitation forming phosphates and other compounds [60-62]. Hernandez-Viezcas et al. [63] also reported a limited dissolution of CeO_2 NPs and surface bio-reduction from Ce (IV) to Ce (III) in soybean plants.

Several research groups have reported in recent years that carbon-based ENM (CNM) are susceptible to biodegradation as well [64-66]. Much work has been performed with human cells lines in view of the biomedical uses of CNM. Bhattacharya et al. [67] recently reviewed this topic, so the readers are encouraged to follow that reference (and references therein) for more information as the present work is mainly focused on the Bio-Nano interface from an environmental point of view. In this regard, it has been proved that lignin peroxidase (a ligninolytic enzyme) released from white rot fungi can induce the oxidative biodegradation of both oxidized and reduced graphene oxide nanoribbons [68]. Similarly, several studies have proved the biodegradation of different CNM by bacterial communities [69, 70]. Liu et al. [69] suggested that the direct contact between bacterial cells and materials promotes the oxidation of carbonaceous material. Interestingly, a fungi-bacteria soil microcosm rapidly mineralized a CNM. Carbon could also be incorporated into the biomass of a range of microorganisms, particularly Gram-negative bacteria and fungi [71]. However, more research is needed in this field to further confirm all these results; Parks et al. [72] showed that pristine and minimally-oxidized CNM are not easily biodegraded under environmental conditions such as exposure to the fungi or bacteria present in contaminated sediments and aerated sludge, indicating that this CNM might be likely persistent in environmental media.

Biological transformations of ENM that have been taken up by microorganisms have been observed in vivo using mussels [73] or worms [74]. Montes et al. [73] showed that CeO_2 and ZnO NPs were taken up by mussels, but, while CeO_2 NP remained unchanged in the pseudofeces, the ZnO NPs were completely transformed and excreted in Zn dissolved species. However, although CeO_2NP seemed to be unaltered, it is interesting to note that the biotransformation of CeO_2 could make them more bioavailable for other organisms such as deposit feeders (e.g., polychaete worms, amphipods, crabs) or grazers (sea urchins), among others. Several authors also reported the biotransformation of superparamagnetic iron oxide NP (SPION) in the nematode *C. elegans* [74, 75]. Gonzalez-Moragas et al. [74] observed a size decrease in SPION coated with citrate during digestion in the intestinal microenvironment of *C. elegans* while SPION coated with BSA proteins did not suffer any changes. Interestingly, the uptake of BSA-SPION was higher than citrate-SPION in larval population, indicating that different result could be obtained using different growth stages of the same organism or different coatings. On the other hand, extracellular biotransformation has been observed for a fungal organism (*Humicola sp*). This species could transform 150–200 nm TiO_2 (with an anatase structure) to 5–28 nm TiO_2 (with a brookite structure) [76]. Unfortunately, the biotransformation mechanism was not proposed, so there are no clues regarding how the process was performed.

These results show that the biotransformation can produce new nanomaterials with a different toxic profile. Clearly, it is information of critical importance for assessing the biological impacts of nanoparticles and the kinetics of such impacts. Considerable research effort is still needed to clarify and fully understand the implications of the environmentally transformed ENM and their behavior within the environment. As shown earlier, it has been

hypothesized that different ENM, once inside the environment, might be transformed into the same material [42]. This can be due, for example, to strong aggregation processes or the ENM surface adsorption of NOM, so imparting the same environmental identity to different ENM. Lombi et al. [77] showed that neither surface coatings, at least for three different types, nor core composition (Ag or AgCl) of AgNP prevented the formation of Ag_2S, indicating that whatever the original AgNP is, the outcome of wastewater treatment in terms of speciation would be the same. The new environmental identity derived from such transformations could result in a complete loss of the individual nano-properties. Conversely, the release and subsequent transformation of NP may result in an increase of ENM diversity [42], due to the diversity of aging/transformation reactions that could end up in different transformed ENM. Besides, the coverage of ENM surface by an eco-corona could facilitate the grouping and read-across of different ENM based on their environmental fate, making it easier to deal with the huge variety of existing and future ENM.

2.5 Biological identity of ENM

Once ENM interact with the environment and get in contact with living organisms, they become exposed to a huge variety of transformations. In particular, active biomolecules may form a corona around them, transforming the bare or pristine ENM into a modified ENM potentially bearing a biological component. The biological identity of an ENM depends on the composition of the surrounding biological environment and could determine the subsequent interactions with cells: It is what the organism ‘sees’ and interacts with [32].

From now on, we will focus on how these transformations and, specifically, the acquisition of an environmental corona, will impact the interaction with biological systems, membranes and cell envelopes, paying special attention to ENM-cellular uptake and endocytosis.

The ENM specific interaction with biological surface (cell membranes or cell walls) and the way they enter cells is a complicated issue. Many efforts have been done using modelling programs and artificial phospholipid bilayers to try to understand the parameters and processes that drive the bio-NP interaction in a simplified scenario [78-80]. Nevertheless, in vivo studies with whole organisms are also being performed. Jacobson et al. [81] recently studied the interaction between gold nanoparticles and the Gram-negative bacteria *Shewanella oneidensis*. The authors demonstrated an electrostatic association of cationic NP with the negatively charged polysaccharide portions of lipopolysaccharides in the cell envelope. However, bacteria constitute a large domain of prokaryotic microorganisms with a huge diversity on their cell envelope and content of lipopolysaccharides, so the mode of contact and outcomes of the NP-biological interaction may be completely different depending on the composition of the bacterial surface.

Whether ENM might pass through the biological barriers and enter into cells (or not) has been a matter of intense research during last years [82-84]. Zhu et al. [85] suggested that the internalization of NPs is mainly a size-dependent process in eukaryotic cells, due to the well-designed endocytic machinery involved (Figure 2.4). It has been noted, however, that NP-hydrophobicity could be an important parameter due to the lipophilic nature of cytoplasmic membranes [80]. In this regard, there are five endocytic pathways that can be used for nanoparticle endocytosis: phagocytosis, macropinocytosis, clathrin-

mediated, caveolin-mediated, and clathrin/caveolin-independent endocytosis (Figure 2.4). In addition to them, there is another one which is independent of endocytosis: ENM direct penetration, suggested from particles with very low sizes (<10 nm) [86].

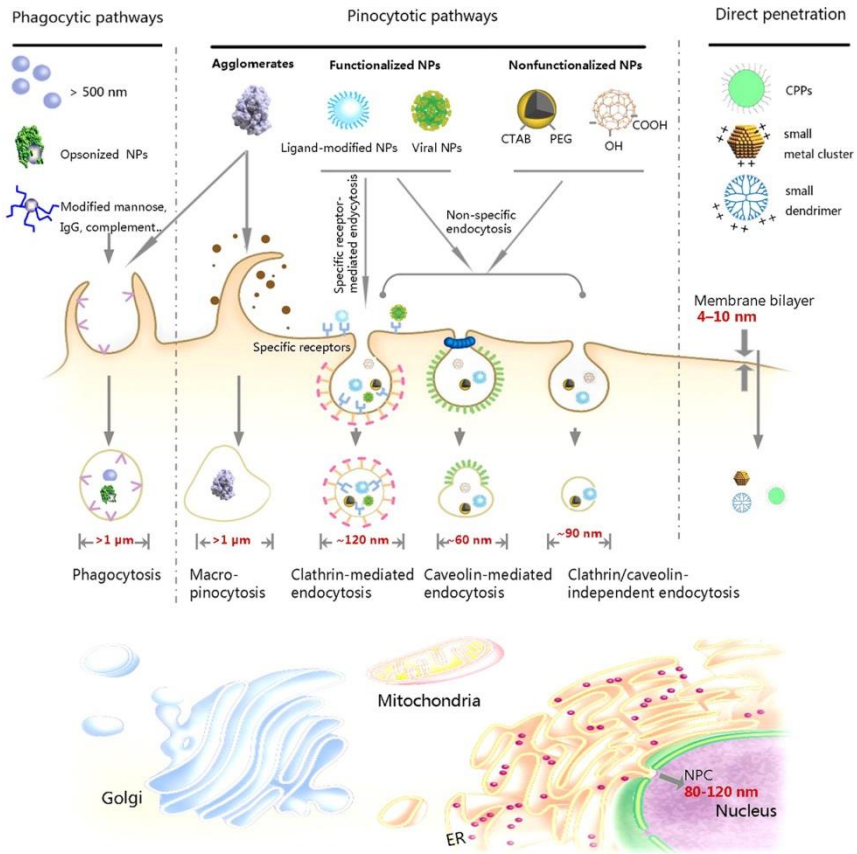

Figure 2.4.- Routes of ENM entry, depending on the size of the initial material. Phagocytosis could be the way used for large particles or aggregates. Other ways include pinocytosis (mediated by specific receptors or not) and direct penetration. Reprinted with permission from (Zhu, M., Nie, G., Meng, H., Xia, T., Nel, A., & Zhao, Y. (2012). Physicochemical properties determine nanomaterial cellular uptake, transport, and fate. Accounts of chemical research, 46(3), 622-631.). Copyright (2012) American Chemical Society).

The same routes of entry outlined in Fig. 2.4 should explain the internalization of ENM in several environmentally revelant eukaryotic organisms [75, 87-89]. In many microorganisms (such as bacteria and algae) the cell wall protects cells with pores in the 5-20 nm range [90]. Accordingly, it has been found that stabilized CdTe Quantum Dots (QD) could enter the freshwater alga *Ochromonas danica* directly through macropinocytosis [91]. Interestingly, the CdTe quatum dots suffered further modifications inside the algal cells as the photoluminescence pattern decayed sharply due to the adsorption of different biomolecules to the surface of QD. Moreover, Hoepflinger et al. [92] recently reported that clathrin pathway played an important role in the endocytosis process in a multicellular green algae (*Chara australis*). *Chlamydomonas reinhardtii,* a model unicellular microalga, has also been shown to possess a chlatrin-mediated endocytosis pathway which is a probable way for ENM internalization [93, 94]. NP internalization has been recently described in *C. reinhardtii* for QdTe/CdS QD [95], CeO_2 [96], Ag [97] , PAMAM-dendrimers [98] and CuO NPs [99]. Futher research is needed for determining the effect of coatings in ENM uptake; some results pointing towards an increased internalization of ENM having organic coatings [96, 97, 99]. However, how the ENM cross the cell wall and use these pathways to enter inside cells is not fully understood yet. Ma et al. [89] extensively reviewed the scientific literature on this topic and provided a thorough classification of the nano-bio interactions between ENM and different organisms: Bacteria, algae, invertebrates and fish. The readers are encouraged to follow this article and their referred studies.

The specific interactions at the Bio-Nano interface, the localization of ENM, inside organisms and cells, and the potential toxicity of ENM may vary depending on their biological identity. There are several factors influencing

the composition and evolution of the biological identity, namely exposure temperature, exposure time, nanoparticle hydrophobicity, size/surface curvature, surface charge, surface functionalization, physiological media/nanoparticle concentration ratio and topology [25]. Once the biological identity is formed, the effect of the ENM with their biological identity could be different, depending on which type of biomolecule is adsorbed or the medium where they are suspended. It has been shown that the formation of the ENM-corona decreased ENM-induced toxicity because of a reduced cellular uptake [100, 101] or the inhibition of ROS formation [102]. Additional environmental examples can be found for AgNPs [21, 103-105] or fullerenes [106] for which the adsorption of NOM decreased the toxicological effects towards several model organisms. Conversely, the adsorption of biomolecules on the ENM surface can induce protein denaturation and cell damage [107-109] and it has also been reported an increased accumulation of NP in biofilms of *Pseudomonas putida* [110]. It is therefore not surprising that the corona effect is contradictory in various biological systems considering that different cell types and environment may generate different corona composition and also favor the uptake of specific surface biomolecules.

Clearly, it is the biomolecular corona that primarily interacts with biological systems and thereby constitutes a major element of the ENM biological identity. The molecular corona may be conveyed when the ENM moves from one biological environment to another [25]. Lundqvist et al. [111] simulated the passage of a ENM from one biological fluid (plasma) into another (cytosolic fluid) and concluded that there was a significant evolution of the PC from the first to the second biological solution, but the NP retained a “fingerprint” of its history in the final corona. The time evolution of PC under realistic in vivo conditions was recently considered by Hadjidemetriou et al.

[112]. Their results showed that a complex PC formed in only 10 min and, although the total amount of protein adsorbed did not significantly vary, the abundance of each protein identified fluctuated over time indicating a competitive exchange processes. As cells constantly excrete to their microenvironment several proteins, nutrients, small solutes, ions,…, it is also interesting to know how conditioning of the cell culture medium influences the biological identity of nanoparticles. Albanese et al. [113] demonstrated that the secretion of different molecules alters the extracellular environment and can lead to nanoparticle aggregation and changes in the PC, which affect the rate and mechanism of cellular uptake.The same process could be observed in the natural environment. Aquatic plants (*Potamogeton diversifolius* and *Egeria densa*) exposed to AgNPs produced exudates (mainly dissolved organic matter) that altered their aggregation state and ability to release Ag^+ [114, 115]. Hayashi et al [116] explored the importance of corona composition for ENM recognition by coelomocytes (leukocyte cells) of the earthworm *Eisenia fetida*. The authors showed that the earthworm was able to recognize AgNPs covered with a corona of native *E. fetida* coelomic proteins, compared with the same particles coated with a non-native corona made from fetal bovine serum.

Table 2.1 lists the main articles characterizing the interaction between ENM and biomolecules (mainly proteins) in studies using environmentally relevant organisms. Hayashi et al. [117] and Canesi et al. [118] used different biological fluids from the model fish *D. rerio* and the marine bivalve *Mytilus galloprovincialis*, to study the spontaneous macromolecular adsorption forming a corona of biomolecules onto ENM. In order to detach the adsorbed biomolecules to the ENM surface, several steps of centrifugation and washing were conducted. Interestingly, NP could adsorb particular biomolecules from

a species specific [116, 118] or gender specific environment [117] and this corona was recognized and even accumulated more easily than other coronas in blood or immunocyte cells, indicating that ENM can acquire a completely different corona, and thus a completely different biological identity, depending of the biomolecular environment where they are suspended. Furthermore, that corona might evolve when the ENM move into a new environment with different biomolecules which have higher affinity than those previously adsorbed as it has been already mentioned [111-113].

Table 2.1.- Studying the eco-corona from its composition to its biological effect using environmentally relevant organisms.

Organism	ENM	Method of Separation	Method of characterization	Ref.
Daphnia magna	PSNP	Sedimentation, centrifugation and washing	Gel Electrophoresis (PAGE)	Nasser et al. [119]
Mytilus galloprovincialis **(hemocytes)**	PSNP	Centrifugation	Gel Electrophoresis and nano-HPLC-MS/MS	Canesi et al. [118]
Danio rerio **(blood cells)**	SiO_2NP	Centrifugation	TEM, DLS, NTA, Gel Electrophoresis (PAGE)	Hayashi et al. [117]
Eisenia fetida **(coelomocytes)**	AgNPs	Centrifugation	TEM, DLS, NTA, Gel Electrophoresis (PAGE)	Hayashi et al. [116]

PSNP: Polystyrene based-NP. PAGE: polyacrylamide gel electrophoresis. HPLC-MS: High-performance liquid chromatography coupled with a mass spectrometer.

Besides the aquatic plant assays stated above, other works assume the hypothetical crossing of ENM through the different biological barriers and entry into the biological fluids in their studies about the effects of specific biomolecular coronas. There is an interesting example of a complete characterization of an eco-corona in an environmentally realistic scenario [119]. The authors elegantly assessed the toxicity and the interaction of two different polystyrene NP (PSNP) with the biomolecules secreted by *Daphnia magna* and the impact of these interactions on the ratio of NP uptake/removal. They observed that the eco-corona increased the uptake and toxicity of PSNP. Interestingly, the removal of eco-corona modified polystyrene nanoparticles was less efficient than uncoated polystyrene in the gastrointestinal tract of *Daphnia magna.*

Evolving or changing the environment where the eco- or PC has formed and how it changes through time adds, thus, novel additional levels of complexity in the study of bio-nano interactions. The vast majority of works dealing with PC refer to biomedical applications, with little attention to environmental scenarios. The evolution of eco-corona through different conditions and time, the biological consequences of eco-corona towards different trofic levels are important issues to be addressed. Further studies are needed to cover those research gaps.

2.6 Studying and characterizing the Bio-Nano interface

To fully understand the behavior of ENM in contact with biological entities, the ENM need to be characterized both in their pristine state and in complex environments, which include their eco or protein corona. This task requires

the use of several techniques from diverse disciplines, including physical, chemical and biological sciences. Characterizing the surface adsorption of molecules on ENM is problematic due to several reasons. For example, discriminating between species adsorbed to the nanoparticle surface and those in solution can be challenging because of their similar chemical signatures and the high chemical complexity of biologically relevant media (which may contain many different biomolecules together with a complex background of coloidal organic matter). This difficulty can be avoided by isolating the ENM from other colloidal species in the sample matrix prior to analysis and characterization. Currently available separation methods include column chromatography, field flow fractionation and their derivatives.

A liquid chromatography method has been recently used to separate AgNP and Ag^+ in environmental water samples such as lake water and wastewater treatment plant influent and effluent [120]. The authors developed an approach for rapid and baseline separation of soluble Ag(I) from AgNP covering the 1 to 100 nm range. Proulx et al. [121] have also used chromatography coupled to single particle ICP-MS method for distinguishing Ag, Au and polystyrene NP spiked into naturally sampled river water. The hydrodynamic chromatography was able to remove much of the background signal due to environmental colloids and natural organic matter, allowing for a reasonable separation of the NP.

Although chromatography has been used to separate NP, the most widely used method to separate NP from complex matrixes is field-flow fractionation (FFF). AgNP with different coating agents could be separated from sandy and clay soils by FFF with in-line UV–vis spectroscopy used to detect the concentration of eluted particles and DLS to determine nanoparticle size

[122]. Poda et al. [123] developted and applicated an FFF–ICP-MS method for the separation and characterization of AgNP mixtures. The technique was also applied for biological media to characterize silver nanoparticles before and after exposure to the freshwater oligochaete, *Lumbriculus variegatus*. After exposure, the tissues were extracted and analyzed by FFF–ICP-MS. The size of the extracted AgNP increased from approximately 31 to 46 nm, indicating a significant change in the NP characteristics during exposure. The ability to discern particle size along with its composition further demonstrated the utility of this method for environmental applications.

The above mentioned techniques separate ENM from complex samples, but do not deeply characterize the biomolecules adsorbed onto their surface. While the assessment of the biomolecule interactions with ENM is becoming routine in medical and human toxicological analyses, much work is still needed in the environmental or ecological context. Some methods coming from biomedicine are normally used (see Table 2.1), demonstrating their suitability for characterizing environmental coronas. As a non-exhaustive list, Table 2.2 shows the most used techniques for PC isolation, separation, and identification, which, as proved by the articles reviewed before, are also suitable for eco-corona studies.

Table 2.2.- Techniques currently in use to study ENM corona and the Bio-Nano interface.

Analytical Methods for Corona Evaluation
▪ Centrifugation
▪ Field-Flow Fractionation (FFF)
▪ Column Chromatography
▪ Nanoparticle tracking analysis (NTA)
▪ Circular Dichroism
▪ Isothermal Titration Calorimetry
▪ SDS-PAGE
- Capillary Electrophoresis
- One-Dimensional Gel Electrophoresis
- Two-Dimensional Gel Electrophoresis
▪ UV–Visible Spectroscopy
▪ Fluorescence Spectroscopy
▪ Mass Spectrometry
▪ Fourier Transform Infrared and Raman Spectroscopies
▪ Nuclear Magnetic Resonance (NMR)
▪ Differential Centrifugation Sedimentation
▪ X-ray Photoelectron Spectroscopy (XPS).
▪ Electron and Atomic Force Microscopies.

In many cases, a direct observation of the Bio-Nano interface is required. Electron microscopy techniques such as Transmission electron microscopy (TEM) and Scanning electron microscope (SEM) provide very high resolution,

making them useful for observing the Bio-Nano interface. Numerous groups used TEM [14, 124, 125] (see Figure 2.5) or SEM [125-127] for studying the interaction of ENM on environmentally relevant organisms. Atomic Force Microscopy (AFM) has also been used to study ENM interactions with whole cells. Dorobantu et al. [128] successfully used AFM and acquired images of several prokaryotic and eukaryotic cells following exposure to AgNP. TEM, SEM and AFM images generally identify adsorbed nanoparticles on the cell surface and prove useful for demonstrating changes in cell morphology and membrane integrity following ENM exposure (TEM coupled with an energy-dispersive X-ray spectroscopy could determine potential metallic ENM internalization as well). Studying Bio-Nano interfaces is not a trivial task. The effort of researchers from different disciplines is required to deal with the numerous analytical problems that appear in the evaluation of real environmental samples. The application of the multiple analytical methodologies required for fully characterizing the Bio-Nano interface is frequently beyond the capabilities of individual laboratories, making collaborative research a need to understand this complex interface.

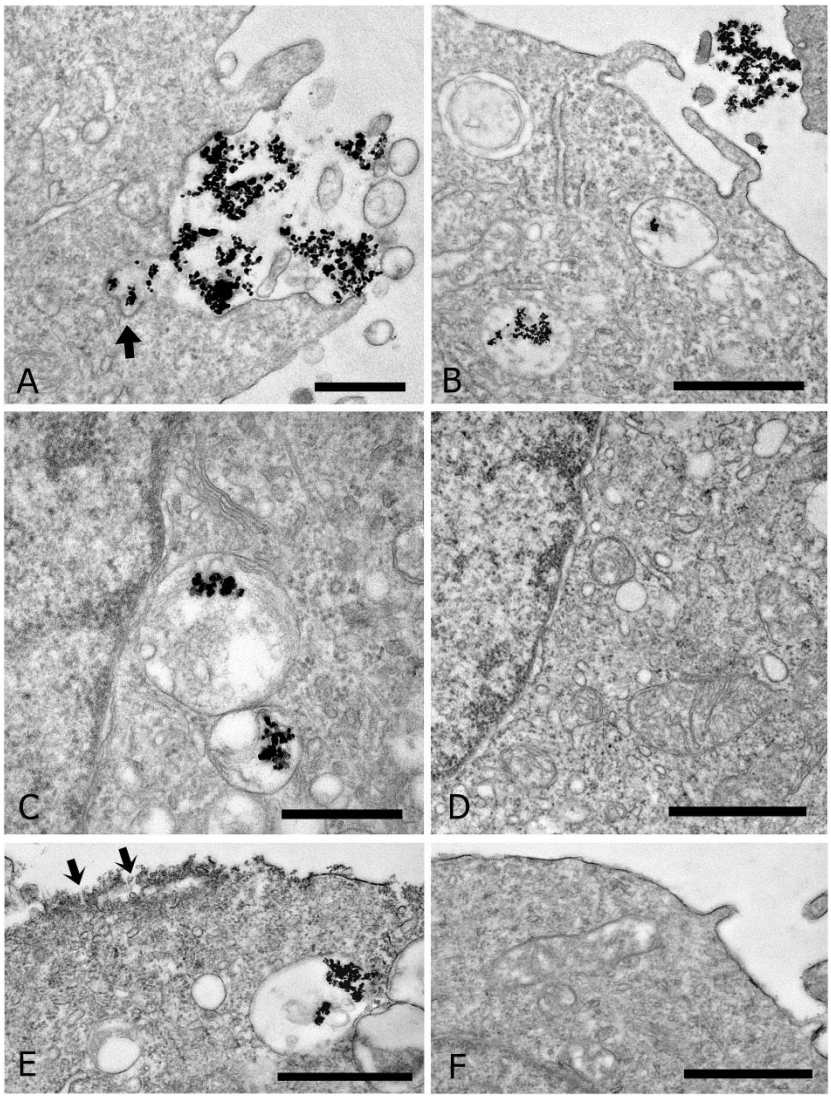

Figure 2.5.- Internalization of TiO_2 NP in a embryonic cell line of sea bass observed by TEM. Reprinted with permission from Picchietti, S., Bernini, C., Stocchi, V., Taddei, A. R., Meschini, R., Fausto, A. M., Rocco L., Buonocore F., Cervia D., & Scapigliati, G. (2017). Engineered nanoparticles of titanium dioxide (TIO 2): Uptake and biological effects in a sea bass cell line. Fish & Shellfish Immunology, 63, 53-67.

2.7 Critical opinion & research needed in the Bio-Nano interface field

The traditional assessment of the biological effects of ENM is not valid anymore. As discussed along this article, the ENM are affected by many physicochemical and biological transformations which endow ENM with new identities from the pristine or “as manufactured” materials. Therefore, a case-by-case approach to assess nanotoxicity is questionable due to the high volume of work required and the continuous advances of nanotechnology. It is necessary to consider not only the current diversity of ENM and the enormous variety of transformed ENM, but all the new ENM that are expected to come to market. High-throughput based-methods could rise as key strategies to fill current gaps in ENM knowledge. The work of Kaweeteerawat et al. [129] is a good example of what can be done and obtained using this approach. The authors analyzed a data set consisting of the toxicological response of *Escherichia coli* to a library of 24 metal oxide nanoparticles and identified the physicochemical drivers (ENM conduction band energy and metal ion hydration enthalpy) for the observed biological effect. An enormous ENM library as Chen et al. [130] developed, where a broad range of single and multimetallic NP made of different combinations of five different metals were synthesized, could be also used as reference materials for future toxicity and ecotoxicity studies to withdraw general toxicological descriptors.

The environmental transformation of ENM in the environment and the biological effects of transformed ENM is a research field requiring particular attention. Although some processes have been outlined during the last years, as covered in the ‘Transformation of ENM in the environment’ section, additional studies using realistic environmental conditions, which reflect the complexity of actual environmental systems, should be implemented. In this

sense, microcosm and mesocosm experiments, which mimic the environmental conditions in a given compartment, could help to study the evolution of pristine to transformed ENM and the resulting biological consequences. Recently, some recommendations and considerations regarding the exposure and design of mesocosm studies in the assessment of ENM environmental hazards have been listed [131]. Among them, controlling the aging of ENM along the mesocosm experiment is of vital importance. The aging process for which ENM could undergo further transformations is somewhat overlooked in the scientific literature and their effects might be underestimated. There is a need for establishing standard methods for aging ENM that provide useful information and also reproducibility among laboratories. Gubicza et al. [132] showed that coated gold nanoparticles grew during a long-time experiment from 2-5 nm to about 25 nm exhibiting drastic morphology changes from initial spherical type to different regular shapes such as bipyramid, decahedron, deca-tetrahedron, triangular plate and rod. Ellis et al. [133] studied the environmental fate and migration of AgNP by using static water 'microcosms' and highlighted the relevance of surface coating as well as water chemistry on the fate of AgNP. This basic microcosm approach, associated with the addition of different trophic organisms to the system, will help to study the behavior and fate of AgNP in a more realistic scenario. The huge variety of physicochemical variation that ENM face in the environment (namely tides and seasons) may enhance or even accelerate all these morphological and transformational changes described above.

More realistic scenarios imply the study of complex matrices. Though multiple ENM may exist jointly in product formulations, different ENM are rarely studied together [134]. Neither the mixture of NP and water pollutants has been frequently addressed [124, 135]. An interesting example has been

provided by Fries et al. [136] who studied the interaction of the antibiotic ciprofloxacin, TiO_2NP and NOM in an aqueous environment. Regarding the study of corona, an ideal scenario involved the understanding of how it is formed in the suspending medium, how it is modified in the vicinity of the cell surface (uptake surface), in blood or other biological liquids, and inside the tissues and cells (intracellular environment) [137]. More research is still needed to cover the existing knowledge gaps regarding the eco-corona formation and evolution in the environment as only a few articles addressed this topic (Table 2.1). Moreover, it is necessary to enlighten whether or not the eco-corona governs the interaction between ENM and cells and also to develop methods that allow characterizing ENM as a function of the eco-corona. Although this strategy was implemented for biomedical applications, the vision of grouping ENM [32] by their eco-corona might also be applied to environmental samples. A thorough characterizing of ENM eco-coronas would provide a mechanism of grouping and reading-across of ENM that could allow a further insight on predicting the fate and behavior of ENM in the environment. The characterization of samples containing very low concentration of NP with heterogeneous size distribution, as well as those susceptible to undergo dissolution or other transformations, is a challenging task for current analytical instruments. The implementation of improved methods to separate ENM from interfering colloidal species would facilitate a more accurate ENM characterization in complex matrices. Current methods also need to be adapted and new ones developed to generate consistent results for separation, detection and quantification of ENM at environmentally relevant concentrations. Moreover, it is necessary to implement more studies which use techniques that could characterize the corona as formed, given the fact that the current techniques to study the adsorbed biomolecules could

greatly alter the corona and induce some artifacts. Instruments for tracking ENM in situ or in vivo are lacking. Besides, the bioaccumulation of ENM through the trophic chain has seldom been examined due to the lack of suitable techniques. In this sense, methods such as the one proposed by Yang et al. [138] might open a new door in the in vivo quantification of ENM in single cells. The authors proposed a single-cell mass cytometry, a method coupling time-of-flight ICP-MS with flow cytometry, for the quantitative determination of ENM combined with multivariate phenotypic analysis. It would be interesting to know whether this technique may be applied with common single cell organisms used in toxicological studies such as *C. reinhardtii* or other unicellular entities.

Due to the high amount of money spent by national and international research agencies to study the impact of nanotechnology at all levels, the promotion of international collaboration should be a priority. In this regard, the discussions on global Environment, Health and Safety (EHS) research needs and challenges led to a joint initiative to create the EU-USA Communities of Research [137], which include voluntary activities of EU and US scientists to facilitate collaboration in nanosafety research. This could be a good scenario for collaborative research among groups from different disciplines as required by the study of Bio-Nano interface phenomena. Cooperative efforts involving different areas of expertise and background (physical, chemical, and biological sciences), are needed to provide fruitful interdisciplinarity and cross-fertilization.

2.8 References

[1] Flynn H. 2014. Nanotechnology update: corporations up their spending as revenues for nano-enabled products increase. *Lux research*.

[2] McWilliams A. 2010. Nanotechnology: a realistic market assessment. *BCC Research*.

[3] Vance ME, Kuiken T, Vejerano EP, McGinnis SP, Hochella Jr MF, Rejeski D, Hull MS. 2015. Nanotechnology in the real world: Redeveloping the nanomaterial consumer products inventory. *Beilstein journal of nanotechnology* 6:1769-1780.

[4] Stark W, Stoessel P, Wohlleben W, Hafner A. 2015. Industrial applications of nanoparticles. *Chemical Society reviews* 44:5793-5805.

[5] Maynard AD, Aitken RJ. 2016. 'Safe handling of nanotechnology' ten years on. *Nat Nano* 11:998-1000.

[6] Council NR. 2009. *Review of the Federal Strategy for Nanotechnology-Related Environmental, Health, and Safety Research*. National Academies Press.

[7] Council NR. 2012. *A research strategy for environmental, health, and safety aspects of engineered nanomaterials*. National Academies Press.

[8] Rasmussen K, González M, Kearns P, Sintes JR, Rossi F, Sayre P. 2016. Review of achievements of the OECD Working Party on Manufactured Nanomaterials' Testing and Assessment Programme. From exploratory testing to test guidelines. *Regulatory Toxicology and Pharmacology* 74:147-160.

[9] Nel AE, Madler L, Velegol D, Xia T, Hoek EM, Somasundaran P, Klaessig F, Castranova V, Thompson M. 2009. Understanding biophysicochemical interactions at the nano-bio interface. *Nature materials* 8:543-557.

[10] Verma A, Stellacci F. 2010. Effect of surface properties on nanoparticle–cell interactions. *Small* 6:12-21.

[11] Yeh Y-C, Creran B, Rotello VM. 2012. Gold nanoparticles: preparation, properties, and applications in bionanotechnology. *Nanoscale* 4:1871-1880.

[12] Satzer P, Svec F, Sekot G, Jungbauer A. 2015. Protein adsorption onto nanoparticles induces conformational changes: Particle size dependency, kinetics, and mechanisms. *Engineering in Life Sciences*.

[13] Huang R, Carney RP, Ikuma K, Stellacci F, Lau BL. 2014. Effects of surface compositional and structural heterogeneity on nanoparticle–protein interactions: different protein configurations. *ACS nano* 8:5402-5412.

[14] Pulido-Reyes G, Rodea-Palomares I, Das S, Sakthivel TS, Leganes F, Rosal R, Seal S, Fernández-Piñas F. 2015. Untangling the biological effects of cerium oxide nanoparticles: the role of surface valence states. *Scientific Reports* 5:15613.

[15] Badawy AME, Luxton TP, Silva RG, Scheckel KG, Suidan MT, Tolaymat TM. 2010. Impact of environmental conditions (pH, ionic strength, and electrolyte type) on the surface charge and aggregation of silver nanoparticles suspensions. *Environmental science & technology* 44:1260-1266.

[16] Bian S-W, Mudunkotuwa IA, Rupasinghe T, Grassian VH. 2011. Aggregation and dissolution of 4 nm ZnO nanoparticles in aqueous environments: influence of pH, ionic strength, size, and adsorption of humic acid. *Langmuir : the ACS journal of surfaces and colloids* 27:6059-6068.

[17] Sousa VS, Teixeira MR. 2013. Aggregation kinetics and surface charge of CuO nanoparticles: the influence of pH, ionic strength and humic acids. *Environmental Chemistry* 10:313-322.

[18] Gonzalo S, Llaneza V, Pulido-Reyes G, Fernandez-Pinas F, Bonzongo JC, Leganes F, Rosal R, Garcia-Calvo E, Rodea-Palomares I. 2014. A colloidal singularity reveals the crucial role of colloidal stability for nanomaterials in-vitro toxicity testing: nZVI-microalgae colloidal system as a case study. *PloS one* 9:e109645.

[19] Gunawan C, Teoh WY, Marquis CP, Amal R. 2011. Cytotoxic origin of copper (II) oxide nanoparticles: comparative studies with micron-sized particles, leachate, and metal salts. *ACS nano* 5:7214-7225.

[20] Zhang Y, Chen Y, Westerhoff P, Crittenden J. 2009. Impact of natural organic matter and divalent cations on the stability of aqueous nanoparticles. *Water research* 43:4249-4257.

[21] Gunsolus IL, Mousavi MP, Hussein K, Bühlmann P, Haynes CL. 2015. Effects of humic and fulvic acids on silver nanoparticle stability, dissolution, and toxicity. *Environmental science & technology* 49:8078-8086.

[22] Louie SM, Spielman-Sun ER, Small MJ, Tilton RD, Lowry GV. 2015. Correlation of the physicochemical properties of natural organic matter samples from different sources to their effects on gold nanoparticle aggregation in monovalent electrolyte. *Environmental science & technology* 49:2188-2198.

[23] Lynch I, Cedervall T, Lundqvist M, Cabaleiro-Lago C, Linse S, Dawson KA. 2007. The nanoparticle–protein complex as a biological entity; a complex fluids and surface science challenge for the 21st century. *Advances in colloid and interface science* 134:167-174.

[24] Kuruvilla J, Farinha AP, Bayat N, Cristobal S. 2017. Surface proteomics on nanoparticles: a step to simplify the rapid prototyping of nanoparticles. *Nanoscale Horizons* 2:55-64.

[25] Docter D, Strieth S, Westmeier D, Hayden O, Gao M, Knauer SK, Stauber RH. 2015. No king without a crown–impact of the nanomaterial-protein corona on nanobiomedicine. *Nanomedicine : nanotechnology, biology, and medicine* 10:503-519.

[26] Walkey CD, Olsen JB, Song F, Liu R, Guo H, Olsen DWH, Cohen Y, Emili A, Chan WC. 2014. Protein corona fingerprinting predicts the cellular interaction of gold and silver nanoparticles. *ACS nano* 8:2439-2455.

[27] Walkey CD, Chan WC. 2012. Understanding and controlling the interaction of nanomaterials with proteins in a physiological environment. *Chemical Society reviews* 41:2780-2799.

[28] Del Pino P, Pelaz B, Zhang Q, Maffre P, Nienhaus GU, Parak WJ. 2014. Protein corona formation around nanoparticles–from the past to the future. *Materials Horizons* 1:301-313.

[29] Treuel L, Brandholt S, Maffre P, Wiegele S, Shang L, Nienhaus GU. 2014. Impact of protein modification on the protein corona on nanoparticles and nanoparticle–cell interactions. *ACS nano* 8:503-513.

[30] Lynch I, Dawson KA. 2008. Protein-nanoparticle interactions. *Nano today* 3:40-47.

[31] Yang ST, Liu Y, Wang YW, Cao A. 2013. Biosafety and bioapplication of nanomaterials by designing protein–nanoparticle interactions. *Small* 9:1635-1653.

[32] Lynch I, Dawson K, Lead J, Valsami-Jones E. 2014. Macromolecular Coronas and their importance in Nanotoxicology and Nanoecotoxicology. *Frontiers of Nanoscience Elsevier, Amsterdam*.

[33] Sheng G-P, Yu H-Q, Li X-Y. 2010. Extracellular polymeric substances (EPS) of microbial aggregates in biological wastewater treatment systems: a review. *Biotechnology advances* 28:882-894.

[34] Grunér M, Kauscher U, Linder M, Monopoli M. 2016. An environmental route of exposure affects the formation of nanoparticle coronas in blood plasma. *Journal of proteomics* 137:52-58.

[35] Su R, Jin Y, Liu Y, Tong M, Kim H. 2013. Bactericidal activity of Ag-doped multi-walled carbon nanotubes and the effects of extracellular polymeric substances and natural organic matter. *Colloids and Surfaces B: Biointerfaces* 104:133-139.

[36] Zhou K, Hu Y, Zhang L, Yang K, Lin D. 2016. The role of exopolymeric substances in the bioaccumulation and toxicity of Ag nanoparticles to algae. *Scientific Reports* 6.

[37] Fu F, Dionysiou DD, Liu H. 2014. The use of zero-valent iron for groundwater remediation and wastewater treatment: a review. *Journal of hazardous materials* 267:194-205.

[38] Reinsch BC, Forsberg B, Penn RL, Kim CS, Lowry GV. 2010. Chemical transformations during aging of zerovalent iron nanoparticles in the presence of common groundwater dissolved constituents. *Environmental science & technology* 44:3455-3461.

[39] Auffan M, Achouak W, Rose J, Roncato M-A, Chanéac C, Waite DT, Masion A, Woicik JC, Wiesner MR, Bottero J-Y. 2008. Relation between the redox state of iron-based nanoparticles and their cytotoxicity toward Escherichia coli. *Environmental science & technology* 42:6730-6735.

[40] Ivask A, Juganson K, Bondarenko O, Mortimer M, Aruoja V, Kasemets K, Blinova I, Heinlaan M, Slaveykova V, Kahru A. 2014. Mechanisms of toxic action of Ag, ZnO and CuO nanoparticles to selected ecotoxicological test organisms and mammalian cells in vitro: a comparative review. *Nanotoxicology* 8:57-71.

[41] Notter DA, Mitrano DM, Nowack B. 2014. Are nanosized or dissolved metals more toxic in the environment? A meta-analysis. *Environmental toxicology and chemistry* 33:2733-2739.

[42] Mitrano DM, Motellier S, Clavaguera S, Nowack B. 2015. Review of nanomaterial aging and transformations through the life cycle of nano-enhanced products. *Environment international* 77:132-147.

[43] Yin Y, Yang X, Zhou X, Wang W, Yu S, Liu J, Jiang G. 2015. Water chemistry controlled aggregation and photo-transformation of silver nanoparticles in environmental waters. *Journal of Environmental Sciences* 34:116-125.

[44] Cheng Y, Yin L, Lin S, Wiesner M, Bernhardt E, Liu J. 2011. Toxicity reduction of polymer-stabilized silver nanoparticles by sunlight. *The Journal of Physical Chemistry C* 115:4425-4432.

[45] Hwang YS, Qu X, Li Q. 2013. The role of photochemical transformations in the aggregation and deposition of carboxylated multiwall carbon nanotubes suspended in water. *Carbon* 55:81-89.

[46] Hou W-C, He C-J, Wang Y-S, Wang DK, Zepp RG. 2016. Phototransformation-induced aggregation of functionalized single-walled carbon nanotubes: the importance of amorphous carbon. *Environmental science & technology* 50:3494-3502.

[47] Hou W-C, Stuart B, Howes R, Zepp RG. 2013. Sunlight-driven reduction of silver ions by natural organic matter: formation and transformation of silver nanoparticles. *Environmental science & technology* 47:7713-7721.

[48] Glover RD, Miller JM, Hutchison JE. 2011. Generation of metal nanoparticles from silver and copper objects: nanoparticle dynamics on surfaces and potential sources of nanoparticles in the environment. *ACS nano* 5:8950-8957.

[49] Kent RD, Oser JG, Vikesland PJ. 2014. Controlled evaluation of silver nanoparticle sulfidation in a full-scale wastewater treatment plant. *Environmental science & technology* 48:8564-8572.

[50] Lowry GV, Espinasse BP, Badireddy AR, Richardson CJ, Reinsch BC, Bryant LD, Bone AJ, Deonarine A, Chae S, Therezien M. 2012. Long-term transformation and fate of manufactured Ag nanoparticles in a simulated large scale freshwater emergent wetland. *Environmental science & technology* 46:7027-7036.

[51] Starnes DL, Unrine JM, Starnes CP, Collin BE, Oostveen EK, Ma R, Lowry GV, Bertsch PM, Tsyusko OV. 2015. Impact of sulfidation on the bioavailability and toxicity of silver nanoparticles to Caenorhabditis elegans. *Environmental pollution* 196:239-246.

[52] Devi GP, Ahmed KBA, Varsha MS, Shrijha B, Lal KS, Anbazhagan V, Thiagarajan R. 2015. Sulfidation of silver nanoparticle reduces its toxicity in zebrafish. *Aquatic toxicology* 158:149-156.

[53] Levard C, Hotze EM, Colman BP, Dale AL, Truong L, Yang X, Bone AJ, Brown Jr GE, Tanguay RL, Di Giulio RT. 2013. Sulfidation of silver nanoparticles: natural antidote to their toxicity. *Environmental science & technology* 47:13440-13448.

[54] Starnes DL, Lichtenberg SS, Unrine JM, Starnes CP, Oostveen EK, Lowry GV, Bertsch PM, Tsyusko OV. 2016. Distinct transcriptomic responses of Caenorhabditis elegans to pristine and sulfidized silver nanoparticles. *Environmental pollution* 213:314-321.

[55] Mitrano DM, Nowack B. 2017. The need for a life-cycle based aging paradigm for nanomaterials: importance of real-world test systems to identify realistic particle transformations. *Nanotechnology* 28:072001.

[56] Kirschling TL, Golas PL, Unrine JM, Matyjaszewski K, Gregory KB, Lowry GV, Tilton R, D. 2011. Microbial bioavailability of covalently bound polymer coatings on model engineered nanomaterials. *Environmental science & technology* 45:5253-5259.

[57] Parsons JG, Lopez ML, Gonzalez CM, Peralta-Videa JR, Gardea-Torresdey JL. 2010. Toxicity and biotransformation of uncoated and coated nickel hydroxide nanoparticles on mesquite plants. *Environmental toxicology and chemistry* 29:1146-1154.

[58] Yin L, Cheng Y, Espinasse B, Colman BP, Auffan M, Wiesner M, Rose J, Liu J, Bernhardt ES. 2011. More than the ions: the effects of silver nanoparticles on Lolium multiflorum. *Environmental science & technology* 45:2360-2367.

[59] Wang Z, Xie X, Zhao J, Liu X, Feng W, White JC, Xing B. 2012. Xylem- and phloem-based transport of CuO nanoparticles in maize (Zea mays L.). *Environmental science & technology* 46:4434-4441.

[60] Ma Y, He X, Zhang P, Zhang Z, Guo Z, Tai R, Xu Z, Zhang L, Ding Y, Zhao Y. 2011. Phytotoxicity and biotransformation of La2O3 nanoparticles in a terrestrial plant cucumber (Cucumis sativus). *Nanotoxicology* 5:743-753.

[61] Zhang P, Ma Y, Zhang Z, He X, Zhang J, Guo Z, Tai R, Zhao Y, Chai Z. 2012. Biotransformation of ceria nanoparticles in cucumber plants. *ACS nano* 6:9943-9950.

[62] Zhang P, Ma Y, Zhang Z, He X, Guo Z, Tai R, Ding Y, Zhao Y, Chai Z. 2012. Comparative toxicity of nanoparticulate/bulk Yb2O3 and YbCl3 to cucumber (Cucumis sativus). *Environmental science & technology* 46:1834-1841.

[63] Hernandez-Viezcas JA, Castillo-Michel H, Andrews JC, Cotte M, Rico C, Peralta-Videa JR, Ge Y, Priester JH, Holden PA, Gardea-Torresdey JL. 2013. In situ synchrotron X-ray fluorescence mapping and speciation of CeO2 and ZnO nanoparticles in soil cultivated soybean (Glycine max). *ACS nano* 7:1415-1423.

[64] Kotchey GP, Zhao Y, Kagan VE, Star A. 2013. Peroxidase-mediated biodegradation of carbon nanotubes in vitro and in vivo. *Advanced drug delivery reviews* 65:1921-1932.

[65] Russier J, Ménard-Moyon C, Venturelli E, Gravel E, Marcolongo G, Meneghetti M, Doris E, Bianco A. 2011. Oxidative biodegradation of single-and multi-walled carbon nanotubes. *Nanoscale* 3:893-896.

[66] Lu N, Li J, Tian R, Peng Y-Y. 2014. Binding of human serum albumin to single-walled carbon nanotubes activated neutrophils to increase production of hypochlorous acid, the oxidant capable of degrading nanotubes. *Chemical research in toxicology* 27:1070-1077.

[67] Bhattacharya K, Mukherjee SP, Gallud A, Burkert SC, Bistarelli S, Bellucci S, Bottini M, Star A, Fadeel B. 2016. Biological interactions of carbon-based nanomaterials: from coronation to degradation. *Nanomedicine: Nanotechnology, Biology and Medicine* 12:333-351.

[68] Lalwani G, Xing W, Sitharaman B. 2014. Enzymatic degradation of oxidized and reduced graphene nanoribbons by lignin peroxidase. *Journal of Materials Chemistry B* 2:6354-6362.

[69] Liu L, Zhu C, Fan M, Chen C, Huang Y, Hao Q, Yang J, Wang H, Sun D. 2015. Oxidation and degradation of graphitic materials by naphthalene-degrading bacteria. *Nanoscale* 7:13619-13628.

[70] Zhang L, Petersen EJ, Habteselassie MY, Mao L, Huang Q. 2013. Degradation of multiwall carbon nanotubes by bacteria. *Environmental pollution* 181:335-339.

[71] Berry TD, Filley TR, Clavijo AP, Bischoff Gray M, Turco R. 2017. Degradation and microbial uptake of C60 fullerols in contrasting agricultural soils. *Environmental science & technology* 51:1387-1394.

[72] Parks AN, Chandler GT, Ho KT, Burgess RM, Ferguson PL. 2015. Environmental biodegradability of [14C] single-walled carbon nanotubes by Trametes versicolor and natural microbial cultures found in New Bedford Harbor sediment and aerated wastewater treatment plant sludge. *Environmental Toxicology and Chemistry* 34:247-251.

[73] Montes MO, Hanna SK, Lenihan HS, Keller AA. 2012. Uptake, accumulation, and biotransformation of metal oxide nanoparticles by a marine suspension-feeder. *Journal of hazardous materials* 225:139-145.

[74] Gonzalez-Moragas L, Yu S-M, Carenza E, Laromaine A, Roig A. 2015. Protective Effects of Bovine Serum Albumin on Superparamagnetic Iron Oxide Nanoparticles Evaluated in the Nematode Caenorhabditis elegans. *ACS Biomaterials Science & Engineering* 1:1129-1138.

[75] Yu S-M, Gonzalez-Moragas L, Milla M, Kolovou A, Santarella-Mellwig R, Schwab Y, Laromaine A, Roig A. 2016. Bio-identity and fate of albumin-coated SPIONs evaluated in cells and by the C. elegans model. *Acta biomaterialia* 43:348-357.

[76] Khan SA, Ahmad A. 2013. Phase, size and shape transformation by fungal biotransformation of bulk TiO 2. *Chemical engineering journal* 230:367-371.

[77] Lombi E, Donner E, Taheri S, Tavakkoli E, Jämting ÅK, McClure S, Naidu R, Miller BW, Scheckel KG, Vasilev K. 2013. Transformation of four silver/silver

chloride nanoparticles during anaerobic treatment of wastewater and post-processing of sewage sludge. *Environmental pollution* 176:193-197.

[78] Lin J, Zhang H, Chen Z, Zheng Y. 2010. Penetration of lipid membranes by gold nanoparticles: insights into cellular uptake, cytotoxicity, and their relationship. *ACS nano* 4:5421-5429.

[79] Bonnaud C, Monnier CA, Demurtas D, Jud C, Vanhecke D, Montet X, Hovius R, Lattuada M, Rothen-Rutishauser B, Petri-Fink A. 2014. Insertion of nanoparticle clusters into vesicle bilayers. *ACS nano* 8:3451-3460.

[80] Guo Y, Terazzi E, Seemann R, Fleury JB, Baulin VA. 2016. Direct proof of spontaneous translocation of lipid-covered hydrophobic nanoparticles through a phospholipid bilayer. *Science Advances* 2:e1600261.

[81] Jacobson KH, Gunsolus IL, Kuech TR, Troiano JM, Melby ES, Lohse SE, Hu D, Chrisler WB, Murphy CJ, Orr G. 2015. Lipopolysaccharide density and structure govern the extent and distance of nanoparticle interaction with actual and model bacterial outer membranes. *Environmental science & technology* 49:10642-10650.

[82] Bannunah AM, Vllasaliu D, Lord J, Stolnik S. 2014. Mechanisms of nanoparticle internalization and transport across an intestinal epithelial cell model: effect of size and surface charge. *Molecular pharmaceutics* 11:4363-4373.

[83] Gonzalez-Rodriguez D, Barakat AI. 2015. Dynamics of receptor-mediated nanoparticle internalization into endothelial cells. *PloS one* 10:e0122097.

[84] Gottstein C, Wu G, Wong BJ, Zasadzinski JA. 2013. Precise quantification of nanoparticle internalization. *ACS nano* 7:4933-4945.

[85] Zhu M, Nie G, Meng H, Xia T, Nel A, Zhao Y. 2012. Physicochemical properties determine nanomaterial cellular uptake, transport, and fate. *Accounts of chemical research* 46:622-631.

[86] Huang K, Ma H, Liu J, Huo S, Kumar A, Wei T, Zhang X, Jin S, Gan Y, Wang PC. 2012. Size-dependent localization and penetration of ultrasmall gold

nanoparticles in cancer cells, multicellular spheroids, and tumors in vivo. *ACS nano* 6:4483-4493.

[87] Wang Z, Li J, Zhao J, Xing B. 2011. Toxicity and internalization of CuO nanoparticles to prokaryotic alga Microcystis aeruginosa as affected by dissolved organic matter. *Environmental science & technology* 45:6032-6040.

[88] Yue Y, Li X, Sigg L, Suter MJ, Pillai S, Behra R, Schirmer K. 2017. Interaction of silver nanoparticles with algae and fish cells: a side by side comparison. *Journal of nanobiotechnology* 15:16.

[89] Ma S, Lin D. 2013. The biophysicochemical interactions at the interfaces between nanoparticles and aquatic organisms: adsorption and internalization. *Environmental Science: Processes & Impacts* 15:145-160.

[90] Navarro E, Baun A, Behra R, Hartmann NB, Filser J, Miao A-J, Quigg A, Santschi PH, Sigg L. 2008. Environmental behavior and ecotoxicity of engineered nanoparticles to algae, plants, and fungi. *Ecotoxicology* 17:372-386.

[91] Wang Y, Miao A-J, Luo J, Wei Z-B, Zhu J-J, Yang L-Y. 2013. Bioaccumulation of CdTe quantum dots in a freshwater alga Ochromonas danica: a kinetics study. *Environmental science & technology* 47:10601-10610.

[92] Hoepflinger MC, Hoeftberger M, Sommer A, Hametner C, Foissner I. 2017. Clathrin in Chara australis: Molecular Analysis and Involvement in Charasome Degradation and Constitutive Endocytosis. *Frontiers in plant science* 8.

[93] Merchant SS, Prochnik SE, Vallon O, Harris EH, Karpowicz SJ, Witman GB, Terry A, Salamov A, Fritz-Laylin LK, Maréchal-Drouard L. 2007. The Chlamydomonas genome reveals the evolution of key animal and plant functions. *Science* 318:245-250.

[94] http://www.genome.jp/kegg-bin/show_pathway?cre04144. Endocytosis - Chlamydomonas reinhardtii.

[95] Domingos RF, Simon DF, Hauser C, Wilkinson KJ. 2011. Bioaccumulation and effects of CdTe/CdS quantum dots on Chlamydomonas

reinhardtii–nanoparticles or the free ions? *Environmental science & technology* 45:7664-7669.

[96] Taylor NS, Merrifield R, Williams TD, Chipman JK, Lead JR, Viant MR. 2015. Molecular toxicity of cerium oxide nanoparticles to the freshwater alga Chlamydomonas reinhardtii is associated with supra-environmental exposure concentrations. *Nanotoxicology*:1-10.

[97] Wang S, Lv J, Ma J, Zhang S. 2016. Cellular internalization and intracellular biotransformation of silver nanoparticles in Chlamydomonas reinhardtii. *Nanotoxicology* 10:1129-1135.

[98] Gonzalo S, Rodea-Palomares I, Leganes F, Garcia-Calvo E, Rosal R, Fernandez-Pinas F. 2014. First evidences of PAMAM dendrimer internalization in microorganisms of environmental relevance: A linkage with toxicity and oxidative stress. *Nanotoxicology*:1-13.

[99] Perreault F, Oukarroum A, Melegari SP, Matias WG, Popovic R. 2012. Polymer coating of copper oxide nanoparticles increases nanoparticles uptake and toxicity in the green alga Chlamydomonas reinhardtii. *Chemosphere* 87:1388-1394.

[100] Tenzer S, Docter D, Kuharev J, Musyanovych A, Fetz V, Hecht R, Schlenk F, Fischer D, Kiouptsi K, Reinhardt C. 2013. Rapid formation of plasma protein corona critically affects nanoparticle pathophysiology. *Nature nanotechnology* 8:772-781.

[101] Docter D, Bantz C, Westmeier D, Galla HJ, Wang Q, Kirkpatrick JC, Nielsen P, Maskos M, Stauber RH. 2014. The protein corona protects against size-and dose-dependent toxicity of amorphous silica nanoparticles. *Beilstein journal of nanotechnology* 5:1380-1392.

[102] Yin H, Chen R, Casey PS, Ke PC, Davis TP, Chen C. 2015. Reducing the cytotoxicity of ZnO nanoparticles by a pre-formed protein corona in a supplemented cell culture medium. *RSC Advances* 5:73963-73973.

[103] Fabrega J, Fawcett SR, Renshaw JC, Lead JR. 2009. Silver nanoparticle impact on bacterial growth: effect of pH, concentration, and organic matter. *Environmental science & technology* 43:7285-7290.

[104] Yang X, Jiang C, Hsu-Kim H, Badireddy AR, Dykstra M, Wiesner M, Hinton DE, Meyer JN. 2014. Silver nanoparticle behavior, uptake, and toxicity in Caenorhabditis elegans: effects of natural organic matter. *Environmental science & technology* 48:3486-3495.

[105] Wirth SM, Lowry GV, Tilton RD. 2012. Natural organic matter alters biofilm tolerance to silver nanoparticles and dissolved silver. *Environmental science & technology* 46:12687-12696.

[106] Li D, Lyon DY, Li Q, Alvarez PJ. 2008. Effect of soil sorption and aquatic natural organic matter on the antibacterial activity of a fullerene water suspension. *Environmental Toxicology and Chemistry* 27:1888-1894.

[107] Deng ZJ, Liang M, Monteiro M, Toth I, Minchin RF. 2011. Nanoparticle-induced unfolding of fibrinogen promotes Mac-1 receptor activation and inflammation. *Nature nanotechnology* 6:39-44.

[108] Gheshlaghi ZN, Riazi GH, Ahmadian S, Ghafari M, Mahinpour R. 2008. Toxicity and interaction of titanium dioxide nanoparticles with microtubule protein. *Acta biochimica et biophysica Sinica* 40:777-782.

[109] Mahmoudi M, Shokrgozar MA, Sardari S, Moghadam MK, Vali H, Laurent S, Stroeve P. 2011. Irreversible changes in protein conformation due to interaction with superparamagnetic iron oxide nanoparticles. *Nanoscale* 3:1127-1138.

[110] Fabrega J, Renshaw JC, Lead JR. 2009. Interactions of silver nanoparticles with Pseudomonas putida biofilms. *Environmental science & technology* 43:9004-9009.

[111] Lundqvist M, Stigler J, Cedervall T, Berggård T, Flanagan MB, Lynch I, Elia G, Dawson K. 2011. The evolution of the protein corona around nanoparticles: a test study. *ACS nano* 5:7503-7509.

[112] Hadjidemetriou M, Al-Ahmady Z, Kostarelos K. 2016. Time-evolution of in vivo protein corona onto blood-circulating PEGylated liposomal doxorubicin (DOXIL) nanoparticles. *Nanoscale* 8:6948-6957.

[113] Albanese A, Walkey CD, Olsen JB, Guo H, Emili A, Chan WC. 2014. Secreted biomolecules alter the biological identity and cellular interactions of nanoparticles. *ACS nano* 8:5515-5526.

[114] Bone AJ, Colman BP, Gondikas AP, Newton KM, Harrold KH, Cory RM, Unrine JM, Klaine SJ, Matson CW, Di Giulio RT. 2012. Biotic and abiotic interactions in aquatic microcosms determine fate and toxicity of Ag nanoparticles: part 2–toxicity and Ag speciation. *Environmental science & technology* 46:6925-6933.

[115] Unrine JM, Colman BP, Bone AJ, Gondikas AP, Matson CW. 2012. Biotic and abiotic interactions in aquatic microcosms determine fate and toxicity of Ag nanoparticles. Part 1. Aggregation and dissolution. *Environmental science & technology* 46:6915-6924.

[116] Hayashi Y, Miclaus T, Scavenius C, Kwiatkowska K, Sobota A, Engelmann P, Scott-Fordsmand JJ, Enghild JJ, Sutherland DS. 2013. Species differences take shape at nanoparticles: protein corona made of the native repertoire assists cellular interaction. *Environmental science & technology* 47:14367-14375.

[117] Hayashi Y, Miclaus T, Murugadoss S, Takamiya M, Scavenius C, Kjaer-Sorensen K, Enghild JJ, Strähle U, Oxvig C, Weiss C. 2017. Female versus male biological identities of nanoparticles determine the interaction with immune cells in fish. *Environmental Science: Nano* 4:895-906.

[118] Canesi L, Ciacci C, Fabbri R, Balbi T, Salis A, Damonte G, Cortese K, Caratto V, Monopoli MP, Dawson K. 2016. Interactions of cationic polystyrene nanoparticles with marine bivalve hemocytes in a physiological environment: Role of soluble hemolymph proteins. *Environmental research* 150:73-81.

[119] Nasser F, Lynch I. 2016. Secreted protein eco-corona mediates uptake and impacts of polystyrene nanoparticles on Daphnia magna. *Journal of proteomics* 137:45-51.

[120] Zhou X-X, Liu R, Liu J-F. 2014. Rapid chromatographic separation of dissoluble Ag (I) and silver-containing nanoparticles of 1–100 nanometer in antibacterial products and environmental waters. *Environmental science & technology* 48:14516-14524.

[121] Proulx K, Wilkinson KJ. 2014. Separation, detection and characterisation of engineered nanoparticles in natural waters using hydrodynamic chromatography and multi-method detection (light scattering, analytical ultracentrifugation and single particle ICP-MS). *Environmental Chemistry* 11:392-401.

[122] Koopmans G, Hiemstra T, Regelink I, Molleman B, Comans R. 2015. Asymmetric flow field-flow fractionation of manufactured silver nanoparticles spiked into soil solution. *Journal of Chromatography A* 1392:100-109.

[123] Poda A, Bednar A, Kennedy A, Harmon A, Hull M, Mitrano D, Ranville J, Steevens J. 2011. Characterization of silver nanoparticles using flow-field flow fractionation interfaced to inductively coupled plasma mass spectrometry. *Journal of Chromatography A* 1218:4219-4225.

[124] Martín-de-Lucía I, Campos-Mañas MC, Agüera A, Rodea-Palomares I, Pulido-Reyes G, Leganés F, Fernández-Piñas F, Rosal R. 2017. Reverse Trojan-horse effect decreased wastewater toxicity in the presence of inorganic nanoparticles. *Environmental Science: Nano*.

[125] Picchietti S, Bernini C, Stocchi V, Taddei A, Meschini R, Fausto A, Rocco L, Buonocore F, Cervia D, Scapigliati G. 2017. Engineered nanoparticles of titanium dioxide (TIO 2): Uptake and biological effects in a sea bass cell line. *Fish & Shellfish Immunology* 63:53-67.

[126] Zhao J, Cao X, Liu X, Wang Z, Zhang C, White JC, Xing B. 2016. Interactions of CuO nanoparticles with the algae Chlorella pyrenoidosa: adhesion, uptake, and toxicity. *Nanotoxicology* 10:1297-1305.

[127] Wang Z, Li J, Zhao J, Xing B. 2011. Toxicity and internalization of CuO nanoparticles to prokaryotic alga Microcystis aeruginosa as affected by dissolved organic matter. *Environmental science & technology* 45:6032-6040.

[128] Dorobantu LS, Fallone C, Noble AJ, Veinot J, Ma G, Goss GG, Burrell RE. 2015. Toxicity of silver nanoparticles against bacteria, yeast, and algae. *Journal of Nanoparticle Research* 17:172.

[129] Kaweeteerawat C, Ivask A, Liu R, Zhang H, Chang CH, Low-Kam C, Fischer H, Ji Z, Pokhrel S, Cohen Y. 2015. Toxicity of metal oxide nanoparticles in Escherichia coli correlates with conduction band and hydration energies. *Environmental science & technology* 49:1105-1112.

[130] Chen P-C, Liu X, Hedrick JL, Xie Z, Wang S, Lin Q-Y, Hersam MC, Dravid VP, Mirkin CA. 2016. Polyelemental nanoparticle libraries. *Science* 352:1565-1569.

[131] Holden PA, Gardea-Torresdey JL, Klaessig F, Turco RF, Mortimer M, Hund-Rinke K, Cohen Hubal EA, Avery D, Barceló D, Behra R. 2016. Considerations of environmentally relevant test conditions for improved evaluation of ecological hazards of engineered nanomaterials. *Environmental science & technology* 50:6124-6145.

[132] Gubicza J, Labar JL, Quynh LM, Nam NH, Luong NH. 2013. Evolution of size and shape of gold nanoparticles during long-time aging. *Materials Chemistry and Physics* 138:449-453.

[133] Ellis L-JA, Valsami-Jones E, Lead JR, Baalousha M. 2016. Impact of surface coating and environmental conditions on the fate and transport of silver nanoparticles in the aquatic environment. *Science of The Total Environment* 568:95-106.

[134] Zou X, Shi J, Zhang H. 2014. Coexistence of silver and titanium dioxide nanoparticles: enhancing or reducing environmental risks? *Aquatic toxicology* 154:168-175.

[135] Canesi L, Frenzilli G, Balbi T, Bernardeschi M, Ciacci C, Corsolini S, Della Torre C, Fabbri R, Faleri C, Focardi S. 2014. Interactive effects of n-TiO 2 and 2, 3, 7, 8-TCDD on the marine bivalve Mytilus galloprovincialis. *Aquatic toxicology* 153:53-65.

[136] Fries E, Crouzet C, Michel C, Togola A. 2016. Interactions of ciprofloxacin (CIP), titanium dioxide (TiO 2) nanoparticles and natural organic matter (NOM) in aqueous suspensions. *Science of the Total Environment* 563:971-976.

[137] Selck H, Handy RD, Fernandes TF, Klaine SJ, Petersen EJ. 2016. Nanomaterials in the aquatic environment: A European Union–United States perspective on the status of ecotoxicity testing, research priorities, and challenges ahead. *Environmental Toxicology and Chemistry* 35:1055-1067.

[138] Yang Y-SS, Atukorale PU, Moynihan KD, Bekdemir A, Rakhra K, Tang L, Stellacci F, Irvine DJ. 2017. High-throughput quantitation of inorganic nanoparticle biodistribution at the single-cell level using mass cytometry. *Nature communications* 8:14069.

CHAPTER 3

UNTANGLING THE BIOLOGICAL EFFECTS OF CERIUM OXIDE NANOPARTICLES: THE ROLE OF SURFACE VALENCE STATES

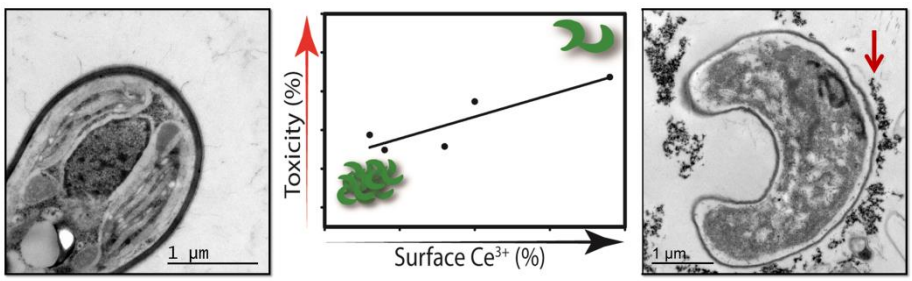

CHAPTER 3. UNTANGLING THE BIOLOGICAL EFFECTS OF CERIUM OXIDE NANOPARTICLES: THE ROLE OF SURFACE VALENCE STATES

3.1 Abstract

Cerium oxide nanoparticles (nanoceria; CNPs) have been found to have both pro-oxidant and anti-oxidant effects on different cell systems or organisms. In order to untangle the mechanisms which underlie the biological activity of nanoceria, we have studied the effect of five different CNPs on a model relevant aquatic microorganism. Neither shape, concentration, synthesis method, surface charge (ζ-potential), nor nominal size had any influence in the observed biological activity. The main driver of toxicity was found to be the percentage of surface content of Ce^{3+} sites: CNP1 (58%) and CNP5 (40%) were found to be toxic whereas CNP2 (28%), CNP3 (36%) and CNP4 (26%) were found to be non-toxic. The colloidal stability and redox chemistry of the most and least toxic CNPs, CNP1 and CNP2, respectively, were modified by incubation with iron and phosphate buffers. Blocking surface Ce^{3+} sites of the most toxic CNP, CNP1, with phosphate treatment reverted toxicity and stimulated growth. Colloidal destabilization with Fe treatment only increased toxicity of CNP1. The results of this study are relevant in the understanding of the main drivers of biological activity of nanoceria and to define global descriptors of engineered nanoparticles (ENPs) bioactivity which may be useful in safer-by-design strategies of nanomaterials.

3.2 Introduction

Cerium (Ce) is a rare-earth element which belongs to the lanthanide series. In solution Ce may exist as Ce^{3+} and Ce^{4+} and depending on environmental conditions can cycle between both oxidation states [1]. Ce may also exist as oxide form, CeO_2, which has been used widely as glass polishing [2] and is used as fertilizer in Chinese agriculture for crop improvement [3]. As a further advance in Ce applications, nanoceria or cerium oxide nanoparticles (CNPs) are gaining interest in many industrial fields [4-6], in plants to increase photosynthesis *via* suppression of reactive oxygen species (ROS) [7]; also as an antioxidant, there are a number of reports in biomedicine concerning the protective effects of nanoceria in certain neurological disorders [8]; to provide cells protection from radiation[9] and to be cytotoxic to cancer cells [10].

Although nanoceria shares similar physicochemical properties with bulk cerium, nanoceria has a large number of point surface defects [11] which correspond mainly to oxygen vacancies at the surface of the nanoparticle lattice [12]. These defects explain the autocatalytic properties of nanoceria, Esch et al [13] determined that Ce^{3+} atoms occupy the center of the oxygen vacancies surrounded by Ce^{4+} atoms. This particular configuration seems to underlie the unique redox-chemistry of nanoceria which is able to switch oxidation states between Ce^{3+} and Ce^{4+} depending on the prevailing environmental conditions [14]. This reduction/oxidation behavior is responsible for the observed antioxidant properties of nanoceria. It has been found that nanoceria displays superoxide-dismutase mimetic activity [15], catalase mimetic activity [16] or the capacity to scavenge nitric oxide radicals [17]. These antioxidant activities have been shown to depend on the Ce^{3+}/Ce^{4+} ratio at the particle surface. In this regard, it has been reported that exposure

of CNPs to phosphate shifted the redox state and altered their catalytic properties *in* vitro [18, 19].

On the other side of the coin, nanoceria has also been found to display oxidase activities [20] and to generate damaging oxygen radicals in a range of organisms and cell systems [14, 21-26].

Besides cerium valence states at the surfaces of CNPs, there are a number of factors which may influence CNPs interaction and thus biological effects on living cells. In this regard, a deep understanding of the colloidal chemistry of nanoceria (ζ-potential, solution pH, use of dispersants, particle size, *etc*.) in the tested biological media is of outmost relevance, processes such as aggregation/agglomeration have been found to modulate the toxicity of CNPs in aquatic organisms [24, 25, 27-29]. Another relevant factor could be the dissolution of free Ce^{3+} in CNPs suspensions, although most studies have found that this phenomenon in most biological media is almost negligible and given the low intrinsic toxicity of Ce^{3+} does not account for the observed toxicity of nanoceria [24, 25, 27, 29]. CNPs internalization has been found to be an issue mostly in human cell lines [10], however, in environmentally relevant organisms such as microalgae, no cell internalization has been reported [25, 28, 29].

As there are so many contradicting reports regarding the effects of nanoceria and so many factors which may contribute to the biological effects, the aim of this study was to perform a thorough study of the effect of five different CNPs in an effort to untangle the mechanisms which underlie the biological activity of nanoceria. The study was performed on a model aquatic microorganism, the green alga *Pseudokirchneriella subcapitata*.

The tested nanoceria have defined percentages of surface content of Ce^{3+} sites, they show distinct morphologies (spheres, rods or cubes) and different nominal sizes. In addition, they were synthesized by two different methods. Furthermore, to get deeper insights into the biological mechanisms of CNPs, the colloidal stability and redox chemistry of the most and least toxic CNPs were modified and the effect of these modifications on the model organism were tested.

3.3 Results

3.3.1 Physicochemical characterization of CNPs

The different CNPs were synthesized by two different methods and with varying % surface Ce^{3+}, morphology and sizes. Fig. 3.1a-e show particle sizes and shapes of all CNPs as observed by Transmission Electron Microscopy (TEM). CNP1, CNP2 and CNP5 had spheres shape with diameters approximately of 5, 7 and 18 nm, respectively. CNP3 had rod shape (350 nm long with a width of 20 nm) and CNP4 had cubic shape with a particle size around 50 nm. Fig. 3.1f-j show selected area electron diffraction (SAED) patterns which confirm the crystalline nature and fluorite structure of the nanoparticles. A(111), B(200), C(220) and D(311) in SAED correspond to the different lattice planes of fluorite crystal structure. Fig. 3.1k-o show the hydrodynamic sizes of all CNPs in ddH_2O. As can be seen in the figure, hydrodynamic size ranged from 20 to 350 nm, depending on morphology. The deconvoluted Ce (3d) XPS spectra of all CNPs are also shown in Fig. 3.1p-t. CNP1 had the highest % surface Ce^{3+} (58%) followed by CNP5 (40%), CNP3 (36%), CNP2 (28%) and CNP4 (26%). Fig. 3.1u-y illustrate UV-visible

absorbance spectra of CNPs. Absorbance spectra fluctuated depending on the % surface content of Ce^{3+} and Ce^{4+} of each nanoparticle[30]. A strong absorption at 250 nm was observed in CNP1, which is directly related to Ce^{3+} [31]. The other CNPs (CNP2-5) had a maximum of absorption at 298 nm, indicative of their higher Ce^{4+} content.

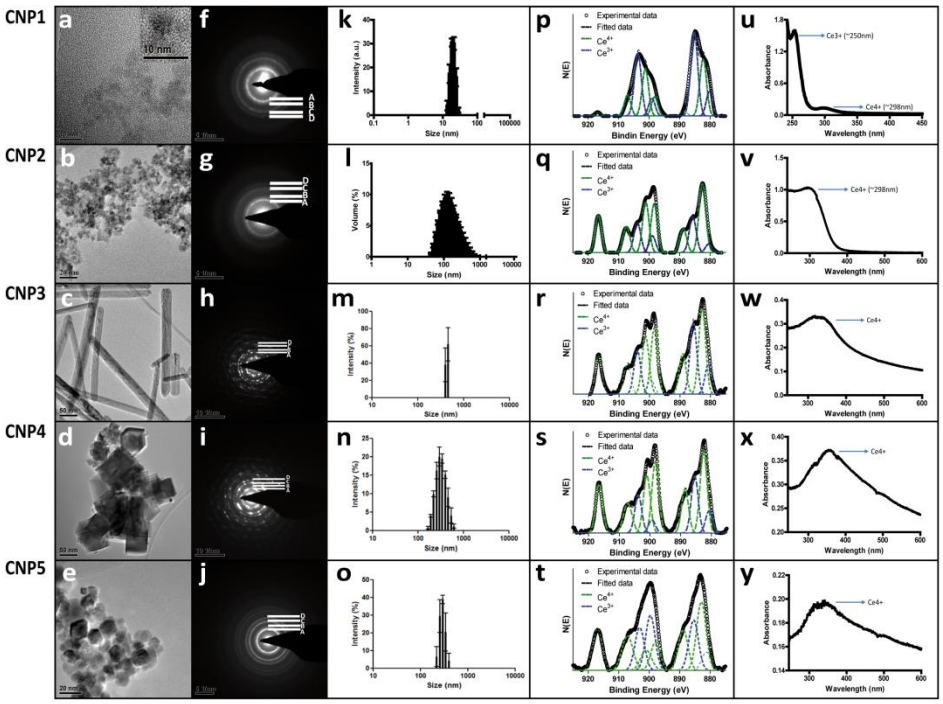

Figure 3.1.- Characterization of synthesized CNPs. a-e photographs show TEM images of the five CNPs (inset on CNP1: high magnification image). f-j show selected areas of electron diffraction pattern of CNPs (different crystal planes of fluorite crystal structure). k-o graphs represent the nanoparticle hydrodynamic radius. p-t images show deconvoluted XPS spectra of all CNPs. The UV−vis absorption spectra of CNPs suspension is represented in u-y.

Table 3.1 shows the physicochemical characteristics of the five CNPs at 10 mg/L suspended in either ddH_2O or OECD algal exposure medium. Measured ζ-potential values of CNP1, CNP2, CNP3, and CNP5 in ddH_2O were positive with the exception of CNP4 which showed a high negative value. However, when the CNPs were suspended in OECD algal medium, there was a shift to negative values for CNP1, CNP2, CNP3, and CNP5. CNP1 (-12.2 mV) had the lowest absolute values of all samples (near to neutrality) indicating a less stable suspension as compared to the other tested CNPs. The other CNPs had more negative values, around -22 mV which indicated that they were stably dispersed [32, 33].

Table 3.1.- Physicochemical properties of the five tested Cerium Oxide Nanoparticles (CNPs). See Figure 3.1 for more details.

				ddH_2O	**OECD medium**	
Sample Name	**% Ce^{3+}**	**Morphology**	**Size from HRTEM (nm)**	**ζ-potential (mV)**	**ζ-potential (mV)**	**ED* (nm)**
CNP1	58	spheres	≈5	18.1±0.7	-12.2 ± 0.6	793.8
CNP2	28	spheres	≈7	30.2±1.5	-25.6 ± 2.5	298.5
CNP3	36	rod	>50	22.8±0.72	-21.2 ± 0.8	511.6
CNP4	26	cube	≈50	-28.7±1.25	-24.4 ± 1.0	256.1
CNP5	40	spheres	≈18	28.3±0.59	-21.1 ± 1.0	286.9

*ED: Effective diameter;

Furthermore, it is worth noticing that CNPs appeared aggregated in OECD medium with higher sizes than in ddH_2O, a phenomenon frequently found in the literature due to the complexity and usually high conductivity of most culture media [25, 28, 29]. According to DLS measurements, the effective diameters were between 250–795 nm (see Table 3.1). CNP1 had the largest effective diameter indicating increased agglomeration/aggregation under these conditions which is in agreement with a less stable suspension as stated above.

Spontaneous cerium dissolution in the exposure media was tested for all CNPs by performing ICP-MS analyses of ultrafiltrated samples. The results indicated negligible (<0.0008 mg/L for 10 mg/L of each tested CNP; Supplementary Table S3.1) amounts of dissolved Ce in OECD medium.

3.3.2 Toxicity of the CNPs towards *P. subcapitata*

The effect of the CNPs on growth of *P. subcapitata* was assessed by measuring *in-vivo* fluorescence of chlorophyll [32]. Results of exposure to the five CNPs in the concentration range of 1 to 50 mg/L are shown in Figure 3.2. Growth inhibition significantly ($p<0.05$) increased with concentrations higher than 1 mg/L for CNP1 and 5 mg/L for CNP5. But, while the highest algal growth inhibition produced by CNP5 was approximately 30% at 50 mg/L, CNP1 reached a maximum growth inhibition of near 65% at the same concentration. In contrast, the growth of *P. subcapitata* was not affected significantly by CNP2, CNP3 and CNP4 exposure, even at the highest concentration tested (50 mg/L). Interestingly, CNP2 and CNP3 statistically ($p<0.05$) stimulated the growth of *P. subcapitata* at a concentration of 10 mg/L. In conclusion, from the five tested CNPs, only CNP1 and CNP5 caused algal growth inhibition, with CNP1 as the most toxic cerium oxide nanoparticle. For none of these CNPs,

dissolved free Ce^{3+} explained the observed toxicity as the concentrations found by ICP-MS did not exert any toxic effect (Supplementary Figure S3.1).

From the data in Table 3.1 and those in Figure 3.2, it appears that some particle properties, such as % surface Ce^{3+}, ζ-potential or effective diameter may probably correlate with toxicity, but other parameters such as nominal size or shape might also be involved. Thus, correlation analyses were performed in order to identify which physicochemical property of the tested CNPs, if any, might explain the observed biological effects. Nominal size,

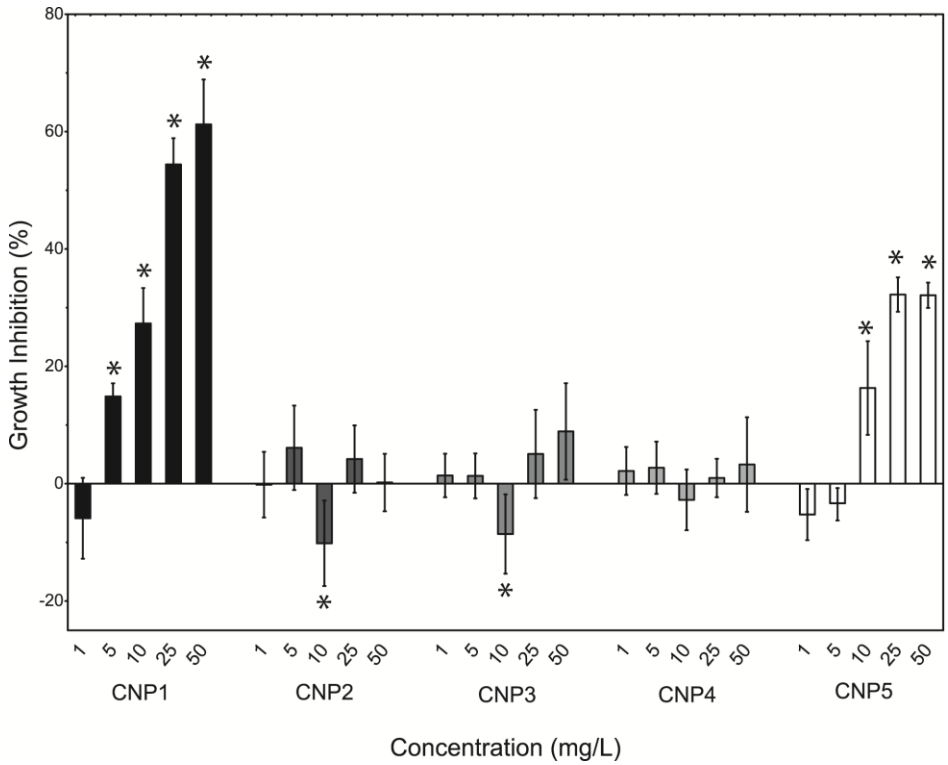

Figure 3.2.- Effect of 72 h exposure to the five CNPs on growth of *P. subcapitata*. Data are expressed as percentages of the value of untreated cells (mean ± standard deviation). Statistically significant differences ($p<0.05$) are marked by asterisks.

effective diameter, nanoparticle ζ-potential, shape and % surface Ce^{3+} were evaluated as potential explanatory variables (Figure 3.3, Supplementary Table S3.2 and Supplementary Figure S3.2). Both % surface Ce^{3+} and ζ-potential correlated equally well ($R^2 \approx 0.7$ with significant *p*-values) with algal growth inhibition (Figure 3.3a,b; Supplementary Table S3.2). Size did not show any significant correlation (Supplementary Table S3.2) and regarding shape, as it is a categorical variable, a different statistical approach was followed. Algal growth was only significantly (ANOVA, $\alpha = 0.05$) affected by spherical nanoceria: CNP1, CNP2 and CNP5 (Supplementary Figure S3.2a) and as also shown in Supplementary Figure S3.2b, within spheres, CNP1 and CNP5 with the higher % surface Ce^{3+} significantly inhibited growth, while CNP2 with a lower % surface Ce^{3+} slightly stimulated growth (already shown in Figure 3.2). So, shape *per se* did not affect toxicity, in fact, CNP2, CNP3 and CNP4 which were non-toxic had different morphology: sphere, rod and cube, respectively.

Both parameters % surface Ce^{3+} and ζ-potential measured in OECD medium presented a very high and statistically significant correlation ($R^2 \approx 0.97$, $p = 0.001$) (Figure 3.3C). However, to our knowledge there is no previous evidence of such a direct influence of surface Ce^{3+} on ζ-potential of cerium oxide nanoparticles. It may be possible that % surface Ce^{3+} may alter the state of nanoceria in a specific medium and thus, may affect toxicity. In this regard, it is well known that surface chemistry of nanoparticles can alter their physicochemical properties in fluids, such as ζ-potential and colloidal stability [34] and it is important to note that measured ζ-potential values are quite different in OECD algal medium as compared to distilled water (See Table 3.1). Therefore, either ζ-potential or % surface Ce^{3+} might explain the observed toxicity pattern. However, which is the actual driving factor of the observed toxicity? Are the differential toxic responses driven by the distinct % of surface

Ce^{3+} and Ce^{4+} content? Or, are the observed differences driven by the found divergences in ζ-potential which usually correlate with the colloidal stability of the CNPs suspensions [32]? Are both factors responsible?

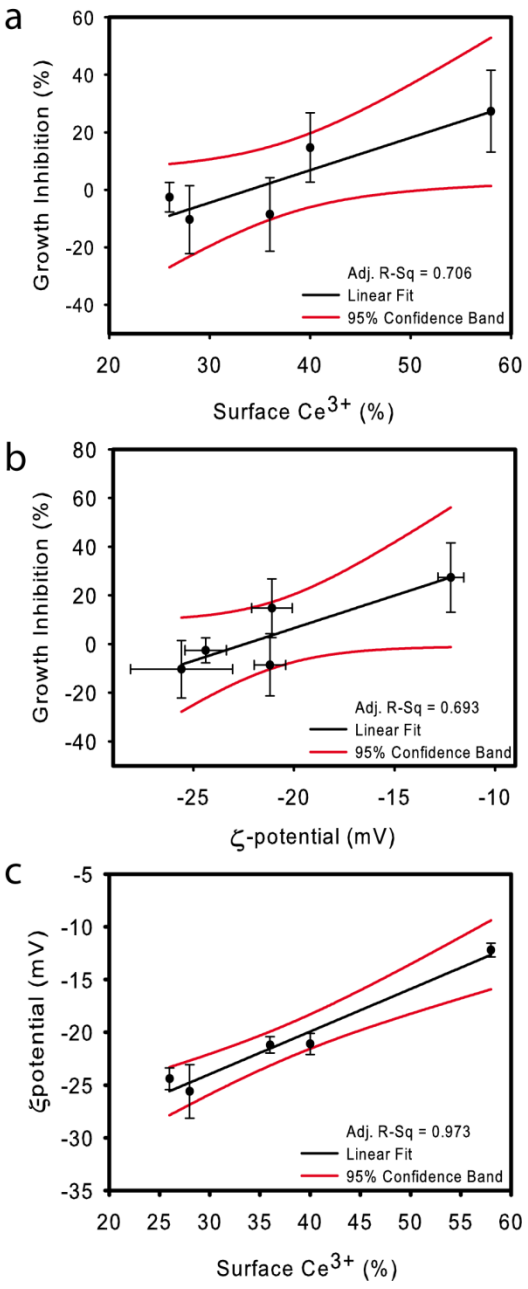

Figure 3.3- Correlation analyses. a) Correlation between algal growth inhibition (%) caused by CNPs exposure and % surface Ce^{3+} of each tested CNP. b) Correlation between algal growth inhibition (%) and ζ-potential (mV) in OECD-medium. c) correlation between ζ-potential (mV) in OECD-medium and % surface Ce^{3+} of each tested CNP.

3.3.3 Untangling the main drivers of CNP bioactivity.

In order to answer those questions, CNP1 and CNP2 were chosen to further understand which parameter(s) caused the observed toxicity. Both CNPs were synthesized by the same method and had similar sizes and shapes but clearly differed in their biological effect (CNP1 as the most toxic and CNP2 as non-toxic) and in the above identified physicochemical properties of interest (ζ-potential and % surface Ce^{3+}).

Previous works [32, 34, 35] have shown that the addition of specific chemical agents influence nanoparticle surface charge and may have significant effects on colloidal stability and surface chemistry [18, 36]. Stock suspensions of the CNP1 and CNP2 were prepared with specific modifying chemical agents in order to provoke specific changes in colloidal stability and surface reactivity. ζ-potential was modified by using trivalent iron (Fe^{3+}) which is specifically adsorbed on negatively charge surfaces and can neutralize the negative surface charges altering the tendency to homo and/or heteroaggregation of nanoparticles[32,34]. The intrinsic reactivity of Ce^{3+}, generated by its surface catalytic properties, was masked by using phosphate ions (PO_4^{3-}) [18]. PO_4^{3-} was used to block the redox cycling between Ce^{3+} and Ce^{4+} at the particle surface due to strong association among surface Ce^{3+} with phosphate anions [18, 37].

In addition to growth inhibition studies, additional biological characterizations were performed to get a deeper insight into the toxicological mechanisms involved. For this, nano-bio interactions were tracked by flow cytometry, TEM-XEDS and FTIR analysis. As oxidative stress has been found to be a basic mechanism of CNP toxicity [21, 23, 26], intracellular ROS production was also evaluated.

As shown in Supplementary Table S3.3, Fe treatment induced charge reversal on CNP1 (from -12.2 mV to 10.15 mV) and a reduction of 10 mV (in absolute values) on CNP2 surface charge (from -25.6 mV to -15.3 mV) (See Table 3.1 for comparison). Besides, Fe treatment significantly increased the effective diameter for CNP2, but did not increase the effective diameter of CNP1 which was already high, although Fe increased its PDI. These changes induced by Fe treatment indicated colloidal destabilization [32, 34]. The addition of the phosphate buffer did not induce significant changes in the nanoparticle suspensions. According to Singh et al. [18], phosphate shifts the redox state of CNPs but does not significantly alter their colloidal stability.

When cells and nanoparticles co-occur, hetero-aggregation has been frequently observed, in particular in those systems where nanoparticles show some degree of colloidal destabilization [26, 29, 32].

Potential hetero-aggregation between algal cells and CNP1/CNP2 was tracked by using Flow Cytometry. Figure 3.4 shows flow cytograms of cell complexity (internal granularity) as a function of cell size of *P. subcapitata* (control), *P. subcapitata* exposed to CNP1 and CNP2 (Fig. 3.4b,c) and *P. subcapitata* exposed to both CNPs after the treatment with Fe (Fig. 3.4e,f) and phosphate (Fig. 3.4h,i). As can be seen, the flow cytograms of algal cells (control) exhibited a defined ellipsoidal population (denoted as subpopulation R-1) with 99% of cells inside this region. CNP1 exposure reduced the percentage of cells inside subpopulation R-1 (95.2 % of total cells), showing a shift to the left indicating a subpopulation of cells (denoted as R-2) with lower size and diminished cell size/complexity which might indicate highly damaged cells or cell death. In addition, a clearly significant shift to the upper left (subpopulation denoted as R-3 which reached 2.5 % of total cells) was also observed which indicated an increase in cell size and complexity that could be

interpreted as the formation of nanoparticle-cell hetero-aggregates [26, 32]. As expected, CNP2 did not induce hetero-aggregation with algal cells and the flow cytograms was quite similar to that of the non-exposed cells. The treatment with Fe already increased the cell size and complexity of non-exposed cells (subpopulation R-3: 12.3%) indicating that the Fe treatment *per se* induced a slight flocculation of algal cells. It also slightly increased subpopulation R-2 (2.9 %), indicating some extent of cell damage. There was a clear and remarkable change in the populations of algal cells exposed to CNP1 and Fe as this treatment drastically shifted the main population to the upper left of the cytogram (subpopulation R-3) with 39.4 % of total cells showing higher complexity and size. This is probably due to the formation of numerous nanoparticle-cell hetero-aggregates due to the increased colloidal destabilization of CNP1.

Fe treatment also provoked and increase in the R-2 subpopulation (it reached 30.3 % of total cells) indicating increased cell damage. CNP2-Fe treatment exhibited smaller changes than CNP1-Fe with respect to the control: R-3 and R-2 slightly increased (reaching 18.6 % and 8.2 % respectively) indicating that some extent of heteroaggregation and cell damage were occurring for CNP2 treated with Fe. Phosphate treatment did not have any significant effect on cell size or complexity of non-exposed cells or cells exposed to CNP2. However, it significantly decreased the subpopulation of cells with increased cell size and complexity (R-3 comprising only 1.4 % of total cells) observed in cells exposed to CNP1 without treatments (Fig. 3.4b), indicating that phosphate treatment inhibited to some degree the hetero-aggregation process. It also decreased the R-2 subpopulation of damaged cells to 1.9 % of total cells, probably indicating a decrease in toxicity.

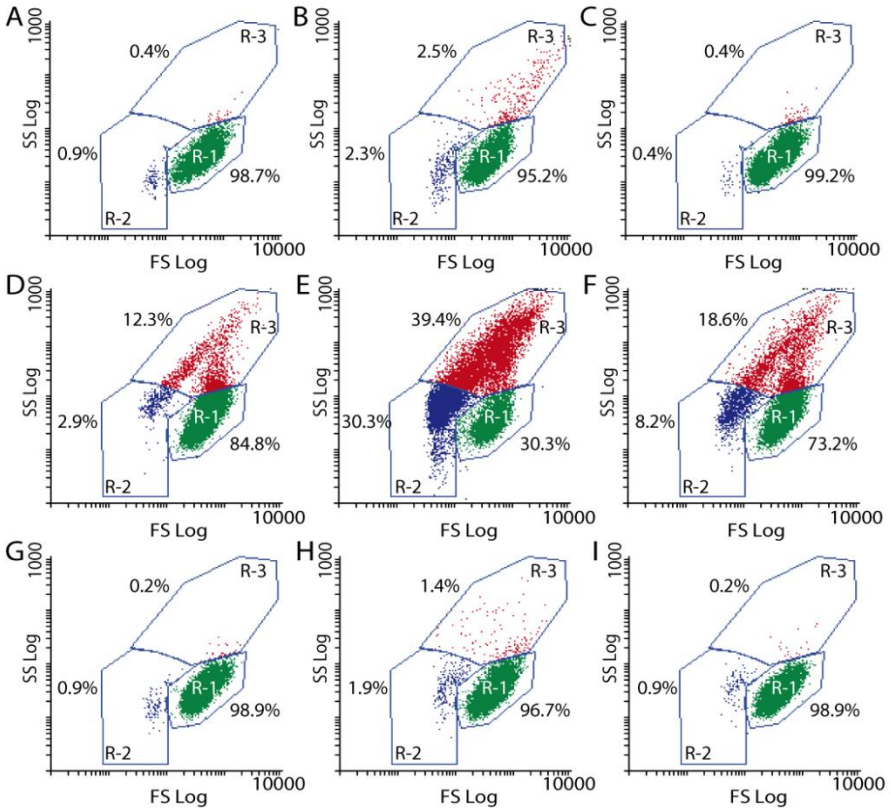

Figure 3.4.- Correlation analyses. a) Correlation between algal growth inhibition (%) caused by CNPs exposure and % surface Ce^{3+} of each tested CNP. b) Correlation between algal growth inhibition (%) and ζ-potential (mV) in OECD-medium. c) correlation between ζ-potential (mV) in OECD-medium and % surface Ce^{3+} of each tested CNP.

In order to correlate the observed hetero-aggregation patterns with toxicity, the effect of the combined treatments CNP1-Fe, CNP2-Fe, CNP1-phosphate and CNP2-phosphate on growth and ROS formation in exposed cells was studied. As can be seen in Figure 3.5a, Fe treatment significantly ($p<0.05$) increased growth inhibition in CNP1 exposed cells. In the case of CNP2, Fe

treatment caused a slight inhibition of growth as compared to the observed growth stimulation when exposed to CNP2 alone. These results correlated with those of the flow cytograms. CNP1 also caused significant (*p<0.05*) ROS formation in exposed cells (Figure 3.5b), indicating that oxidative stress might be an important mechanism of toxicity. However, Fe treatment did not

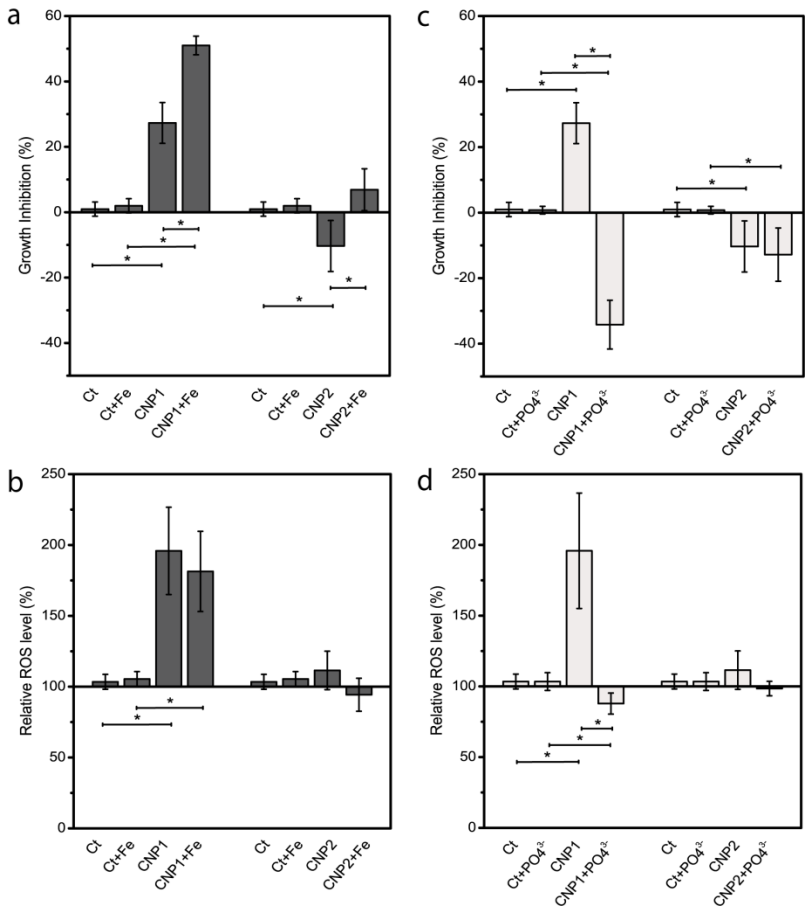

Figure 3.5.- Effect of combined treatments of CNP1 and CNP2 with Fe (left column) or PO_4^{3-} (right column) on the growth of *P. subcapitata* during 72 h (a, c), and intracellular ROS production (b, d). Mean ± standard deviation. Statistically significant differences (*p < 0.05*) are

increase ROS further. CNP2 alone or combined with Fe did not induce ROS formation in the exposed cells. CNP1-Phosphate treatment (Figure 3.5c and d) completely reverted the toxicity of CNP1 resulting in a significant ($p<0.05$) growth stimulation. Moreover, phosphate treatment slightly reduced the ROS levels of the non-exposed cells (Figure 3.5d). CNP2 treated with phosphate maintained its non-toxic profile (Fig. 3.5c and d).

The drastic effect of phosphate treatment on the toxic patterns of cells exposed to CNP1 might be due to the affinity of surface Ce^{3+} for phosphate anions, which occupy surface oxygen vacancies forming $CePO_4$; this modifies the nanoceria surface and blocks the redox cycling between Ce^{3+} and Ce^{4+} [18]. The fact that phosphate treatment totally reverted the toxicity of CNP1 indicates that the % surface Ce^{3+} is probably the main driver of CNP1 toxicity. This is further demonstrated by the fact that CNP2 with a significantly lower % surface Ce^{3+} was not toxic even under Fe treatment which induced heteroaggregation between cells and nanoparticles.

Direct attachment of nanoparticles to cellular envelopes has been found to mediate toxicity of several nanoparticles to algae in which internalization has not been found [25, 28, 32]. In order to confirm whether % surface Ce^{3+} might influence CNP attachment to algal cell envelope, FTIR and TEM-XEDS studies were made. As shown by the FTIR profiles in Figure 3.6, the presence of CNP1 was detected in the envelope of *P. subcapitata* (absorption band at wavenumber 400 cm^{-1}, representing the Ce-O stretch [38] no significant differences were found at wavenumbers in the range 4000-550 cm^{-1} (not shown). No absorption peaks at wavenumber of 400 cm^{-1} or higher were found for CNP2 or CNP1 treated with phosphate indicating that treatment

with phosphate which blocks Ce^{3+}, prevents CNP1 attachment to the cell wall. As expected, the non-toxic CNP2 did not attach to the cell envelope.

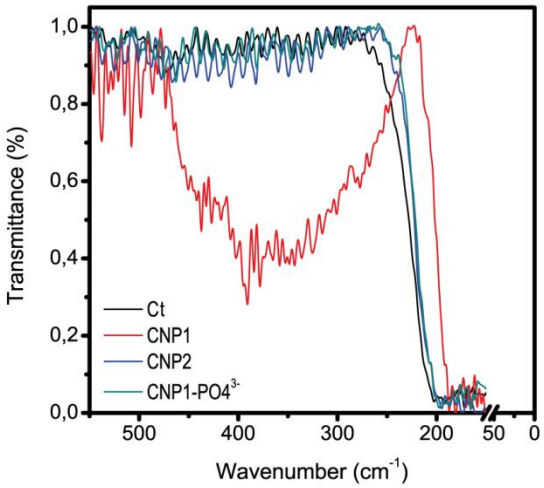

Figure 3.6.- FTIR transmission profiles of *P. subcapitata* control cells (Ct), CNP1, CNP2 and CNP1-PO_4^{3-}. Wavenumber range: 550-50 cm^{-1}.

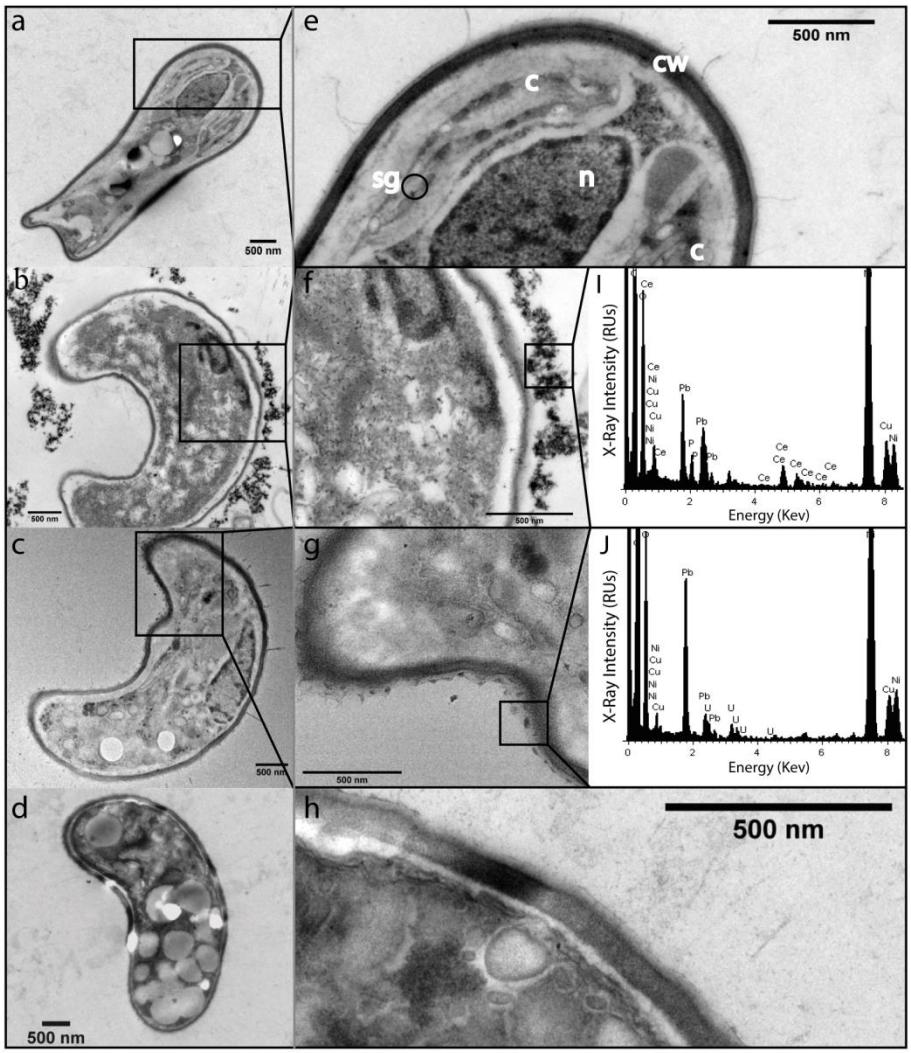

Figure 3.7.- Selected Transmission electron microscopy (TEM) micrographs of *P. subcapitata* non-exposed (a, e) and exposed to CNP1 (b, f), CNP2 (c, g) and CNP1-PO_4^{-3} (d, h) for 72 h, accompanied with XEDS spectrum (i, j). N=nucleus; C=chloroplast; SG=starch grain; CW=cell wall.

Attachment to the algal envelope was further confirmed by TEM-XEDS. As shown in Figure 3.7 (b, f), CNP1 nanoparticles clearly attached to the outer cell

wall as several layers of electron-dense particles surrounding the cell wall were found. No evidence of internalization was observed. XEDS analysis assigned Ce as the main constituent of attached particles. The electron-dense nanoparticles were absent in non-exposed cells (a, e) or cells exposed to CNP2 (c, g). XEDS analysis already confirmed the absence of Ce around the cell wall. Treatment with phosphate (d, h) prevented nanoparticle attachment and no Ce was detected around the cell wall either. It is worth noticing that CNP1 (clearly seen in Figure 3.7f) induced cell wall detachment from the cytoplasmic membrane, cell shrinking and disorganization as internal structures such as the nucleus, chloroplast or storage bodies could not be distinguished, indicating cell damage. CNP2 or CNP1-phosphate did not induce significant ultrastructural cell changes.

In the present study, we have found that CNP1 induced ROS formation in the algal cells (Figure 3.5) which, in the end, may result in oxidative stress. Interestingly, we have also found that treatment with phosphate prevented ROS formation. The relevant question is how adsorbed nanoceria induces ROS formation. Thill et al [22] and Zeyons et al [23] have found a reduction of surface Ce^{4+} to Ce^{3+} when particles are tightly adsorbed to *Escherichia coli* cell walls and have suggested that oxidative stress was triggered by the oxidant activity of Ce^{4+}. In our study, we found that toxicity depended on % surface Ce^{3+}, so that the reactivity of Ce^{3+} sites and not Ce^{4+} is the most likely source of ROS in the algal cells. Xia et al. [39] found that nanoceria induced hydrogen peroxide production abiotically. Based on these findings, we evaluated the possibility of spontaneous abiotic ROS generation by CNP1, CNP2 and CNP1 treated with phosphate by using the OxiSelect™ *in vitro* ROS/RNS Assay Kit. As shown in Figure 3.8, both in distilled water (a) and OECD algal culture medium (b), CNP1 induced significant production of ROS/RNS (152.7 nM as H_2O_2

equivalent concentration in H_2O and almost twofold in OECD medium), while CNP2 or CNP1 treated with phosphate did not. In the experiment depicted in Figure 3.8c, algal cells were exposed 24 h to the CNPs, then removed by centrifugation and ROS/RNS production was assayed in the supernatant. CNP1 significantly induced ROS/RNS formation (208.5 nM) while CNP2 and CNP1-phosphate did not induce significant ROS formation.

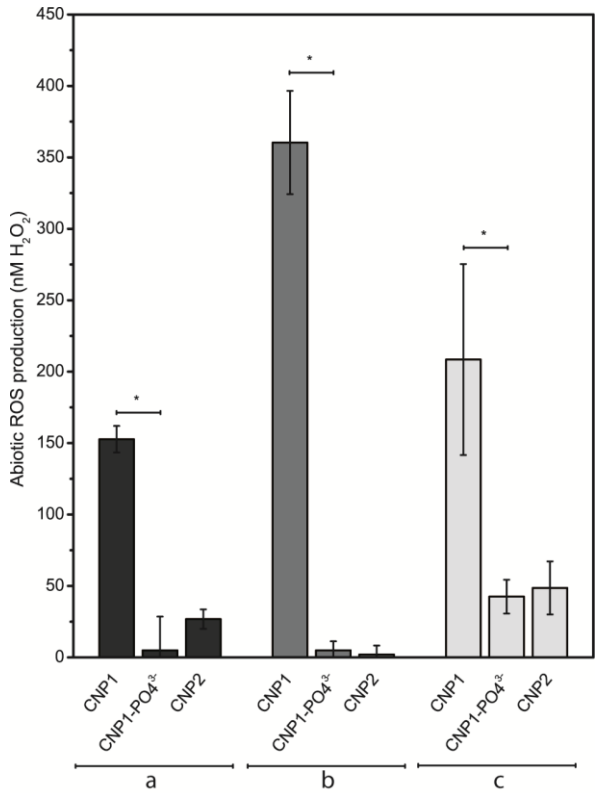

Figure 3.8.- ROS production by 10 mgL^{-1} CNPs in ddH_2O (a), in OECD-medium (b) and OECD-medium after 24h exposure to *P. subcapitata* to CNP1, CNP2 and CNP1-PO_4^{3-} (c) assessed by OxiSelect™ *in vitro* ROS/RNS Assay Kit. ROS/RNS was expressed as H_2O_2 equivalent concentration.

3.4 Discussion

There are contradictory reports on whether nanoceria may act as an oxidant causing toxicity or as an antioxidant being able to scavenge free radical, and protect the cells from oxidative damage. A variety of different nanoceria particles have been used in the bioassays. The tested particles have been synthesized by a variety of methods and have been tested in many different cell types and organisms. In some of the organisms, internalization of nanoceria particles has been observed while not in others. Different mechanisms of nanoceria toxicity have been proposed, although in most cases, toxicity seemed to be related to oxidative stress. Thus, there is a disparity of data on biological activity of nanoceria and no clear consensus on which nanoparticle properties/characteristics are responsible of the observed effects.

As found in this study and reported previously, nanoceria internalization usually does not occur in organisms such as bacteria and algae with thick cell walls [23-25, 27, 28] with a recently reported exception using PVP coated nanoceria [40]. However, nanoceria is able to internalize in human and animal cell lines and tissues [10, 14, 41]. Independently of internalization, evidence for nanoceria toxicity has been found in many of the tested cell systems and organisms. For internalized nanoceria, toxicity has been found to be related to lysosomal injury [10, 41] and oxidative stress [14, 21]. For non-internalized nanoceria toxicity seems to be mediated by direct contact of nanoceria to cell walls of algae and bacteria [22, 23, 26, 28]. Several mechanisms have been postulated to explain how non-internalized nanoceria may exert toxicity: interference with the nutrient transport functions of the membrane [23], mechanical damage membrane disruption [24, 25], or ROS generation and

oxidative stress induction [22, 23, 26]. The observed abiotic production of ROS by CNP1, most probably hydrogen peroxide, is in agreement with Xia et al [39] and Zhao et al. [42] observations. Hydrogen peroxide is able to freely diffuse across cell walls and membranes. Heckert et al. [15] reported that Ce^{3+} ions were capable of redox-cycling with hydrogen peroxide to generate ROS such as hydroxyl radicals. They suggested that surface Ce^{3+} sites rich in oxygen vacancies could be responsible of ROS production by nanoceria. The hydrogen peroxide abiotically produced by CNP1, through oxidative reactions, may generate damaging radicals such as hydroxyl radicals which cause cellular damage.

A step forward to start understanding the enigma of the biological activity of nanoceria are the studies by Ji et al. [43] and Lin et al. [41] in which a library of nanoceria rods with increasing aspect ratio (range between 1 to >100) was constructed and toxicity tested in a human myeloid cell line and in two animal models, mouse lung and zebrafish gastrointestinal tract. They found that nanorods with an aspect ratio ≥ 22 induced cytotoxicity in the human cell line. They also found that the toxicological profile of the tested nanorods in both animal models depended on the aspect ratio, although this was clearly demonstrated only with the longest rod. However, these observations may only be relevant for internalized nanoceria.

In the present study, we demonstrate that neither shape, concentration, surface charge (ζ-potential) synthesis method nor nominal size had any influence in the observed biological activity and present for the first time solid evidence of the involvement of % surface Ce^{3+} in toxicity of nanoceria in an environmentally relevant organism. Our results clearly showed that % surface Ce^{3+} correlated with toxicity and was the main driver explaining the observed

toxic effect of nanoceria: CNP1 with the highest % surface Ce^{3+} (58 %) was also the most toxic followed by CNP5 with a % surface Ce^{3+} of 40 whereas CNP2, CNP3 and CNP4 with lower % surface Ce^{3+} values (between 26-36 %) were apparently safe for the model organism. The fact that a relatively small difference in % surface Ce^{3+} (40 % for CNP5 which is toxic *vs.* 36 % for CNP3 which is non- toxic) accounts for a larger biological effect may be explained by the differential catalytic activity of nanoparticles with varying Ce^{3+}/Ce^{4+} ratios. Nanoceria with higher Ce^{3+} on the surface can efficiently scavenge superoxide radicals (superoxide dismutase mimetic activity) and produce H_2O_2 which becomes toxic to the cells. This is the case with CNP1 and CNP5 while CNP2, CNP3 and CNP4 are less active towards scavenging superoxide radicals [15, 44]. In fact, nanoceria with lower Ce^{3+} and therefore higher Ce^{4+} on the surface (CNP2, CNP3 and CNP4) exhibit catalase mimetic activity [16] which breaks down H_2O_2 to molecular oxygen, protecting the cells against this toxic reactive oxygen species.

It was further demonstrated that surface Ce^{3+} was the source of toxicity as blocking the Ce^{3+} sites of CNP1 with phosphate prevented toxicity and even stimulated growth and slightly reduced ROS levels with respect to the control. This stimulation could be due to an increase of the catalase mimetic activity of phosphate treated nanoceria as found by Singh et al. [18].

Colloidal destabilization by Fe treatment only significantly increased toxicity of the already toxic CNP1. As nanoceria was not internalized, it was proposed that abiotically generated ROS, probably hydrogen peroxide, was the inducing factor of the observed oxidative stress.

Systematic studies such as those of Ji et al. [43] and Lin et al. [41] and those presented here might be useful to untangle the main drivers of the biological

activity of synthesized nanoceria in different cell/organism systems and to define global descriptors of engineered nanoparticles (ENPs) bioactivity which may be useful in safer-by-design strategies and in Environmental Health and Safety (EHS) assessment of nanomaterials.

We demonstrate that the main driver of toxicity of cerium oxide nanoparticles is the percentage of Ce^{3+} at the surface of the nanoparticles: only the nanoparticles with the highest values exert toxicity in the ecologically relevant aquatic organism. As opposed to human and animal cell lines where nanoceria internalization usually occurs, nanoceria did not internalize in the alga. The mechanisms of toxicity rely primarily on the formation of abiotic ROS and on attachment of the nanoparticles to the cell wall which affect cell viability and ultrastructure. Blocking the Ce^{3+} sites of the toxic nanoparticles with phosphate prevented toxicity and even stimulated growth and slightly reduced ROS levels with respect to the control. This study gives clues towards a safer design of nanoparticles which may eventually end up in the aquatic environment.

3.5 METHODS

3.5.1 Synthesis of Different Cerium Oxide Nanoparticles

In this study, five Cerium Oxide Nanoparticles (CNPs) were synthesized using different methods with varying % surface Ce^{3+}, size and morphology. 99.999% pure cerium nitrate hexahydrate was used for all the preparation. CNP1 and CNP2 were synthesized using the wet chemical method, with H_2O_2 (CNP1) and NH_4OH (CNP2) as oxidizing agents [45]. In order to prove that there was no H_2O_2 in CNP1 after the synthesis process, the Amplex® Red Hydrogen

Peroxide/Peroxidase Assay Kit was performed following the manufacturer instructions (Life Technologies). Briefly, reactions containing 50 µM Amplex® Red reagent, 0.1 U/mL horseradish peroxidase (HRP) and increasing concentration of CNP1 (1, 10, 100 mg/l) were incubated for 30 minutes at room temperature. Fluorescence was then measured with a Fluorostar Omega plate reader (BMG LABTECH GmbH, Germany) using excitation at 530 nm and fluorescence detection at 590 nm. H_2O_2 was not detected in any of the concentration tested (see Supplementary Figure S3.3). No differences were found between CNP1 and control (with H_2O). CNP3, CNP4 and CNP5 were prepared using the hydrothermal method, as described elsewhere [44]. The % surface Ce^{3+} for all the nanoparticles were tested several times over the experimental period in the aqueous environment (data not shown) and the % surface Ce^{3+}/Ce^{4+} was stable for all these nanoparticles.

3.5.2 CNPs chemistry

High Resolution Transmission Microscopy (HRTEM), FEI Tecnai F30 was used to analyze size and morphology of the particles. Selected Area Electron Diffraction patterns (SAED) of nanoparticles were analyzed to determine the crystallinity. Surface chemistry (Ce^{3+}/Ce^{4+}) ratios on the surface of nanoparticles was analyzed using X-Ray photoelectron spectroscopy as described elsewhere [46]. The optical properties were analyzed using Ultraviolet–Visible Spectrophotometer (Perkin Elmer, Lambda 750S, 60 mm Int. Sphere). The dissolved fraction of CNPs was examined by centrifugal ultrafiltration (Sartorius AG, Goettingen, Germany) through a membrane with a nominal molecular weight limit of 50 kDa (Vivaspin 6). Suspensions were centrifuged for 15 min at 4000 rpm (Allegra X-12 Series, Beckman Coulter). Dissolution of CNPs was tested at a concentration of 10 mg/L in OECD media

(algal growth medium; composition in Supplementary Table S3.4) under agitation (135 rpm) during 72 h. Nanoparticle suspensions were maintained under identical experimental conditions as the bioassays. The concentration of Ce^{3+} in the filtrate was related to the total Ce concentration as determined by ICP-MS. Cerium (III) chloride (CAS no. 7790-86-5) >99.99% was purchased from Sigma-Aldrich. Water suspensions were prepared with high-purity water obtained from a Milipore Mili-Q system with a resistivity of at least 18 MΩ at 25 ºC.

Hydrodynamic diameter and ζ-potential of the CNP suspensions in the different assay conditions were measured by Dynamic light scattering (DLS) and electrophoretic light scattering respectively using a Zetasizer Nano ZS particle size analyzer from Malvern Instruments Ltd. Measurements were essentially as described elsewhere [32].

3.5.3 Modification of surface chemistry and colloidal stability of CNPs in OECD media

0.1 mM [$Fe_2(SO_4)_3$] was used to induce particle colloidal destabilization of CNPs suspension and heteroaggregation of CNP with algae [34]. Regarding surface chemistry properties, the phosphate treatment consisted on incubation (24 h) with equimolar concentration (100 µM) of phosphate buffer (13.8 g/L monosodium phosphate and 14.1 g/L disodium phosphate, pH 7.4) and CNPs. PO_4^{3-} blocks the redox cycling between Ce^{3+} and Ce^{4+}, which is essential for the catalytic activity of CNPs [18, 37]. All the chemicals were from Merck (Darmstadt, Germany). The chosen concentrations of both buffers did not have any statistically significant effects on the algal studied parameters.

3.5.4 Biological end-points

3.5.4.1 Growth inhibition. Growth inhibition of the green microalga *P. subcapitata* (Microbiotests. Inc.; Denmark) was performed essentially as described in Gonzalo, et al. [32] following the standard TG 201 [47] guideline. Cells were routinely grown in 250 ml flasks on a rotatory shaker at 135 rpm in OECD standard culture medium (pH 8.2); the pH was regularly checked and remained unchanged during the experiment. Exposure experiments to CNPs suspensions were carried out in 1.8 mL of OECD culture medium in 24 well-plates. Growth inhibition experiments were performed during 72h in the same experimental conditions at least in triplicate with serial dilutions. *In-vivo* fluorescence of chlorophyll (485nm/645nm excitation/emission) was measured daily as biomass surrogate as described elsewhere [32] on a Synergy HTmulti-mode microplate reader (BioTek,USA).

3.5.4.2 Intracellular ROS. Intracellular ROS produced by *P. subcapitata* was measured by using the cell permeable fluorescent indicator 2',7'-dichlorodihydrofluorescein diacetate (H_2DCFDA, Invitrogen Molecular Probes; Eugene, OR, USA) as previously described [25]. 3% H2O2 (v/v) was used as a positive control for ROS formation. Fluorescence (488 and 530 nm) was monitored on a Synergy HT multi-mode microplate reader (BioTek, USA). Results were normalized for possible differences in cell number by the measured *in-vivo* fluorescence of chlorophyll of the sample.

3.5.4.2 Flow cytometric analyses. Chlorophyll (cell autofluorescence) and heteroaggregation (as FS *vs* SS distributions) of algal populations were evaluated using a Cytomix FL500 MPL flow cytometer equipped with an argon-ion excitation wavelength (488 nm), detector of forward (FS) and side (SS) light scatter and four fluorescence detectors (FL1:525, FL2:575, FL3:620 and FL4: 675 ± 20 nm) (Beckman Coulter Inc., Fullerton, CA, USA), as described

previously [26]. The flow rate was set at 1 μLs^{-1} and at least 10000 events (algal cells) were counted. Non-algal particles were excluded from the analysis by setting an acquisition threshold value 1 for the forward scatter (FS) parameter. Chlorophyll red autofluorescence was collected with a 610 nm long band pass filter (FL4). Data acquisition was performed using MXP-2.2 software, and the analyses were performed using CXP-2.2 and Flowing Software 2.5.1 software. Fluorescence was analyzed in Log mode.

3.5.4.3 CNP-algal interaction by TEM and FT-IR. For transmission electron microscopy (TEM) analysis, algal cell suspensions exposed to the different CNP treatments were collected by centrifugation at low relative centrifugal forces (RCFs = 1500g) during 3 min in order to reduce the chance for artifacts, cells where prepared essentially as previously described [32]. Cells were fixed in agar blocks in 3.1% glutaraldehyde in phosphate buffer (pH 7.2) for 3 h at 4ºC. Post-fixation was in osmium tetroxide in phosphate buffer for 2 h at 4ºC. Samples were dehydrated in ethanol and embedded in Durcupan resin (Fluka). Samples were sectioned in a Leica Reichert Ultracut S ultramicrotome, stained with uranyl acetate 2%. Ultrathin sections were visualized on a JEOL (JEM 1010) electron microscope (100 kV) or on a JEOL JEM 2100 (200 kV) coupled with XEDS (X-Ray Energy Dispersive Spectroscopy). All reagents used for TEM preparations were Electron Microscopy grade. For Fourier Transformed Infrared (FTIR) analyses, algal cell suspensions exposed to different CNPS treatment were centrifuged and 5µL of pelletized cells were transferred to KBr dish and were dried for 2 h at 25 ºC. Infrared spectra of the algal cell were obtained using a Bruker model IFs 66VFourier Transform Infrared spectrometer in transmission mode.

3.5.4.4 In vitro ROS assessment. Spontaneous ROS generation by CNPs was determined by using the OxiSelect *in vitro* ROS/RNS assay kit (Cell BioLabs, San Diego, USA). The kit was used according to the recommendations of the manufacturer. ROS and the reactive nitrogen species (RNS) content were determined in ddH_2O and OECD algal exposure medium by fluorescence (480nm/530nm), measured in 96 well opake microttiter plates in a Synergy HT multi-mode microplate reader (BioTek, USA). Quantitative determinations of ROS/RNS content were estimated using a hydrogen peroxide standard curve. For the assay, 10 mg/L of CNPs suspensions were added to ddH_2O or algal medium and ROS/RNS content was determined after 15 min. In addition, ROS/RNS content was also determined in used culture medium (medium where the cells were previously exposed to CNPs particles (see below) (after removing cells by centrifugation, 5min, 10000 rpm).

3.5.5 Statistical Analysis

Statistical analyses were performed by using R software 3.0.2. (The R Foundation for Statistical Computing©) and Rcmdr 2.0-4 package [48]. A one way ANOVA coupled with Tukey's HSD (honestly significant difference) post-hoc test was performed for comparison of means. Statistically significant differences were considered to exist when $p<0.05$.

3.6 References

[1] Hayes, S. A., Yu, P., O'Keefe, T. J., O'Keefe, M. J. & Stoffer, J. O. The Phase Stability of Cerium Species in Aqueous Systems: I. E-pH Diagram for the

Ce - HClO 4 - H 2 O System. *Journal of The Electrochemical Society* 149, C623-C630 (2002).

[2] Reed, K. *et al.* Exploring the properties and applications of nanoceria: is there still plenty of room at the bottom? *Environmental Science: Nano* 1, 390-405, doi:10.1039/C4EN00079J (2014).

[3] Pang, X., Li, D. & Peng, A. Application of rare-earth elements in the agriculture of china and its environmental behavior in soil. *J Soils Sediments* 1, 124-129, doi:10.1007/BF02987718 (2001).

[4] Patil, S., Kuiry, S. C., Seal, S. & Vanfleet, R. Synthesis of Nanocrystalline Ceria Particles for High Temperature Oxidation Resistant Coating. *Journal of Nanoparticle Research* 4, 433-438, doi:10.1023/A:1021696107498 (2002).

[5] Jasinski, P., Suzuki, T. & Anderson, H. U. Nanocrystalline undoped ceria oxygen sensor. *Sensors and Actuators B: Chemical* 95, 73-77, doi:http://dx.doi.org/10.1016/S0925-4005(03)00407-6 (2003).

[6] Croy, J. R. *et al.* Support dependence of MeOH decomposition over size-selected Pt nanoparticles. *Catalysis Letters* 119, 209-216 (2007).

[7] Giraldo, J. P. *et al.* Plant nanobionics approach to augment photosynthesis and biochemical sensing. *Nature materials* 13, 400-408, doi:10.1038/nmat3890 (2014).

[8] Das, M. *et al.* Auto-catalytic ceria nanoparticles offer neuroprotection to adult rat spinal cord neurons. *Biomaterials* 28, 1918-1925 (2007).

[9] Tarnuzzer, R. W., Colon, J., Patil, S. & Seal, S. Vacancy engineered ceria nanostructures for protection from radiation-induced cellular damage. *Nano letters* 5, 2573-2577, doi:10.1021/nl052024f (2005).

[10] Asati, A., Santra, S., Kaittanis, C. & Perez, J. M. Surface-charge-dependent cell localization and cytotoxicity of cerium oxide nanoparticles. *ACS nano* 4, 5321-5331 (2010).

[11] Karakoti, A. S. *et al.* Nanoceria as Antioxidant: Synthesis and Biomedical Applications. *JOM (Warrendale, Pa. : 1989)* 60, 33-37, doi:10.1007/s11837-008-0029-8 (2008).

[12] Campbell, C. T. & Peden, C. H. F. Oxygen Vacancies and Catalysis on Ceria Surfaces. *Science* 309, 713-714, doi:10.1126/science.1113955 (2005).

[13] Esch, F. *et al.* Electron Localization Determines Defect Formation on Ceria Substrates. *Science* 309, 752-755, doi:10.1126/science.1111568 (2005).

[14] Zhang, H. *et al.* Nano-CeO2 exhibits adverse effects at environmental relevant concentrations. *Environmental science & technology* 45, 3725-3730, doi:10.1021/es103309n (2011).

[15] Heckert, E. G., Karakoti, A. S., Seal, S. & Self, W. T. The role of cerium redox state in the SOD mimetic activity of nanoceria. *Biomaterials* 29, 2705-2709, doi:10.1016/j.biomaterials.2008.03.014 (2008).

[16] Pirmohamed, T. *et al.* Nanoceria exhibit redox state-dependent catalase mimetic activity. *Chemical communications* 46, 2736-2738, doi:10.1039/b922024k (2010).

[17] Dowding, J. M., Dosani, T., Kumar, A., Seal, S. & Self, W. T. Cerium oxide nanoparticles scavenge nitric oxide radical (NO). *Chemical communications* 48, 4896-4898, doi:10.1039/c2cc30485f (2012).

[18] Singh, S. *et al.* A phosphate-dependent shift in redox state of cerium oxide nanoparticles and its effects on catalytic properties. *Biomaterials* 32, 6745-6753, doi:10.1016/j.biomaterials.2011.05.073 (2011).

[19] Naganuma, T. & Traversa, E. The effect of cerium valence states at cerium oxide nanoparticle surfaces on cell proliferation. *Biomaterials* 35, 4441-4453, doi:10.1016/j.biomaterials.2014.01.074 (2014).

[20] Asati, A., Santra, S., Kaittanis, C., Nath, S. & Perez, J. M. Oxidase-like activity of polymer-coated cerium oxide nanoparticles. *Angewandte Chemie* 48, 2308-2312, doi:10.1002/anie.200805279 (2009).

[21] Lin, W., Huang, Y. W., Zhou, X. D. & Ma, Y. Toxicity of cerium oxide nanoparticles in human lung cancer cells. *International journal of toxicology* 25, 451-457, doi:10.1080/10915810600959543 (2006).

[22] Thill, A. *et al.* Cytotoxicity of CeO2 Nanoparticles for Escherichia coli. Physico-Chemical Insight of the Cytotoxicity Mechanism. *Environmental science & technology* 40, 6151-6156, doi:10.1021/es060999b (2006).

[23] Zeyons, O. *et al.* Direct and indirect CeO2nanoparticles toxicity forEscherichia coliandSynechocystis. *Nanotoxicology* 3, 284-295, doi:10.3109/17435390903305260 (2009).

[24] Rogers, N. J. *et al.* Physico-chemical behaviour and algal toxicity of nanoparticulate CeO2 in freshwater. *Environmental Chemistry* 7, 50-60, doi:http://dx.doi.org/10.1071/EN09123 (2010).

[25] Rodea-Palomares, I. *et al.* Physicochemical characterization and ecotoxicological assessment of CeO2 nanoparticles using two aquatic microorganisms. *Toxicological sciences : an official journal of the Society of Toxicology* 119, 135-145, doi:10.1093/toxsci/kfq311 (2011).

[26] Rodea-Palomares, I. *et al.* An insight into the mechanisms of nanoceria toxicity in aquatic photosynthetic organisms. *Aquatic toxicology* 122-123, 133-143, doi:10.1016/j.aquatox.2012.06.005 (2012).

[27] Van Hoecke, K. *et al.* Fate and effects of CeO2 nanoparticles in aquatic ecotoxicity tests. *Environmental science & technology* 43, 4537-4546 (2009).

[28] Manier, N., Bado-Nilles, A., Delalain, P., Aguerre-Chariol, O. & Pandard, P. Ecotoxicity of non-aged and aged CeO2 nanomaterials towards freshwater microalgae. *Environmental pollution* 180, 63-70, doi:10.1016/j.envpol.2013.04.040 (2013).

[29] Rohder, L. A., Brandt, T., Sigg, L. & Behra, R. Influence of agglomeration of cerium oxide nanoparticles and speciation of cerium(III) on short term effects to the green algae Chlamydomonas reinhardtii. *Aquatic toxicology* 152, 121-130, doi:10.1016/j.aquatox.2014.03.027 (2014).

[30] Kuchibhatla, S. V. *et al.* Influence of Aging and Environment on Nanoparticle Chemistry - Implication to Confinement Effects in Nanoceria. *The journal of physical chemistry. C, Nanomaterials and interfaces* 116, 14108-14114, doi:10.1021/jp300725s (2012).

[31] McCormack, R. N. *et al.* Inhibition of Nanoceria's Catalytic Activity due to Ce3+Site-Specific Interaction with Phosphate Ions. *The Journal of Physical Chemistry C* 118, 18992-19006, doi:10.1021/jp500791j (2014).

[32] Gonzalo, S. *et al.* A colloidal singularity reveals the crucial role of colloidal stability for nanomaterials in-vitro toxicity testing: nZVI-microalgae colloidal system as a case study. *PloS one* 9, e109645, doi:10.1371/journal.pone.0109645 (2014).

[33] Booth, A. *et al.* Freshwater dispersion stability of PAA-stabilised cerium oxide nanoparticles and toxicity towards Pseudokirchneriella subcapitata. *The Science of the total environment* 505, 596-605, doi:10.1016/j.scitotenv.2014.10.010 (2015).

[34] Gregory, J. *Particles in water: properties and processes*. (CRC Press, 2005).

[35] Stankus, D. P., Lohse, S. E., Hutchison, J. E. & Nason, J. A. Interactions between Natural Organic Matter and Gold Nanoparticles Stabilized with Different Organic Capping Agents. *Environmental science & technology* 45, 3238-3244, doi:10.1021/es102603p (2011).

[36] Dowding, J. M. *et al.* Cellular interaction and toxicity depend on physicochemical properties and surface modification of redox-active nanomaterials. *ACS nano* 7, 4855-4868, doi:10.1021/nn305872d (2013).

[37] Xue, Y. *et al.* The vital role of buffer anions in the antioxidant activity of CeO2 nanoparticles. *Chemistry* 18, 11115-11122, doi:10.1002/chem.201200983 (2012).

[38] Jalilpour, M. & Fathalilou, M. Effect of aging time and calcination temperature on the cerium oxide nanoparticles synthesis via reverse co-precipitation method. *International Journal of the Physical Sciences* 7 (2012).

[39] Xia, T. *et al.* Comparison of the mechanism of toxicity of zinc oxide and cerium oxide nanoparticles based on dissolution and oxidative stress properties. *ACS nano* 2, 2121-2134 (2008).

[40] Taylor, N. S. *et al.* Molecular toxicity of cerium oxide nanoparticles to the freshwater alga Chlamydomonas reinhardtii is associated with supra-environmental exposure concentrations. *Nanotoxicology*, 1-10, doi:10.3109/17435390.2014.1002868 (2015).

[41] Lin, S. *et al.* Aspect Ratio Plays a Role in the Hazard Potential of CeO2 Nanoparticles in Mouse Lung and Zebrafish Gastrointestinal Tract. *ACS nano* 8, 4450-4464, doi:10.1021/nn5012754 (2014).

[42] Zhao, L. *et al.* Stress Response and Tolerance of Zea mays to CeO2 Nanoparticles: Cross Talk among H2O2, Heat Shock Protein, and Lipid Peroxidation. *ACS nano* 6, 9615-9622, doi:10.1021/nn302975u (2012).

[43] Ji, Z. *et al.* Designed Synthesis of CeO2 Nanorods and Nanowires for Studying Toxicological Effects of High Aspect Ratio Nanomaterials. *ACS nano* 6, 5366-5380, doi:10.1021/nn3012114 (2012).

[44] Sakthivel, T. *et al.* Morphological phase diagram of biocatalytically active ceria nanostructures as a function of processing variables and their properties. *ChemPlusChem* 78, 1446-1455 (2013).

[45] Das, S. *et al.* The induction of angiogenesis by cerium oxide nanoparticles through the modulation of oxygen in intracellular environments. *Biomaterials* 33, 7746-7755, doi:10.1016/j.biomaterials.2012.07.019 (2012).

[46] Deshpande, S., Patil, S., Kuchibhatla, S. V. & Seal, S. Size dependency variation in lattice parameter and valency states in nanocrystalline cerium oxide. *Applied Physics Letters* 87, 133113-133113-133113 (2005).

[47] OECD. Test No. 201: Freshwater Alga and Cyanobacteria, Growth Inhibition Test.

[48] Fox, J. Getting started with the R commander: a basic-statistics graphical user interface to R. *Journal of statistical software* 14, 1-42 (2005).

3.7 Supplementary information

Suplementary Table S3.1.- Spontaneous cerium dissolution in the exposure media for all CNPs was tested by performing ICP-MS analyses of ultrafiltrated samples (10 mg/l).

Sample	Concentration (mg/l)	Stand. Dev
CNP1	0,00045	4.13%
CNP2	0,00001	29.22%
CNP3	0,00081	8.95%
CNP4	0,00003	4.05%
CNP5	n.d.*	-
CNP6	n.d.*	-
CNP7	n.d.*	-
***No detected**		

Supplementary Figure S3.1.- Effect of free ion Ce^{3+} on growth of *P. subcapitata*.

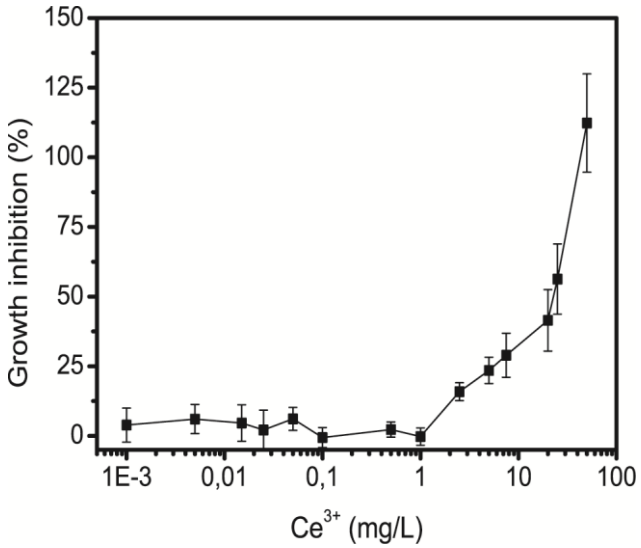

Supplementary Table S3.2.- Summary table of correlation analyses between algal growth inhibition and different tested factors, showing the adjusted R^2 values and their associated *p*-values (ANOVA, F<P). α = 0.05 is stablished as significance criterion (marked by asterisks).

Tested factors	R^2	*p*-value
Surface Ce^{3+}	0.706	0.047*
ζ-Potential	0.693	0.049*
Nominal Size	0.007	0.384
Effective Size	0.152	0.281

Supplementary Figure S3.2. Box plots which show agal growth inhibition as function of nanoparticle shape (cube: CNP4, rod: CNP3 and sphere: CNP1, CNP2 and CNP5; Figure S2a) and just as function of spheric-shaped nanoceria (CNP1, CNP2 and CNP5; Figure S2b). A one way ANOVA coupled with Tukey's HSD (honestly significant difference) post-hoc test was performed for comparison of means. Statistically significant differences ($\alpha = 0.05$) are marked by asterisks.

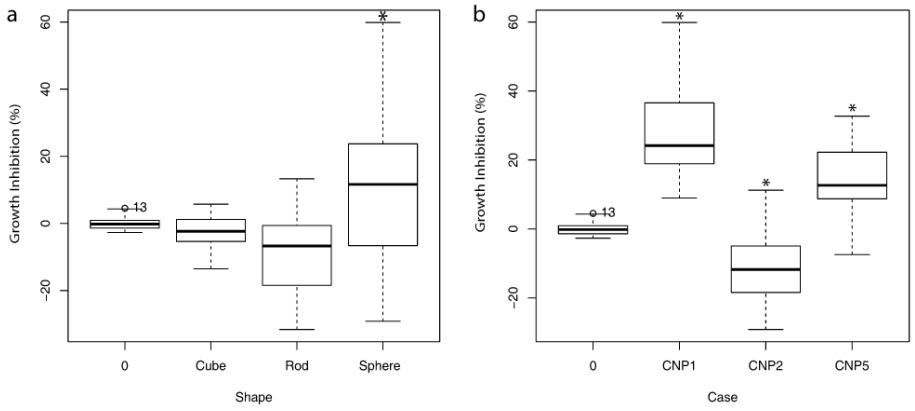

Suplementary Table S3.3.- ζ-potential and effective diameter of CNP1 and CNP2 with the addition of Fe or phosphate.

10 mgL^{-1} OECD medium						
	0.1 mM Fe			0.2 mM Phosphate		
Sample Name	**ζ-potential (mV)**	**Effective Diameter (nm)**	**PDI***	**ζ-potential (mV)**	**Effective Diameter (nm)**	**PDI***
CNP1	10.15 ± 0.9	787.3	0.979	-19.9 ± 0.6	817.2	0.53
CNP2	-15.30 ± 1.9	1073	0.362	-10.1 ± 1.1	450.7	0.57

*PDI=Polydispersity index

Supplementary Figure S3.3.- Detection of H_2O_2 using the Amplex® Red Hydrogen Peroxide/Peroxidase Assay Kit. Reactions containing 50 µM Amplex® Red reagent, 0.1 U/mL HRP and the indicated amount of CNP1 (a) or H_2O_2 as standard curve (b) were incubated for 30 minutes at room temperature. The fluorescence (excitation 535 nm, emission 595 nm) was measured on a Fluorostar Omega plate reader (BMG LABTECH GmbH, Germany). Background fluorescence, determined for a control reaction (H_2O), has been subtracted from each value.

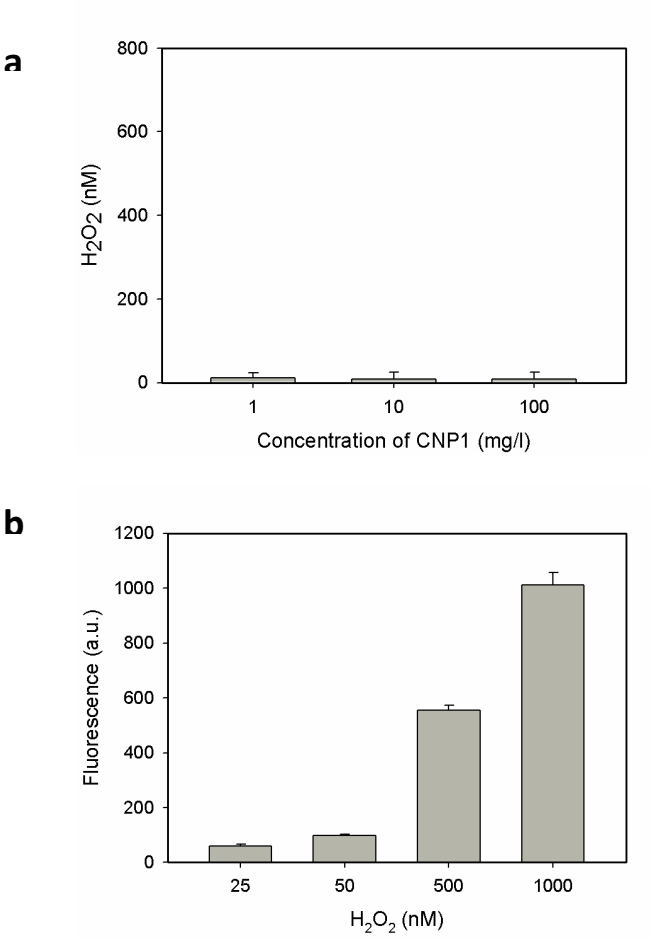

Supplementary Table S3.4.- Composition of the OECD TG 201 medium.

Component	OECD	
	mg/L	mM
$NaHCO_3$	50.0	0.595
$NaNO_3$	15.0	0.280
NH_4Cl		
$MgCl_2 \cdot 6(H_2O)$	12.0	0.0590
$CaCl_2 \cdot 2(H_2O)$	18.0	0.122
$MgSO_4 \cdot 7(H_2O)$	15.0	0.0609
K_2HPO_4	1.60	0.00919
KH_2PO_4		
$FeCl_3 \cdot 6(H_2O)$	0.0640	0.000237
$Na_2EDTA \cdot 2(H_2O)$	0.100	0.000269
H_3BO_3	0.185	0.00299
$MnCl_2 \cdot 4(H_2O)$	0.415	0.00210
$ZnCl_2$	0.00300	0.0000220
$CoCl_2 \cdot 6(H_2O)$	0.00150	0.00000630
$Na_2MoO_4 \cdot 2(H_2O)$	0.00700	0.0000289
$CuCl_2.2(H_2O)$	0.00001	0.00000006

CHAPTER 4

INTERNALIZATION AND TOXICOLOGICAL MECHANISMS OF UNCOATED AND PVP-COATED CERIUM OXIDE NANOPARTICLES IN THE FRESHWATER ALGA CHLAMYDOMONAS REINHARDTII

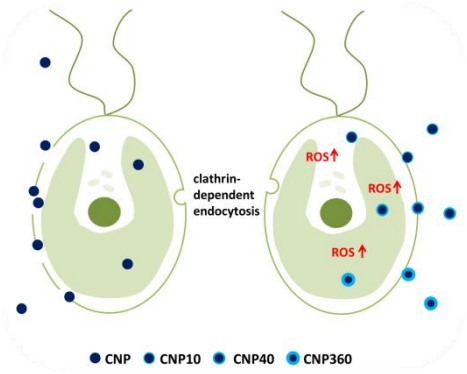

CHAPTER 4. INTERNALIZATION AND TOXICOLOGICAL MECHANISMS OF UNCOATED AND PVP-COATED CERIUM OXIDE NANOPARTICLES IN THE FRESHWATER ALGA CHLAMYDOMONAS REINHARDTII

4.1 Abstract

Due to the wide range of applications of cerium oxide nanoparticles (CNPs), an environmental assessment of their biological effects using environmentally relevant species becomes of high importance. There are contradictory reports on the effects of CNPs, which may be related to the use of different types of nanoparticles and coatings. It has been shown that the catalytic activity of CNPs is influenced by the type of coating and shell thickness. CNPs may act as an oxidant causing toxicity or as an antioxidant able to scavenge free radicals. As a consequence of such complexity, the toxicological behaviour of these nanoparticles is still poorly understood. Moreover, little is known about the internalization process of CNPs in algae. There is evidence of CNP-internalization by *Chlamydomonas reinhardtii (C. reinhardtii)*, but the internalization mechanism and route of uptake are still unknown. In this study, we used an uncoated and different polyvinylpyrrolidone(PVP)-coated CNPs with the aim of identifying their toxicological mechanisms in *C. reinhardtii* and exploring their possible internalization. PVP coated-CNPs significantly increased the formation of reactive oxygen species in exposed cells, indicating that oxidative stress is an important toxicity mechanism for these particles. Direct contact and damage through the cellular membrane

was identified as the mechanism causing the toxicity of uncoated nanoparticles. Using different endocytosis inhibitors, the clathrin-dependent endocytosis revealed as the main internalization route for all nanoparticles. However, due to the fact that uncoated uncoated CNPs provoked severe cellular membrane damage, direct pass of nanoparticles through membrane holes could not be discarded. To our knowledge, this is the first report with evidences of direct linking between nanoparticle internalization and a specific endocytic pathway. The results presented here will help to unravel the toxicological mechanism and behaviour of CNPs and provide input information for the Environmental Health and Safety assessment of CNPs.

4.2 Introduction

Surface coatings of nanoparticles are applied to selectively change or influence several particle properties [1]. The surface of a particle can be covered with a wide variety of substances such as dendrimers [2], polymers [3], silica [4], peptides [5] or polysaccharides [6]. The increase of particle stability [7], the prevention of particle core dissolution [7], the protection of particle functionality or the enhacement of biocompatibility [8] are some different purposes by which those coatings are used.

Cerium oxide nanoparticles (CNPs) have become an exceptionally versatile material due to their high surface area and redox-active nature [9, 10]. A diversity of applications has emerged for them thanks to their singular surface chemistry as electrochemical bio-sensors [11], radiation protector [12], corrosion-resistant coatings [13] and antioxidant agents in the biomedical field [14-16], among others [10]. Controlling the surface properties of CNPs is essential for them to behave as designed. As nanoobject, the reactivity of CNPs strongly depend on nanoparticle size. However, it has also been shown that surface coatings also play a significant role [17]. In recent years, CNPs have been synthesized and functionalized with a variety of molecules such as small ligands [18], polymers [19, 20], surfactants [21] and other organic molecules [22] using different strategies [23].

Due to their variety of applications and volume of use CNPs may be released to the aquatic environment, where the exposure of aquatic organisms is unavoidable. Until now, several authors showed that CNPs may cause some harmful effects in different environmentally relevant microorganisms [24-27]. Considerable efforts are being conducted in the scientific community in order

to untangle the toxicological mechanisms of CNPs [26, 28], which is a difficult task due to the existence of contradictory results [27, 29-31]. Recently, it has been shown that internalization processes might be involved in the effects of CNPs in the model aquatic algae *Chlamydomonas reinhardtii* (*C. reinhardtii*) [32], but it is unclear how CNPs can pass through cell envelopes.The cell wall constitutes the first barrier with a pore diameter in the 5-20 nm range [33]. Overall, whether CNPs are internalized by using some endocytic routes or not is not fully undertstood in green algae yet. Besides, futher research is needed to determine the effect of coatings on nanoparticle uptake. In this regard, some results point towards an enhanced internalization of nanomaterials with organic coatings [32, 34, 35].

Besides, the biological effect of different types of coatings in the toxicity of CNPs towards environmentally relevant microorganisms has not been completely assessed. Whether CNPs are being synthesized with coatings to enhance their colloidal stability, they, thus, should be evaluated even with those coatings as they will be possibly encountered in the environment in that form. In this study, we used neat and and PVP-coated CNPs with the aim of identifying the mechanism by which they affect the green alga C. reinhardtii. Attention was focused on the impact of different coatings and on the potential routes of uptake and internalization.

4.3 Materials and methods

4.3.1 Synthesis of CNPs

Three CNPs were synthesized using the method described by Briffa et al [36]. Briefly, 130 mg of $Ce(NO_3)_3$ were dissolved in a 5 mM solution of

polyvinylpyrrolidone (PVP), with different molecular weights (10, 40 and 360 kDa). The mixture was heated for 3 h at 105 ºC, after which the reaction was stopped by immersion in cold water. When the reaction mixture was cooled, excess PVP was removed by adding acetone to the solution in a 4:1 (acetone:particle suspension) volume ratio and then centrifuged at 4000 rpm for 10 min. The pellet was retained and the excess liquid was discarded. The pellet was re-suspended in double distilled water (ddH_2O). This procedure was repeated to ensure all excess PVP was removed. Finally, the nanoparticles were redispersed in ddH_2O and stored at room temperature in the dark. CNPs without coating were also prepared and tested.

4.3.2 Characterization of CNPs suspension

Synthesized CNPs were thoroughly characterized using different techniques. The optical properties were analysed using Ultraviolet–Visible Spectrophotometer (Perkin Elmer, Lambda 750 S, 60 mm Int. Sphere). Hydrodynamic diameter and ζ-potential of the CNP suspensions in the different assay conditions were measured by Dynamic light scattering (DLS) and electrophoretic light scattering respectively using a Zetasizer Nano ZS particle size analyzer from Malvern Instruments Ltd. Measurements were essentially as described elsewhere [37]. Colloidal stability was measured both in distilled water and algae culture medium (six times diluted Tris-Acetate-Phosphate, TAP/6 [38]).

4.3.3 Biological end-points

Growth inhibition experiments using *C. reinhardtii* were performed in TAP/6 medium essentially as described in the standard OECD TG 201. Exposure experiments to CNPs suspensions were carried out in 12 mL of TAP/6 culture medium in 25 mL flasks. Growth inhibition experiments were performed for 72 h under the same experimental conditions using a set of serial dilutions at least in triplicate. The effect of CNPs on the growth of microalgae was assessed by measuring the optical density at 750 nm after 72 h of exposure.

4.3.4 Flow cytometric analyses (FCM)

FCM analyses of *C. reinhardtii* cells were performed on a Cytomix FL500 MPL flow cytometer equipped with an argon-ion excitation wavelength (488 nm), detector of forward (FS) and side (SS) light scatter and four fluorescence detectors (Beckman Coulter Inc., Fullerton, CA, USA), as described previously [26]. The intracellular reactive oxygen species (ROS), superoxide anion and hydrogen peroxide produced by *C. reinhardtii* were measured by means of the cell permeable fluorescent dye dihydrorhodamine 123 (DHR 123) and hydroethidine (HE), respectively. Changes in cytoplasmic membrane potential were evaluated with the probe $DiBAC_4(3)$. FCM was also used to detect cells with cell membrane damage by using the fluorescent probe Propidium Iodide (PI) and cells with altered metabolic activity by using Fluorescein Diacetate (FDA). Data acquisition was performed using MXP-2.2 software, and the analyses were performed using CXP-2.2 and Flowing 2.5.1 software. Fluorescence was analyzed in Log mode. Cells were incubated with the appropriate fluorochrome for each parameter at room temperature and in the dark, after 24 h of CNPs exposure, prior to FCM analyses. All fluorochrome stock solutions were prepared in dimethyl sulfoxide (DMSO) and stored at −20

°C, with the exception of the solution of propidium iodide (PI), which was made in ddH_2O and stored at 4 °C. The fluorochrome concentrations and incubation times were reported elsewhere [39]. Three independent experiments with triplicate samples were carried out for each parameter.

4.3.5 Internalization studies

In order to determine the amount of CNPs inside cells, the algal cells were incubated with 10 mg/L CNPs for 12 h and 48 h. Then, they were collected by centrifugation (4000 rpm) and the supernatant recovered to determine the amount of free suspended CNPs. 20 mM EDTA was used to remove the CNPs bound onto the cell wall [40] and the samples were again centrifuged. This process was repeated three times and the supernatant was used to calculate the content of CNP measured as Ce bound to the algal cells. The remaining algal pellet was acid-digested for 12 h to calculate the intracellular Ce. The Ce content in all samples was measured by Inductively Coupled Plasma Mass Spectrometry (ICP-MS) on an ICP-MS NexION 300XX from Perkin-Elmer. Sodium azide (NaN_3; 0.25 mM), monodansylcadaverine (MDC; 0.2 mM) and 5-(N-ethyl-N-isopropyl)-amiloride (EIPA; 10 µM) were used as endocytic inhibitors to evaluate the impact of endocytosis on CNPs internalization [41, 42]. *In-vivo* fluorescence of chlorophyll a (Chl *a*) (485 nm/645 nm excitation/emission) was measured at 48 h as biomass surrogate on a Synergy HTmulti-mode microplate reader (BioTek, USA).

4.3.6 Statistical Analysis

Means and standard deviation values were calculated for each treatment from three independent replicate experiments. Statistical analyses were performed by using R software 3.0.2. (The R Foundation for Statistical Computing©) and Rcmdr 2.0–4 package. A one way ANOVA coupled with Tukey's HSD (honestly significant difference) post-hoc test was performed for comparison of means. Statistically significant differences were considered to exist when $p < 0.05$.

4.4 Results and discussion

4.4.1 Physicochemical characterization of CNPs

Three CNPs were synthesized with three different molecular weight PVP coatings (10 kDa, 40 kDa and 360 kDa). Accordingly, the CNPs were named CNP10, CNP40 or CNP360, depending on the PVP chain length. CNPs without coating were referred to as CNP. Table 4.1 shows the physicochemical characteristics of the four CNPs at 10 mg/L suspended in the algal exposure medium. The particles had a negative surface charge (ζ-potential) in TAP/6 with similar values in the (-7)-(-13) mV range. There was a slight increase in the effective diameter based on the PVP-chain length: 6.0 nm, 8.2 nm and 12.5 nm for CNP with 10 kDa-PVP, 40 kDa-PVP and 360 kDa-PVP, respectively; whereas the uncoted CNP had a diameter size of 10.2 nm.

Table 4.1: Physicochemical properties of the tested CNPs.

Sample Name	PVP chain length	ζ -Pot (mV)	DLS Diameter (nm)	PDI*
CNP	-	-13.0 ± 1.1	10.2 ± 0.5	0.38
CNP10	10k	-8.11 ± 0.8	6.0 ± 0.1	0.18
CNP40	40k	-7.25 ± 0.4	8.2 ± 0.6	0.15
CNP360	360k	-9.23 ± 0.3	12.5 ± 0.1	0.28

*Polydispersity Index

4.4.2 Toxicity of the CNPs towards *C. reinhardtii growth*

Figure 1 shows the effect of 72 h exposure to CNPs on the growth of *C. reinhardtii* in the 1-50 mg/L range. CNP was more toxic at low concentrations (1-10 mg/L) than PVP-coated CNPs, irrespective of PVP molecular weight. However, CNP10 and CNP40 resulted in higher growth inhibition at 50 mg/L than CNP360 and CNP. In order to clarify the mechanisms underlying the observed toxicity, several cytotoxicity biomarkers (cell membrane integrity, oxidative stress, metabolic activity and cytoplasmic membrane potential) were analyzed by flow cytometry after 48 h of exposure to 10 mg/L of nanoparticles.

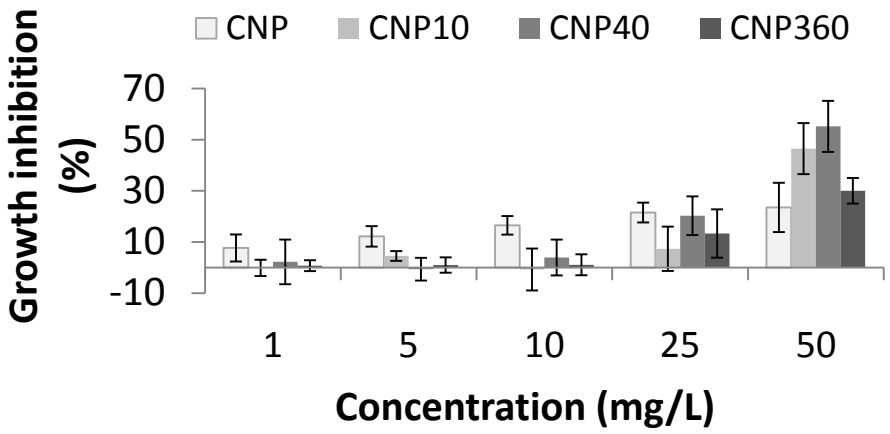

Figure 4.1.- Effect of 72 h exposure to the four CNPs on the growth of *C. reinhardtii*.

4.4.3 The effects of CNPs on relevant cellular biomarkers.

To check the impairment of cytoplasmic membrane, the fluorescent dye PI was used and analyzed by flow cytometry measurements. The flow cytograms

showed the presence of two cell subpopulations, H-2 and H-3, in control cultures (Figure 2A). H-2 comprised around 89% of total cells and corresponded to intact cells (intact membranes). H-3 subpopulation comprised cells with damaged membranes (around 10 % of total cells). FCM results showed that only CNP significantly ($p < 0.05$) affected membrane integrity by increasing the H-3 subpopulation to 21 %, indicating a clear damage to cell membrane. The effect of CNPs on cytoplasmic membrane potential of *C. reinhardtii* was also studied by flow cytometry using the fluorescent dye DIBAC4(3) (Figure 2B). Flow cytograms showed two clear subpopulations (H-2 and H-3) in control cells. H-2 was the largest one comprising around 96 % of total cells while the H-3 subpopulation (showing a slight membrane depolarization) accounted for 4.2 % of total cells. CNP, CNP10 and CNP40 considerably increased membrane depolarization by 13.1 %, 27.4 % and 36.9 % of total cells (H-3 subpopulation; Figure 2B), respectively. CNP360 did not have any significant effect on this parameter. Furthermore, as shown in Figure 2C, the percentage of metabolically non-active cells (H-3), determined by flow cytometry using FDA, increased significantly ($p < 0.05$) in cultures exposed to all treatments, in comparison with control levels. However, CNP10 and CNP40 had the highest percentages with 34 % and 35 % of total cells with a lower metabolic activity.

The production of intracellular ROS in exposed cells has been identified as an important toxicity mechanism for CNPs [26, 43]. The fluorescent indicators HE and DHR123 were used to determine intracellular superoxide anion ($O_2^{\bullet -}$) and H_2O_2, respectively (Figure 3 A and B), by flow cytometry. The CNPs coated with PVP (CNP10, CNP40 and CNP360) caused a significant increase in the intracellular level of both oxidative species, while CNP did not produce any alterations. It is worth noting that CNP40 led to the highest level of

intracellular hydrogen peroxide. The alterations of mitochondrial ROS homeostasis and cellular lipid peroxidation were revealed by MitoTracker-selective probes and C4-BODIPY fluorescent dye, respectively. As shown in Figure 3C, mitochondria were affected in all treated cells with respect to control cells; the highest level of damage being produced by CNP40, followed by CNP10, CNP360 and CNP. Figure 3D shows the results of cellular lipid peroxidation. Statistically significant differences were only detected for CNP-40.

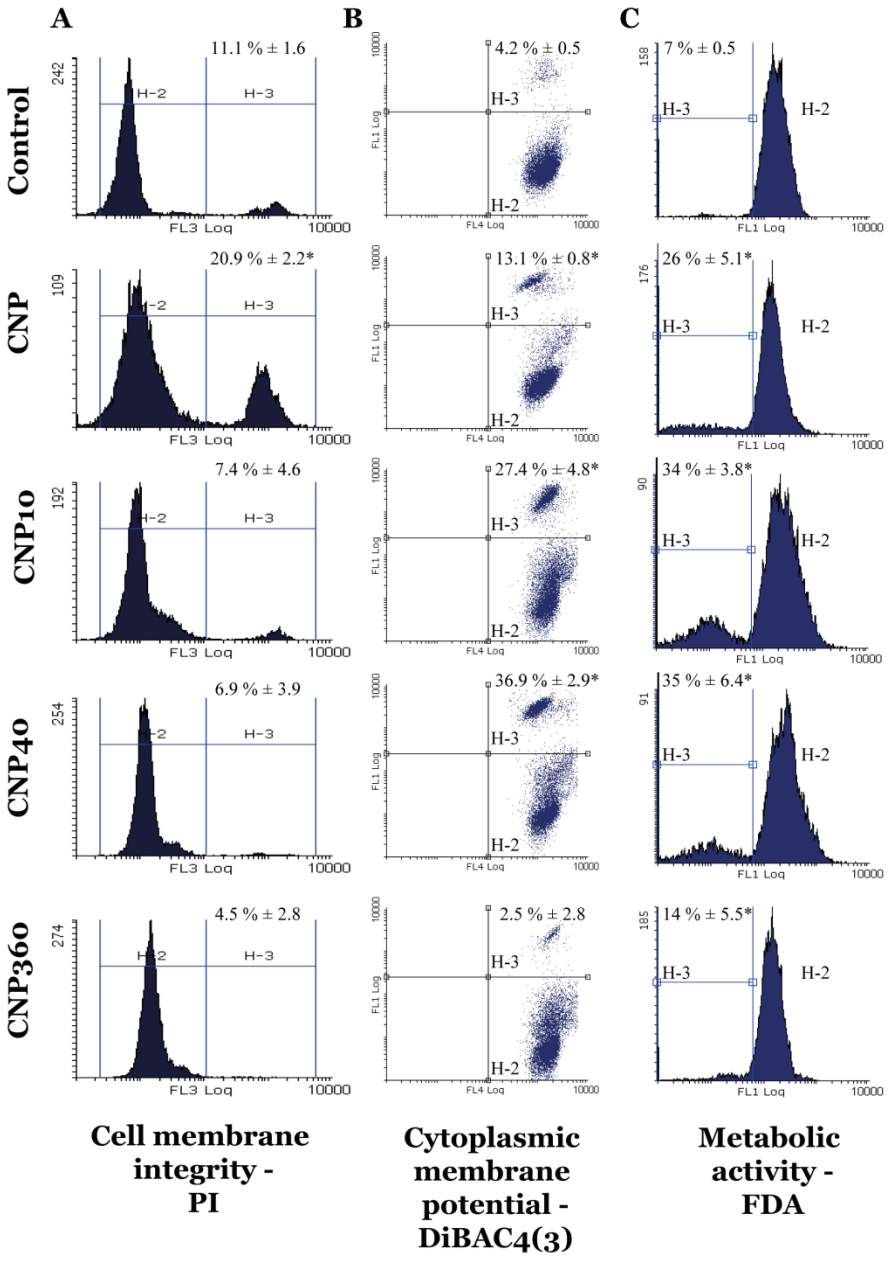

Figure 4.2.- Effect of CNPs on cell membrane integrity (A), cytoplasmic membrane potential (B) and metabolic activity (C) of *C. reinhardtii* by FCM using the fluorochromes PI, $DiBAC_4(3)$ and FDA.

.

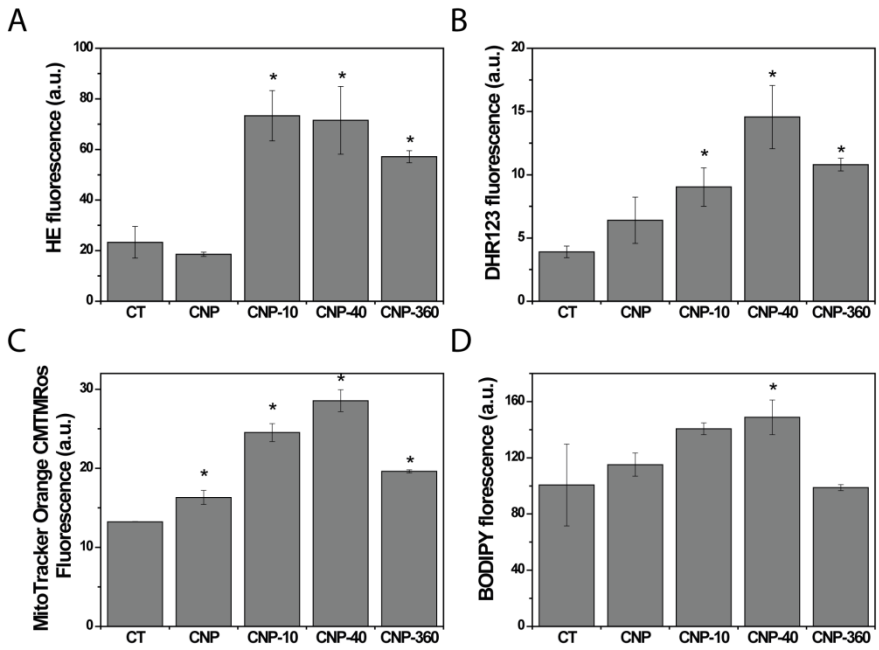

Figure 4.3.- Effect of CNPs on intracellular superoxide anion and hydrogen peroxide levels of *C. reinhardtii* by FCM using the fluorochrome HE (A) and DHR123 (B), respectively. Alterations derived of oxidative stress in mitochondria and intracellular lipid peroxidation are also shown in (C) and (D), respectively.

4.4.4 Internalization of CNPs

To investigate the internalization of CNPs, the distribution of cerium in the culture medium (Figure 4A and D), adsorbed to the cell wall (Figure 4B and E) and measured inside the cells (Figure 4C and F) was analyzed by ICP-MS after 12 h (Figure 4A-C) or 48 h (Figure 4D-F) of exposure. There were no differences in the cerium content in the culture medium between nanoparticles after 12 h of exposure (Figure 4A). Uncoated nanoparticle led to more Ce attached to the cell wall than PVP coated nanoparticles (Figure B),

but much less inside the cell (Figure C) where no differences were found between CNP10, CNP40 or CNP360. Different behavior was observed after 48 h of contact between CNPs and algal cells. CNP appeared prominently in suspension more than the other nanoparticles (Figure 4D), but PVP coated nanoparticles preferentially attached to the cell wall. Also, CNP internalized in higher amount than the other nanoparticles after 48 h.

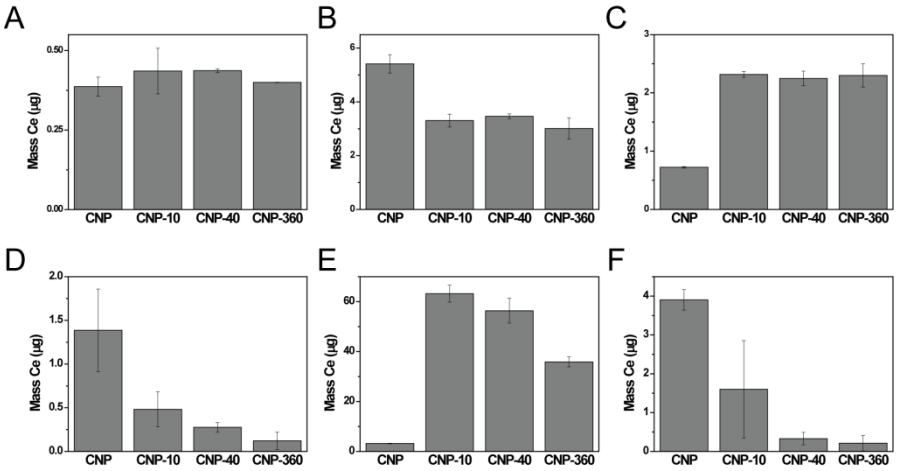

Figure 4.4.- Analysis of the Ce content in three different compartments after 12 h (A-C) and 48 h (D-F) of exposure to CNP, CNP10, CNP40 and CNP360. (A and D) The Ce content as CNPs suspended in the medium. (B and E) The Ce content as CNPs adsorbed to the algal cell envelopes. (C and F) The Ce content inside cell as CNPs internalized.

4.4.5 Endocytosis inhibitors and route of uptake

Different endocytosis inhibitors were used in order to clarify the uptake route involved in the internalization of CNPs. MDC, EIPA and NaN_3 were used to block the clathrin dependent endocytosis, macropinocytosis and energy dependent endocytosis, respectively. These compounds did not cause any harmful effect at the concentrations used in this study (see Supplementary Material Figure S1). It has been shown that several toxics can increase the fluorescence of Chl *a* [44], so this biological endpoint was used to decipher the effect of inhibitors in the internalization of CNPs. We assumed that an inhibitor blocked an endocytic route and, thus, avoided the entry of CNPs if the fluorescence of Chl *a* decreased until control levels. As shown in Figure 4.5, the inhibitor associated with clathrin dependent endocytosis, MDC, was

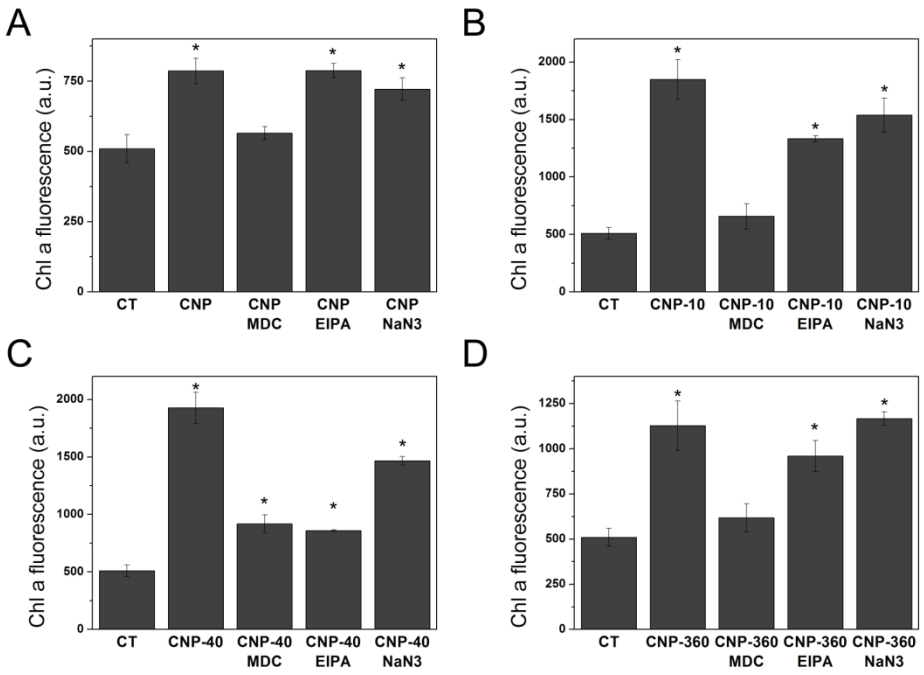

Figure 4.5.- Analysis of the effect of MDC, EIPA and NaN_3 on the increase of Chl *a* fluorescence caused by CNP, CNP10, CNP40 and CNP360 in *C. reinhardtii*.

able to block the entry of CNP, CNP10 and CNP360 as the Chl *a* fluorescence reached the level displayed by the control sample. The other inhibitors also blocked CNPs entry, but statistically significant differences were not found as compared to controls.

4.5 Discussion

The main finding of this study was that CNPs was able to internalize and provoke a strong toxic response in the green alga *C. reinhardtii*, mediated by an increase of intracellular ROS or direct damage to the cytoplasmic membrane. Several studies have previously reported that CNPs are toxic to algae and other aquatic organisms [24, 25, 27], mechanistic studies are less abundant. Here, a combined approach of cellular and physiological analyses has provided novel insights into toxicological mechanisms of coated and uncoated CNPs in the green alga. This is also the first time internalization and toxic mechanisms could be related and associated to CNPs.

PVP-CNPs exerted toxicity by means of a different toxicological mechanism than uncoated CNP. According to the results obtained in this work, cellular membrane integrity was only compromised by CNP (Figure 2A), indicating that the initial effect of CNP takes place by interaction with the algal membrane. Conversely, PVP-coated nanoparticles did not affect the cytoplasmic membrane, but induced a strong increment in intracellular ROS (both $O_2^{\bullet -}$ and H_2O_2; Figure 3A-B), which led to an increase in oxidative-driven mitocondrial alterations (Figure 3C) stress and, also, in the content of intracellular peroxidized lipids for the specific case of CNP40. There was no increase in the intracellular ROS when algal cells were exposed to CNP, demonstrating that

the direct physical damage to the cellular membrane was the main mechanism explaining the observed toxicity. Membrane damage is possibly the main pathway of entry of uncoated CNP into the cells.

Cerium internalization depended on the exposure time: after 12 h, internalization was found mostly for PVP-coated nanoparticles while after 48 h of exposure it was higher for CNP and CNP with the smallest coating (CNP10). Once the membrane is damaged, CNP may pass through more easily and accumulate inside cells (Figure 4F). PVP-coated CNPs also interacted with the cellular membrane since they caused an increase of the percentage of depolarized cells in comparison with control cells. Besides, they were found in higher amount adsorbed to the cell envelopes after 48 h of exposure (Figure 4E). The explanation is that PVP coating protected the cells from the direct contact with the nanoparticle core, but enhaced nanoparticle internalization during the early stages of exposure (12 h; Figure 4C). Once inside the cells, PVP-coated CNPs produced alterations in ROS homeostasis by increasing the amount of $O_2^{\bullet -}$ and H_2O_2.

It has been shown that there exist several routes of endocytosis in eucaryotic organisms [45] that explain the internalization of nanomaterials in several environmentally revelant eukaryotic organisms [46-49]. Accordingly, Wang et al [46] showed that CdTe Quantum Dots (QD) could enter the freshwater alga *Ochromonas danica* directly through macropinocytosis. Moreover, it has been reported that clathrin pathway played an important role in the endocytosis process in a multicellular green algae (*Chara australis*) [50]. Nanoparticle internalization has been recently observed in *C. reinhardtii* for QdTe/CdS QD [51], CeO_2 [32], Ag [34], PAMAM-dendrimers [52] and CuO [35] nanoparticles. In the present study, we have shown that clathrin-dependent endocytosis is

the main route of CNPs entry into the cells of C. *reinhardtii* as MDC (molecule that stabilizes clathrin-coated pits) blocked the entry of all CNPs, avoiding their toxic effects related with the increment of Chl *a* fluorescence. Previously, it has been shown that *C. reinhardtii* possess a chlatrin-mediated endocytosis pathway [53, 54] and that nanoparticles can be internalized. However, as far as we know, this is the first time that it is shown that clathrin pathway is the main route of entry of nanoparticles into C reinhardtii cells. Futher research is needed for determining the effect of other coatings in CNPs uptake and also, the optimal PVP-chain length that could favor the internalization of nanoparticles. The results shown in this work suggest that lower molecular weights, such as 10-40 kDa might be better to interact with the cellular envelopes than larger chain length such as 360 kDa.

4.6 Conclusions

In this work, we have reported a thorough study on the toxicological effects of uncoated and PVP-coated CNPs to *C. reinhardtii*. Monodispersed nanoparticles of cerium oxide and PVP-coated cerium oxide were synthesized and physicochemically characterized in the exposure media. The toxicity of the bare cerium oxide nanoparticles (CNP) took place by damage in cytoplasmic membrane and mitochondrial ROS alterations, which eventually caused a decrease in metabolic activity. PVP-coated nanoparticles exerted their toxicity by the intracellular ROS formation without direct damage to the cell membrane. Different degrees of cell damage were found depending on PVP chain length. CNP-40 was the most toxic nanoparticle, followed by CNP10. Moreover, internalization evidences were found for all nanoparticles, but, after 48 h of exposure, CNP was internalized in higher proportion than PVP-

coated CNPs, which predominantly appeared attached to the algal envelopes. The studies performed using endocytosis inhibitors indicated that clathrin dependent endocytosis is the main pathway for nanoparticle entry. The results shown here highlight the importance of assessing the toxicity of CNPs as they are intended to be used and found in the environment as the fact that the toxicological mechanism could be significantly different, depending on nanoparticle coating. This information will be useful for shedding light regarding the contradictory effects of CNPs that have been reported in the scientific literature and for the synthesis of safer-by-design nanomaterials.

4.7 References

[1] Sperling RA, Parak W. 2010. Surface modification, functionalization and bioconjugation of colloidal inorganic nanoparticles. *Philosophical Transactions of the Royal Society of London A: Mathematical, Physical and Engineering Sciences* 368:1333-1383.

[2] Wang YA, Li JJ, Chen H, Peng X. 2002. Stabilization of inorganic nanocrystals by organic dendrons. *Journal of the American Chemical Society* 124:2293-2298.

[3] Grubbs RB. 2007. Roles of polymer ligands in nanoparticle stabilization. *Polymer Reviews* 47:197-215.

[4] Guerrero-Martínez A, Pérez-Juste J, Liz-Marzán LM. 2010. Recent progress on silica coating of nanoparticles and related nanomaterials. *Advanced materials* 22:1182-1195.

[5] Roma-Rodrigues C, Heuer-Jungemann A, Fernandes AR, Kanaras AG, Baptista PV. 2016. Peptide-coated gold nanoparticles for modulation of angiogenesis in vivo. *International Journal of Nanomedicine* 11:2633.

[6] Uthaman S, Lee SJ, Cherukula K, Cho C-S, Park I-K. 2015. Polysaccharide-coated magnetic nanoparticles for imaging and gene therapy. *BioMed research international* 2015.

[7] Li X, Lenhart JJ, Walker HW. 2012. Aggregation kinetics and dissolution of coated silver nanoparticles. *Langmuir : the ACS journal of surfaces and colloids* 28:1095-1104.

[8] Thanh NT, Green LA. 2010. Functionalisation of nanoparticles for biomedical applications. *Nano Today* 5:213-230.

[9] Sayle TX, Molinari M, Das S, Bhatta UM, Möbus G, Parker SC, Seal S, Sayle DC. 2013. Environment-mediated structure, surface redox activity and reactivity of ceria nanoparticles. *Nanoscale* 5:6063-6073.

[10] Reed K, Cormack A, Kulkarni A, Mayton M, Sayle D, Klaessig F, Stadler B. 2014. Exploring the properties and applications of nanoceria: is there still plenty of room at the bottom? *Environmental Science: Nano* 1:390-405.

[11] Chaturvedi P, Vanegas D, Taguchi M, Burrs S, Sharma P, McLamore E. 2014. A nanoceria–platinum–graphene nanocomposite for electrochemical biosensing. *Biosensors and Bioelectronics* 58:179-185.

[12] Colon J, Herrera L, Smith J, Patil S, Komanski C, Kupelian P, Seal S, Jenkins DW, Baker CH. 2009. Protection from radiation-induced pneumonitis using cerium oxide nanoparticles. *Nanomedicine: Nanotechnology, Biology and Medicine* 5:225-231.

[13] Zandi Zand R, Verbeken K, Adriaens A. 2013. Evaluation of the corrosion inhibition performance of silane coatings filled with cerium salt-activated nanoparticles on hot-dip galvanized steel substrates. *International Journal of Electrochemical Science* 8:4927-4940.

[14] Pulido-Reyes G, Das S, Leganés F, Silva S, Wu S, Self W, Fernández-Piñas F, Rosal R, Seal S. 2016. Hypochlorite scavenging activity of cerium oxide nanoparticles. *RSC Advances* 6:62911-62915.

[15] Xu C, Liu Z, Wu L, Ren J, Qu X. 2014. Nucleoside Triphosphates as Promoters to Enhance Nanoceria Enzyme-like Activity and for Single-Nucleotide Polymorphism Typing. *Advanced Functional Materials* 24:1624-1630.

[16] Xu C, Qu X. 2014. Cerium oxide nanoparticle: a remarkably versatile rare earth nanomaterial for biological applications. *NPG Asia Materials* 6:e90.

[17] Lee SS, Song W, Cho M, Puppala HL, Nguyen P, Zhu H, Segatori L, Colvin VL. 2013. Antioxidant properties of cerium oxide nanocrystals as a function of nanocrystal diameter and surface coating. *ACS nano* 7:9693-9703.

[18] Qi L, Sehgal A, Castaing J-C, Chapel J-P, Fresnais J, Berret J-F, Cousin F. 2008. Redispersible hybrid nanopowders: cerium oxide nanoparticle complexes with phosphonated-PEG oligomers. *ACS nano* 2:879-888.

[19] Asati A, Santra S, Kaittanis C, Nath S, Perez JM. 2009. Oxidase-like activity of polymer-coated cerium oxide nanoparticles. *Angewandte Chemie* 48:2308-2312.

[20] Karakoti AS, Singh S, Kumar A, Malinska M, Kuchibhatla SV, Wozniak K, Self WT, Seal S. 2009. PEGylated nanoceria as radical scavenger with tunable redox chemistry. *Journal of the American Chemical Society* 131:14144-14145.

[21] Wu Z, Zhang J, Benfield RE, Ding Y, Grandjean D, Zhang Z, Ju X. 2002. Structure and chemical transformation in cerium oxide nanoparticles coated by surfactant cetyltrimethylammonium bromide (CTAB): an X-ray absorption spectroscopic study. *The Journal of Physical Chemistry B* 106:4569-4577.

[22] Hijaz M, Das S, Mert I, Gupta A, Al-Wahab Z, Tebbe C, Dar S, Chhina J, Giri S, Munkarah A. 2016. Folic acid tagged nanoceria as a novel therapeutic agent in ovarian cancer. *BMC cancer* 16:220.

[23] Das S, Dowding JM, Klump KE, McGinnis JF, Self W, Seal S. 2013. Cerium oxide nanoparticles: applications and prospects in nanomedicine. *Nanomedicine (London, England)* 8:1483-1508.

[24] Rodea-Palomares I, Boltes K, Fernandez-Pinas F, Leganes F, Garcia-Calvo E, Santiago J, Rosal R. 2011. Physicochemical characterization and ecotoxicological assessment of CeO2 nanoparticles using two aquatic microorganisms. *Toxicological sciences : an official journal of the Society of Toxicology* 119:135-145.

[25] Artells E, Issartel J, Auffan M, Borschneck D, Thill A, Tella M, Brousset L, Rose J, Bottero J-Y, Thiéry A. 2013. Exposure to cerium dioxide nanoparticles differently affect swimming performance and survival in two daphnid species. *PloS one* 8:e71260.

[26] Pulido-Reyes G, Rodea-Palomares I, Das S, Sakthivel TS, Leganes F, Rosal R, Seal S, Fernández-Piñas F. 2015. Untangling the biological effects of

cerium oxide nanoparticles: the role of surface valence states. *Scientific Reports* 5:15613.

[27] Manier N, Bado-Nilles A, Delalain P, Aguerre-Chariol O, Pandard P. 2013. Ecotoxicity of non-aged and aged CeO2 nanomaterials towards freshwater microalgae. *Environmental pollution* 180:63-70.

[28] Mittal S, Pandey AK. 2014. Cerium oxide nanoparticles induced toxicity in human lung cells: role of ROS mediated DNA damage and apoptosis. *BioMed research international* 2014.

[29] Zhang H, He X, Zhang Z, Zhang P, Li Y, Ma Y, Kuang Y, Zhao Y, Chai Z. 2011. Nano-CeO2 exhibits adverse effects at environmental relevant concentrations. *Environmental science & technology* 45:3725-3730.

[30] Caputo F, De Nicola M, Sienkiewicz A, Giovanetti A, Bejarano I, Licoccia S, Traversa E, Ghibelli L. 2015. Cerium oxide nanoparticles, combining antioxidant and UV shielding properties, prevent UV-induced cell damage and mutagenesis. *Nanoscale* 7:15643-15656.

[31] Chaudhury K, Babu KN, Singh AK, Das S, Kumar A, Seal S. 2013. Mitigation of endometriosis using regenerative cerium oxide nanoparticles. *Nanomedicine : nanotechnology, biology, and medicine* 9:439-448.

[32] Taylor NS, Merrifield R, Williams TD, Chipman JK, Lead JR, Viant MR. 2015. Molecular toxicity of cerium oxide nanoparticles to the freshwater alga Chlamydomonas reinhardtii is associated with supra-environmental exposure concentrations. *Nanotoxicology*:1-10.

[33] Navarro E, Baun A, Behra R, Hartmann NB, Filser J, Miao A-J, Quigg A, Santschi PH, Sigg L. 2008. Environmental behavior and ecotoxicity of

engineered nanoparticles to algae, plants, and fungi. *Ecotoxicology* 17:372-386.

[34] Wang S, Lv J, Ma J, Zhang S. 2016. Cellular internalization and intracellular biotransformation of silver nanoparticles in Chlamydomonas reinhardtii. *Nanotoxicology* 10:1129-1135.

[35] Perreault F, Oukarroum A, Melegari SP, Matias WG, Popovic R. 2012. Polymer coating of copper oxide nanoparticles increases nanoparticles uptake and toxicity in the green alga Chlamydomonas reinhardtii. *Chemosphere* 87:1388-1394.

[36] Briffa S, Lynch I, Trouillet V, Bruns M, Hapiuk D, Liu J, Palmer R, Valsami-Jones E. 2017. Development of scalable and versatile nanomaterial libraries for nanosafety studies: polyvinylpyrrolidone (PVP) capped metal oxide nanoparticles. *RSC Advances* 7:3894-3906.

[37] Gonzalo S, Llaneza V, Pulido-Reyes G, Fernandez-Pinas F, Bonzongo JC, Leganes F, Rosal R, Garcia-Calvo E, Rodea-Palomares I. 2014. A colloidal singularity reveals the crucial role of colloidal stability for nanomaterials in-vitro toxicity testing: nZVI-microalgae colloidal system as a case study. *PloS one* 9:e109645.

[38] Gorman DS, Levine RP. 1965. Cytochrome f and plastocyanin: their sequence in the photosynthetic electron transport chain of Chlamydomonas reinhardi. *Proceedings of the National Academy of Sciences of the United States of America* 54:1665-1669.

[39] González-Pleiter M, Rioboo C, Reguera M, Abreu I, Leganés F, Cid Á, Fernández-Piñas F. 2017. Calcium mediates the cellular response of

Chlamydomonas reinhardtii to the emerging aquatic pollutant Triclosan. *Aquatic toxicology* 186:50-66.

[40] Spedding F, Powell J, Wheelwright EJ. 1956. The stability of the rare earth complexes with N-hydroxyethylethylenediaminetriacetic acid. *Journal of the American Chemical Society* 78:34-37.

[41] Vranic S, Boggetto N, Contremoulins V, Mornet S, Reinhardt N, Marano F, Baeza-Squiban A, Boland S. 2013. Deciphering the mechanisms of cellular uptake of engineered nanoparticles by accurate evaluation of internalization using imaging flow cytometry. *Particle and fibre toxicology* 10:2.

[42] Rejman J, Bragonzi A, Conese M. 2005. Role of clathrin-and caveolae-mediated endocytosis in gene transfer mediated by lipo-and polyplexes. *Molecular Therapy* 12:468-474.

[43] von Moos N, Slaveykova VI. 2014. Oxidative stress induced by inorganic nanoparticles in bacteria and aquatic microalgae--state of the art and knowledge gaps. *Nanotoxicology* 8:605-630.

[44] Eullaffroy P, Vernet G. 2003. The F684/F735 chlorophyll fluorescence ratio: a potential tool for rapid detection and determination of herbicide phytotoxicity in algae. *Water research* 37:1983-1990.

[45] Zhu M, Nie G, Meng H, Xia T, Nel A, Zhao Y. 2013. Physicochemical properties determine nanomaterial cellular uptake, transport, and fate. *Accounts of chemical research* 46:622-631.

[46] Wang Y, Miao A-J, Luo J, Wei Z-B, Zhu J-J, Yang L-Y. 2013. Bioaccumulation of CdTe quantum dots in a freshwater alga Ochromonas danica: a kinetics study. *Environmental science & technology* 47:10601-10610.

[47] Wang Z, Li J, Zhao J, Xing B. 2011. Toxicity and internalization of CuO nanoparticles to prokaryotic alga Microcystis aeruginosa as affected by dissolved organic matter. *Environmental science & technology* 45:6032-6040.

[48] Yue Y, Li X, Sigg L, Suter MJ, Pillai S, Behra R, Schirmer K. 2017. Interaction of silver nanoparticles with algae and fish cells: a side by side comparison. *Journal of nanobiotechnology* 15:16.

[49] Ma S, Lin D. 2013. The biophysicochemical interactions at the interfaces between nanoparticles and aquatic organisms: adsorption and internalization. *Environmental Science: Processes & Impacts* 15:145-160.

[50] Hoepflinger MC, Hoeftberger M, Sommer A, Hametner C, Foissner I. 2017. Clathrin in Chara australis: Molecular Analysis and Involvement in Charasome Degradation and Constitutive Endocytosis. *Frontiers in plant science* 8.

[51] Domingos RF, Simon DF, Hauser C, Wilkinson KJ. 2011. Bioaccumulation and effects of CdTe/CdS quantum dots on Chlamydomonas reinhardtii–nanoparticles or the free ions? *Environmental science & technology* 45:7664-7669.

[52] Gonzalo S, Rodea-Palomares I, Leganes F, Garcia-Calvo E, Rosal R, Fernandez-Pinas F. 2014. First evidences of PAMAM dendrimer internalization in microorganisms of environmental relevance: A linkage with toxicity and oxidative stress. *Nanotoxicology*:1-13.

[53] Merchant SS, Prochnik SE, Vallon O, Harris EH, Karpowicz SJ, Witman GB, Terry A, Salamov A, Fritz-Laylin LK, Maréchal-Drouard L. 2007. The Chlamydomonas genome reveals the evolution of key animal and plant functions. *Science* 318:245-250.

[54] http://www.genome.jp/kegg-bin/show_pathway?cre04144. Endocytosis - Chlamydomonas reinhardtii.

4.8 Supplementary Material

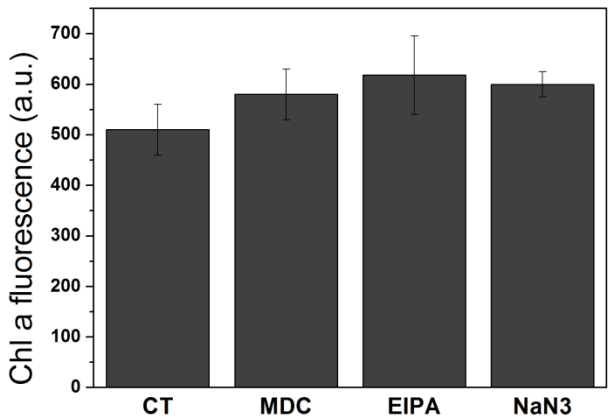

Figure S4.1.- The effect of the different endocytic inhibitors towards chlorophyll *a* fluorescence of *Chlamydomonas reinhardi*. CT: control.

CHAPTER 5

HYPOCHLORITE SCAVENGING ACTIVITY OF CERIUM OXIDE NANOPARTICLES

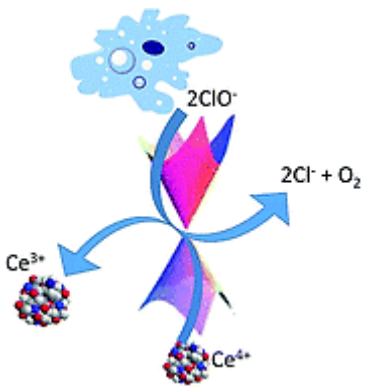

CHAPTER 5. HYPOCHLORITE SCAVENGING ACTIVITY OF CERIUM OXIDE NANOPARTICLES

5.1 Abstract

In this report, we provide evidence that specific synthesis of cerium oxide nanoparticles can scavenge hypochlorite anion, which is a strong extracellular oxidant involved in the inflammatory processes. The scavenging process takes place by a surface reaction involving the evolution of oxygen and the reduction of ce^{4+} to ce^{3+}.

5.2 Introduction

Reactive oxygen species (ROS) or oxidants are associated with different diseases and aging [1]. Among them, HOCl/ClO^- is a strong oxidant produced by activated neutrophils and monocytes. Activated neutrophils or monocytes produce myeloperoxidase, which reacts with hydrogen peroxide and chloride ions giving rise to hypochlorous acid, HOCl, a strong non-selective oxidant [2, 3]. HOCl production is part of the host defense mechanism against microorganisms; however, these properties may involve the risk of tissue damage through the same processes used in the destruction of invading microorganisms. In fact, neutrophil oxidants have been shown to be implicated in the tissue injury associated with inflammatory diseases, including respiratory distress, ischemia-reperfusion injury, acute vasculitis, arthritis, inflammatory bowel diseases, and glomerulonephritis [4].

Antioxidant and some natural compounds have been shown to scavenge hypochlorite such as flavonoids, polyphenols, hydroxycinnamic acids, etc [5-8]. Cerium oxide nanoparticles (CNPs) have recently been shown as an inorganic regenerative antioxidant in biological systems [9]. CNPs are characterized by a complex redox chemistry due to the presence of Ce^{3+} atoms accompanying oxygen vacancies which are surrounded by Ce^{4+} atoms [10]. It has been reported that CNPs display superoxide-dismutase mimetic activity [9], catalase mimetic activity [11] and the capacity to scavenge nitric oxide radicals [12]. Therefore, CNPs could potentially be used in biomedicine to fight against oxidative stress.

Although there are several studies which describe the antioxidant properties of CNPs [13, 14], little is known about the specific process and mechanisms that are taking place. In general, the antioxidant activity of these nanoparticles has been measured indirectly by intermediaries [15, 16] and the reactions and subproducts which are generated after the interaction between CNPs and free radicals have not been fully characterized. Moreover, until now, there has been no evidence that CNPs can scavenge $HOCl/ClO^-$. A complete knowledge of the interaction of all physiological compounds with CNPs is completely necessary before assessing the massively use of CNPs in biomedical applications. In this study, we investigated whether CNPs are capable of scavenging $HOCl/ClO^-$ and explored the reaction mechanism by which this phenomenon occurs. The proposed scavenging method which is shown here improves the speed of scavenging reaction of this particular ROS in comparison with already published articles[17] and clearly shows that it is effective in an in vitro cell model.

5.3 Results and Discussion

It is well established that physicochemical properties of CNPs govern the catalytic activity. Therefore, in this study we have selected four different CNPs (synthesized or commercially available) which have been used in previous studies and named as CNP1 [18], CNP2 [19], CNP3 [12] and CNP4 [18]. Physicochemical properties of the four nanoparticles were thoroughly analyzed and summarized in Table 5.1. In particular, size, morphology, agglomeration status, surface charge and surface Ce^{3+}/Ce^{4+} were measured. These above mentioned parameters were investigated as catalytic activity of CNPs can be highly influenced by these parameters as follows: 1. Size – directly correlated with surface area and density of active site; 2. Morphology and crystallinity –surface energy and stability of the particles; 3. Agglomeration status – directly correlated with available surface for catalytic activity; 4. Surface Ce^{3+}/Ce^{4+} - the presence of both surface oxidation states at nanoscale make nanoparticles catalytically active, CNPs with higher Ce^{3+}/Ce^{4+} scavenge more superoxide radicals whereas lower Ce^{3+}/Ce^{4+} scavenge hydrogen peroxide and nitric oxide radicals [20]. The size and morphology of particles were assessed using High Resolution Transmission Electron Microscopy (HRTEM). They were all round-shaped with particle nominal size in the 3-20 nm range. The Selected area electron diffraction (SAED) pattern revealed that all four particles were crystalline (HRTEM images and SAED pattern are shown in the supplementary document, Supplementary Figure S5.1).

Table 5.1.- Physicochemical characterization of CNPs.

Sample	Surface Ce^{3+} (%)	Shape	ζ-potential (mV)	Effective diameter(DLS) (nm)
CNP1	27	round	52.3 ± 0.5	50.8 ± 0.9
CNP2	40	round	56.5 ± 1.4	58.8 ± 0.8
CNP3	30	round	46.0 ± 2.5	9.4 ± 2.1
CNP4	57	round	18.6 ± 0.6	30.8 ± 2.8

Effective diameter and zeta-potential of the CNPs suspensions were measured by Dynamic light scattering (DLS) and electrophoretic light scattering, respectively (Zetasizer Nano ZS from Malvern Instruments). The data, obtained for 1 mM suspensions in high purity water at pH 7.5, are shown in Table 5.1. X-Ray photoelectron spectroscopy data were collected for Ce $3d_{5/2}$ using 5400 PHI ESCA spectrometer (Mg-Ka X-radiation (1253.6 eV) at a power of 350 W was used during the data collection). Surface Ce^{3+}/Ce^{4+} was calculated as discussed in our previous publication [21].

These well characterized nanoparticles were investigated for ClO^- scavenging activity. The nanoparticle suspensions (from 0.1 to 4 mM) were incubated for 60 min with freshly prepared hypochlorite solutions (5 mM, pH 9.0 ± 0.2). Then, the particles were separated by centrifugation (23000 g, 5 min). The amount of ClO^- (at the working pH, hypochlorous acid, pKa 7.5, is 97% dissociated) in the supernatant, which decreased due to the scavenging activity of CNPs, was tracked by measuring the inactivation of catalase. The method followed the procedure described by Aruoma and Halliwell [22] with minor variations. The scavenging activity was evaluated by measuring the

decrease in absorbance of catalase at 404 nm using microplate readings (FLUOstar Omega microplate reader, BMG LABTECH, Germany). The data are shown in Figure 5.1A for the tested CNPs and the reference antioxidant compound ascorbic acid [23]. Scavenging activity (%) was calculated using the following formula [1].

$$S\text{cavenging Activity }(\%) = \frac{(C_x - C_{t2})}{(C_{t1} - C_t)} \cdot 100 \qquad [1]$$

Where C_{t1} is the catalase absorbance (measured at 404 nm) without ClO^- (intact catalase); C_{t2} is the catalase absorbance in the presence of ClO^- (degraded catalase) and C_x is the catalase absorbance with ClO^- which was previously in contact with CNPs or ascorbic acid.

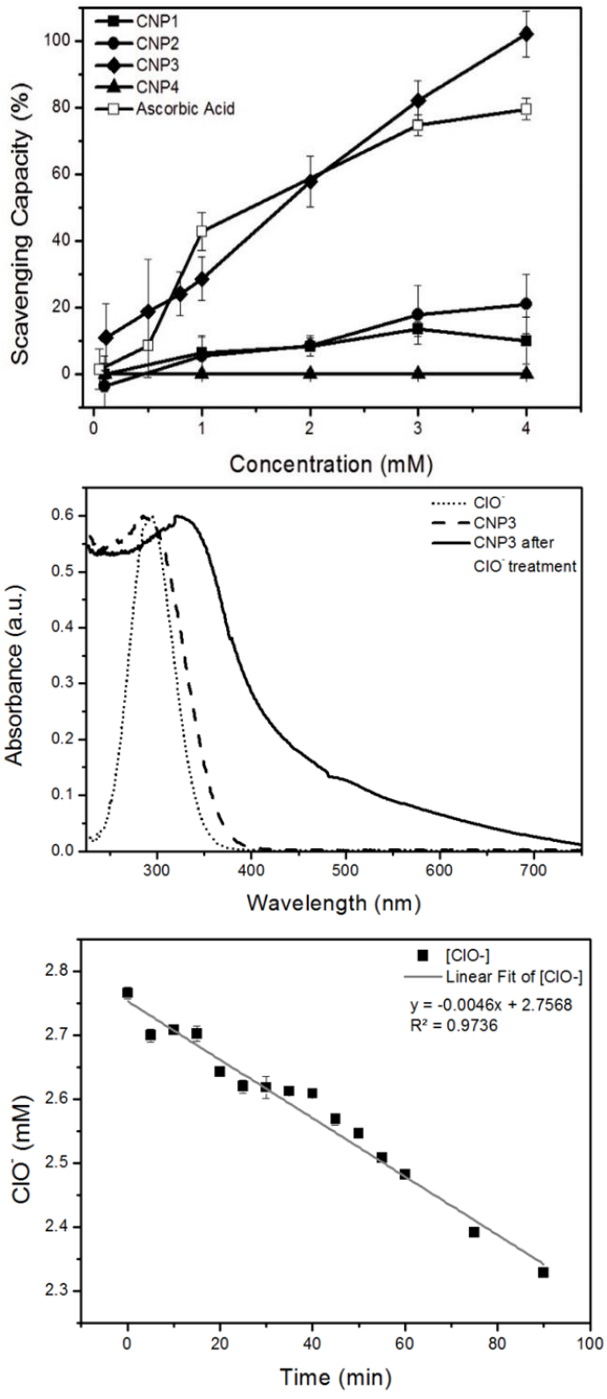

Figure 5.1.- (A) ClO^- scavenging activity of CNP determined from catalase inactivation measurements. (B) UV-vis spectra showing the interaction of CNP3 and ClO^-. (C) Kinetics of ClO^- depletion by CNP3.

The data show that CNP3 has strong ClO^- scavenging activity, with reaction extents comparable to the same concentration of ascorbic acid. The interaction of CNP3 with ClO^- was revealed by absorption spectroscopy. The absorption spectra of CNP3, recorded using a Perkin Elmer Lambda 750S instrument, show a shift in the absorption peak from 300 to 322 nm in CNP exposed to ClO^- (60 min), separated by centrifugation and carefully washed three times before recording the spectrum (Figure 5.1B). A similar phenomenon was found with CNP2 (see supplementary Figure S5.2). Absorbance values at wavelengths 298 and 252 nm are the characteristic UV-Vis absorbance for Ce^{4+} and Ce^{3+}, respectively [24]. Figure 5.1B clearly indicates that there is a shift in CNPs surface oxidation state from Ce^{4+} to Ce^{3+} after reacting with ClO^-. The disappearance of ClO^- from CNPs suspensions could not be attributed to its mere adsorption on the nanoparticle surface. A kinetic study was undertaken in mixtures of ClO^- and CNPs (5 mM) by following the evolution of hypochlorite concentration with time. The UV absorbance at 292 nm (molar absorptivity 350 M-1 cm-1) was measured to estimate the concentration of the ClO^- on the supernatant of centrifuged samples [25]. The corresponding data are shown in Figure 5.1C for CNP3. We selected CNP3 as CNP3 showed highest ClO^- scavenging activity. A Langmuir kinetics assuming surface equilibrium yields the following expression [26]:

$$r = \frac{kKC}{1 + KC} \qquad [2]$$

Where k is the rate of reaction of adsorbed species, K the adsorption equilibrium constant and C is the concentration of ClO^-. Given the relatively low concentration used, the zero-order kinetics depicted in Figure 5.1C points towards a high adsorption constant of ClO^- on CNP.

In order to better understand the interaction between ClO^- and CNP, XPS analysis was performed to further confirm the change in Ce^{3+}/Ce^{4+} on the surface of the nanoparticles seen in UV-Vis data. CNP3 was washed three times with distilled water after 60 min treatment with 5 mM ClO^-, to make sure there was no free ClO^-. The Ce $3d_{5/2}$ spectra recorded (Figure 5.2A and B) showed a significant increase in surface Ce^{3+} (12%) after interaction of CNP3 with ClO^- for 60 min at pH 9.0. The presence of chloride on CNP3 surface after treatment with ClO^- is also apparent (Figure 5.2C). The shift in Cl $2P_{3/2}$ spectrum compared to $CeCl_3$ may signify a complex formation on the surface of the nanoparticles rather than formation of $CeCl_3$ on the surface. Based on these results, we hypothesized the following reaction by means of which ClO^- is depleted by interaction with CNP3:

$$Ce^{4+} + 2ClO^- \rightarrow Ce^{3+} + 2Cl^- + O_2 \qquad (3)$$

The reaction accounts for the formation of chlorine-metal bonds due to chloride adsorption on the positively charged surface and should be accompanied by a release of oxygen. In order to prove that ClO^- decomposes as indicated, we performed direct measurements of oxygen evolution using a Clark-type oxygen electrode. The experiments were performed at 25°C under constant stirring (0.1 g) using a Hansatech apparatus (Kings Lynn, Norfolk, UK) with 1 mM CNPs and 5 mM of ClO^-.

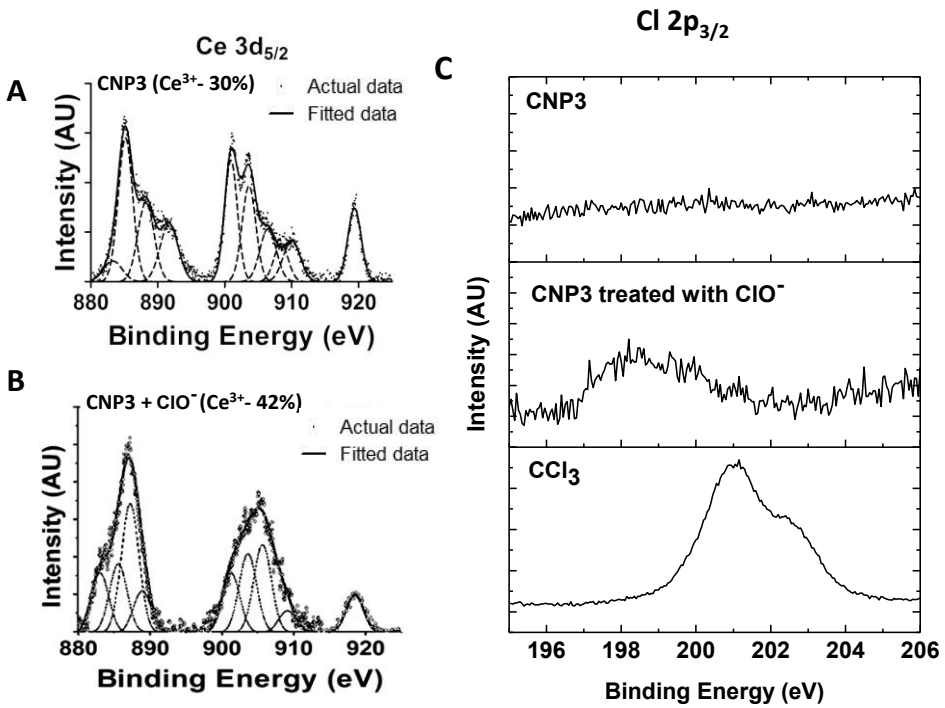

Figure 5.2.- The chemical property of the CNP3 after treatment with ClO^-. (A) and (B) show a significant change in Ce 3d5/2 XPS spectrum after treatment with ClO^-. (C) Shows Cl $2p_{3/2}$ spectra of CNPs, CNPs treated with ClO^- and $CeCl_3$ ($CeCl_3$ was used as reference) and indicates the presence of Cl on the surface of the nanoparticles after reaction of ClO^-.

The results are shown in Figure 5.3 and revealed a significant evolution of oxygen for CNP3 (CNP4 and ClO^- without nanoparticles are also shown for comparison), which amounted to 8 nmol/min or 0.32 mol O_2 mol CNP^{-1} h^{-1}. There was no evidence of oxygen release when nanoparticle or ClO^- alone was added (supplementary Figure S5.3). Lastly, we explored if CNP could scavenge ClO^- in the cellular environment. RAW 264.7 cells culture was selected as in vitro model and boron dipyrromethene-based fluorometric probe, HCS, was

used to detect the ClO^- [27]. Data are shown in Figure 5.4. Confocal images clearly indicate that concentration of ClO^- in the cells pre-treated with CNP3 is comparable to the control. 1 µM concentration of CNP3 was sufficient to scavenge the ClO^- to its basal level (control) in the RAW cell model. Fluorescence intensity was also measured using image J software and is shown in supplementary Figure S5.4.

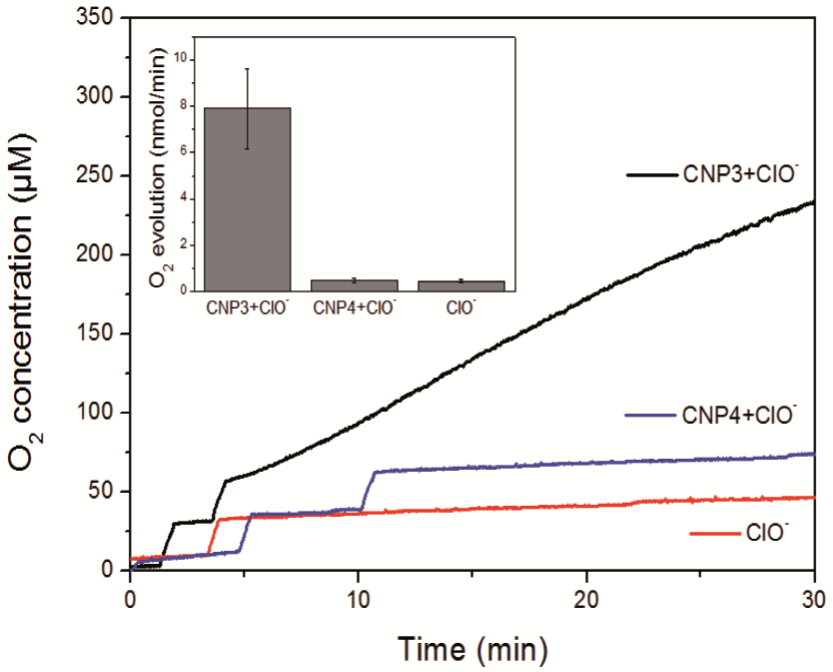

Figure 5.3.- Oxygen evolution for CNP in contact with ClO^-.

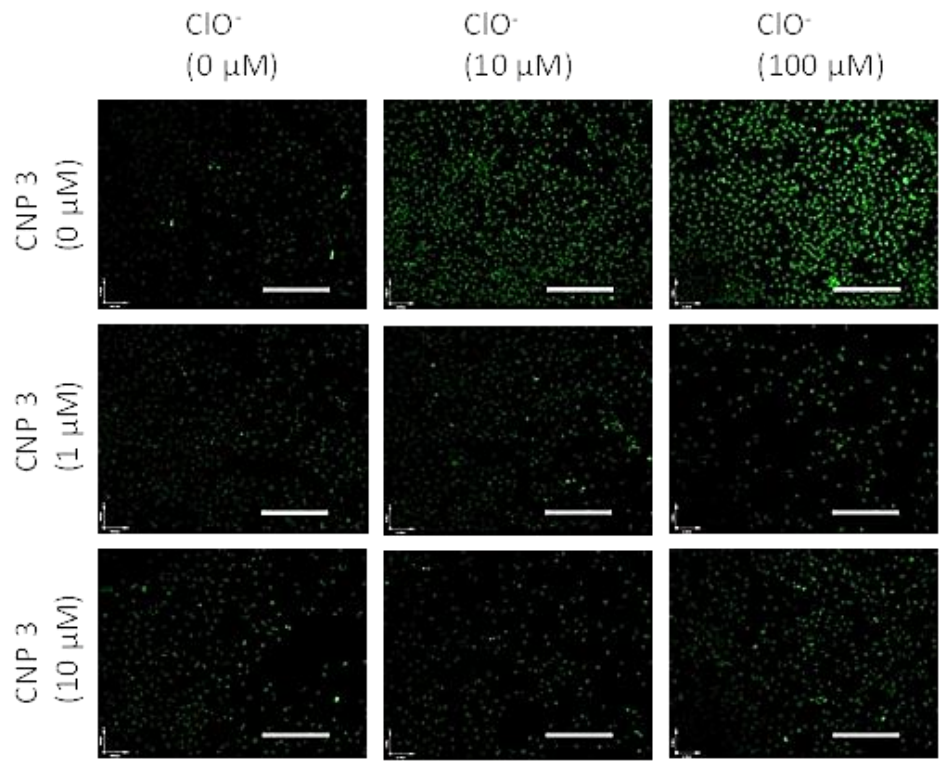

Figure 5.4.- Scavenging of ClO^- by CNP3 in vitro RAW cell culture model. Pretreatment with 1 µM CNP3 able to scavenge the most of the ClO^- (comparable to control); scale bar 50 µm.

5.4 Conclusions

The higher activity of CNP3 in comparison with the other tested nanoparticles is apparent from the data displayed in Figure 5.1, 5.2 and 5.3. We attributed this higher reactivity to its significantly lower effective particle size, with DLS diameters below 10 nm versus 30-50 nm for the other particles and to higher Ce^{4+} on the surface. The effect of particle size on surface chemistry has already been reported for CNPs [28]. Decrease in nanoparticles size and

increase in stability are directly related to increase in the active surface area for the reaction [9]. From the proposed reaction and XPS data it can be concluded that higher surface Ce^{4+} is necessary for better ClO^- scavenging. It is interesting to mention that CNP1 (73%) has a comparable amount of Ce^{4+} to that of CNP3 (70%) and similar nominal size (5-8 nm); however, CNP3 has the highest scavenging activity. Thus, lower stability of CNP1 (higher agglomeration, Table 5.1) contributed towards lower ClO^- scavenging activity. Noteworthy, CNP2, which also showed a minor surface interaction as revealed by absorption spectroscopy, had a surface composition very similar to that of CNP1. In conclusion, we determined that CNPs were able to scavenge ClO^- both in test tube and *in vitro* RAW cell culture model by surface interaction and a reaction involving the evolution of oxygen and the reduction of Ce^{4+} to Ce^{3+}. The results are relevant because $HOCl/ClO^-$ is involved in tissue damage due to overstimulation of inflammatory processes.

5.5 References

[1] A. A. Alfadda and R. M. Sallam, J. Biomed. Biotechnol., 2012, 2012, 936486.

[2] L. J. Palmer, P. R. Cooper, M. R. Ling, H. J. Wright, A. Huissoon and I. L. C. Chapple, Clin. Exp. Immunol., 2012, 167, 261-268.

[3] S. M. McKenna and K. J. Davies, Biochem. J, 1988, 254, 685-692.

[4] J. D. Imig and M. J. Ryan, Compr. Physiol., John Wiley & Sons, Inc., 2013.

[5] B. Bekdeser, N. Durusoy, M. Ozyurek, K. Guclu and R. Apak, J. Agric. Food Chem, 2014, 62, 11109-11115.

[6] O. Firuzi, P. Mladenka, R. Petrucci, G. Marrosu and L. Saso, J. Pharm. Pharmacol., 2004, 56, 801-807.

[7] O. Firuzi, L. Giansanti, R. Vento, C. Seibert, R. Petrucci, G. Marrosu, R. Agostino and L. Saso, J. Pharm. Pharmacol., 2003, 55, 1021-1027.

[8]. J. Pedraza-Chaverri, G. Arriaga-Noblecia and O. N. Medina-Campos, Phytother. Res., 2007, 21, 884-888.

[9] S. Das, J. M. Dowding, K. E. Klump, J. F. McGinnis, W. Self and S. Seal, Nanomedicine, 2013, 8, 1483-1508.

[10] F. Esch, S. Fabris, L. Zhou, T. Montini, C. Africh, P. Fornasiero, G. Comelli and R. Rosei, Science, 2005, 309, 752-755.

[11] E. G. Heckert, A. S. Karakoti, S. Seal and W. T. Self, Biomaterials, 2008, 29, 2705-2709.

[12] J. M. Dowding, T. Dosani, A. Kumar, S. Seal and W. T. Self, Chem. Commun., 2012, 48, 4896-4898.

[13] J. Chen, S. Patil, S. Seal and J. F. McGinnis, Nat. Nanotechnol., 2006, 1, 142-150.

[14] 2014 - US 8795731 B1.

[15] S. Soren, S. R. Jena, L. Samanta and P. Parhi, Appl. Biochem. Biotechnol. 2015, 177, 148-161.

[16] S. Chigurupati, M. R. Mughal, E. Okun, S. Das, A. Kumar, M. McCaffery, S. Seal and M. P. Mattson, Biomaterials, 2013, 34, 2194-2201.

[17] Z. Liu, Y. Yan, S. Wang, W.-Y. Ong, C. N. Ong and D. Huang, Am. J. Biomed. Sci, 2013, 2, 140-153.

[18] S. Das, S. Singh, J. M. Dowding, S. Oommen, A. Kumar, T. X. Sayle, S. Saraf, C. R. Patra, N. E. Vlahakis, D. C. Sayle, W. T. Self and S. Seal, Biomaterials, 2012, 33, 7746-7755.

[19] T. Sakthivel, S. Das, A. Kumar, D. L. Reid, A. Gupta, D. C. Sayle and S. Seal, ChemPlusChem, 2013, 78, 1446-1455.

[20] A. Kumar, S. Das, P. Munusamy, W. Self, D. R. Baer, D. C. Sayle and S. Seal, Environ. Sci.: Nano, 2014, 1, 516-532. 21. S. Deshpande, S. Patil, S. V. N. T. Kuchibhatla and S. Seal, Appl. Phys. Lett., 2005, 87, 133113.

[22] O. I. Aruoma and B. Halliwell, Biochem. J, 1987, 248, 973-976.

[23] S. Shukla, A. Mehta, V. K. Bajpai and S. Shukla, Food Chem. Toxicol., 2009, 47, 2338-2343.

[24] C. J. Neal, S. Das, S. Saraf, L. Tetard and S. Seal, ChemPlusChem, 2015, 80, 1680-1690.

[25] J. Zhang, X. Xu and X. Yang, Analyst, 2012, 137, 3437-3440.

[26] Y. Liu and L. Shen, Langmuir, 2008, 24, 11625-11630.

[27] S.-R. Liu, M. Vedamalai and S.-P. Wu, Anal. Chim. Acta., 2013, 800, 71-76.

[28] S. V. Kuchibhatla, A. S. Karakoti, D. R. Baer, S. Samudrala, M. H. Engelhard, J. E. Amonette, S. Thevuthasan and S. Seal, J. Phys. Chem. C., 2012, 116, 14108-14114.

5.6 Supplementary information

5.6.1 Experimental Section

5.6.1.1. Nanoparticles preparation and characterization

Synthesis of the nanoparticles were described in our previous publications. Briefly, CNP1 was synthesized using precipitation method. Cerium nitrate hexahydrate was dissolved in distilled water and equimolar mixture NH_4OH was used as oxidizer [1]. The solution was the stirred for 4 hours and particles were washed with distilled water for three times. CNP2 was prepared using hydrothermal method. Cerium nitrate hexahydrate was dissolve in water and then NaOH was added to adjust pH to 10. This solution were mixed properly in a Teflon bottle and subjected to hydrothermal treatment at 80° C for 6 h [2]. Then particles were washed with distilled water for three times. CNP3 was also prepared using precipitation method. Cerium nitrate hexahydrate was dissolved in distilled water and excess amount of NH4OH was added. Then solution was stirred for 4 hours and washed with distilled water for three times. Pellet was resuspended in water and 1N HNO_3 was added to decrease the pH to 4 for better stability[3]. Lastly, CNP4 was prepared using wet chemical method, where equimolar H_2O_2 was used as oxidizer. 1N HNO_3 was used to decrease the pH to 4 for better stability [1].

These four nanoparticles were then thoroughly characterized. Size and morphology of the nanoparticles were analyzed using High Resolution Transmission Electron Microscopy (HRTEM). Surface charge and hydrodynamic radius of the nanoparticles were estimated using Zetasizer (Nano-ZS from Malvern Instruments, Houston, TX). X-ray photoelectron spectroscopy (5400 PHI ESCA; Mg KR X-ray irradiation (1253.6 eV) and 350 W) was used to determine the surface chemistry of the nanoparticles.

5.6.1.2. UV-Vis ClO^- absorption study

The interaction of CNP3 with ClO^- was revealed by UV-vis absorption spectrometry. A 10 mM stock solution of hypochlorite (ClO^-) was prepared

immediately before the experiment. The reaction mixture contained, in a final volume of 1.5 ml, ClO^- (5 mM) and increasing concentrations (from 1 to 2.5 mM) of each CNPs (CNP3 and CNP2). After mixing both, the nanoparticles were centrifuged at 23000 g during 5 min and carefully washed three times with distilled water, in order to avoid the presence of free ClO^-. Finally, the absorption spectra (220-750 nm) were recorded using a Perkin Elmer Lambda 750S instrument.

5.6.1.3. Oxygen evolution measurements

Oxygen evolution was measured at 25°C under stirring (0.1 g) with a Clark-type oxygen electrode (Hansatech, Kings Lynn, UK). Firstly, 2 ml of distilled water were added to the chamber and dissolved oxygen was displaced with argon gas. Then, the chamber cap was opened and CNP3 or CNP4 at final concentration of 1 mM was added. Finally, the reaction mixture was completed when ClO^- (5 mM) was added. Oxygen evolution was tracked during 30 min. There was no evidence of oxygen release when nanoparticle or ClO^- alone was added (see supplementary figure S3).

5.6.1.4. ClO^- measurement in RAW cells

30 × 103 RAW cells/cover slips were seeded and then cultured overnight. Cells were then treated with two different concentrations of CNP3 (1 and 10 µM) and incubated for 6 h. After the incubation, 10 µM and 100 µM NaOCl were added to the culture and incubated 30 min for at 37 °C. Following washing with sterile saline solution, cells were treated with 2 µl of 10 mM HCS (HSC was provided by Dr. Shu-pao Wu) dissolved in DMSO and was incubated for 30 min at 37 °C. Finally, cells were washed with sterile saline and immediately, imaged under a confocal (Carl Zeiss confocal microscope with Velocity image

processing software) microscope using 20x water immersion lenses and ten different regions were randomly imaged. Image J was used to get semi-quantitative data from the confocal images.

5.6.2. References

[1]. S. Das, S. Singh, J. M. Dowding, S. Oommen, A. Kumar, T. X. Sayle, S. Saraf, C. R. Patra, N. E. Vlahakis, D. C. Sayle, W. T. Self and S. Seal, *Biomaterials*, 2012, **33**, 7746-7755.

[2]. T. Sakthivel, S. Das, A. Kumar, D. L. Reid, A. Gupta, D. C. Sayle and S. Seal, *ChemPlusChem*, 2013, **78**, 1446-145

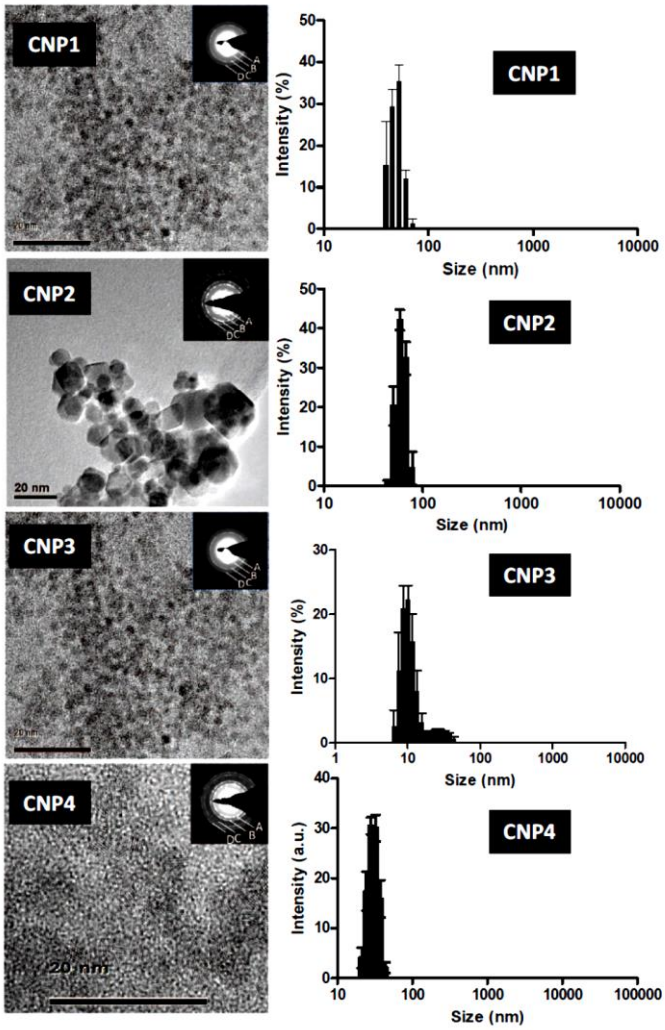

Figure S5.1.- HRTEM images of CNPs show nanoparticles morphology (left panel) and the size distribution histogram using dynamic light scattering (DLS) (Left panel). The nominal sizes of the particles are as follows: CNP1 5-8 nm, CNP2 15-20 nm, CNP3 5-8 nm, CNP4 3-5 nm. Selected area electron diffraction patterns (SAED) of the particles are shown in the inset. SAED patterns confirm the crystalline nature and A(111), B(200), C(220) and D(311) are different lattice planes of CNPs fluorite crystal structure. Scale bars 20 nm. DLS data showed size of the different nanoparticles as follows: CNP1 – 50.8 ± 0.9 nm; CNP2 – 58.8 ± 0.8nm; CNP3 – 9.4 ±2.1 nm; CNP4 – 30.8 ± 2.8 nm. The increase in the size of the nanoparticles is due to partial agglomeration of the nanoparticles.

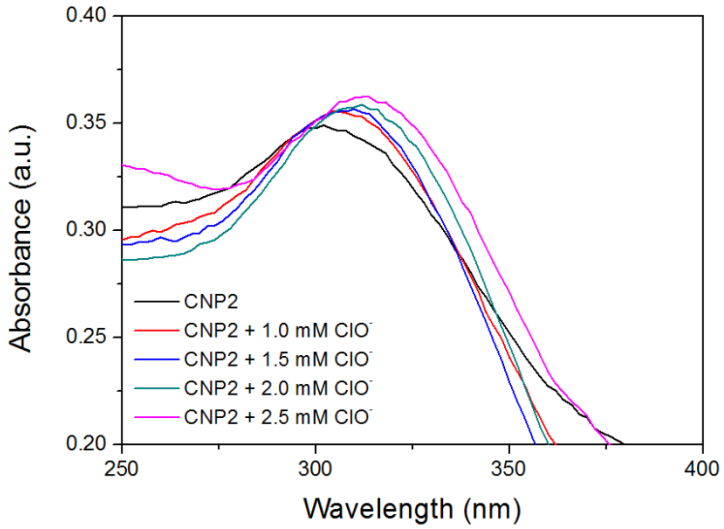

Figure S5.2.- UV-vis spectra showing the interaction of CNP2 and ClO^-.

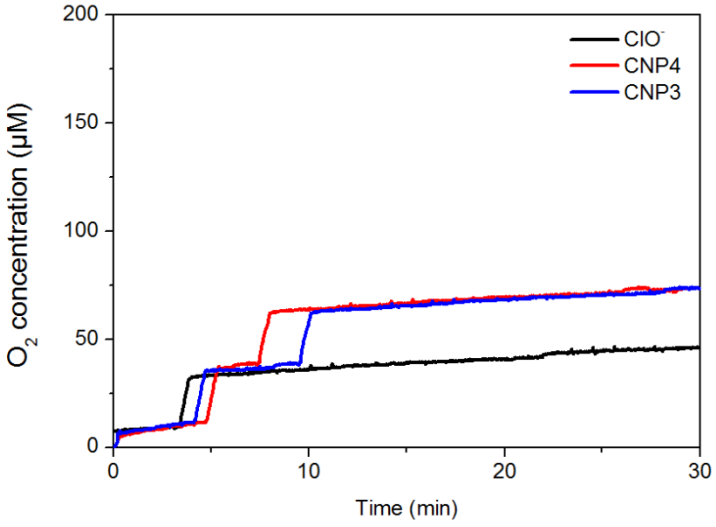

Figure S5.3.- Oxygen evolution for CNP3, CNP4 and ClO^- alone, indicating that there was no evidence of oxygen release when nanoparticle or ClO^- alone was added.

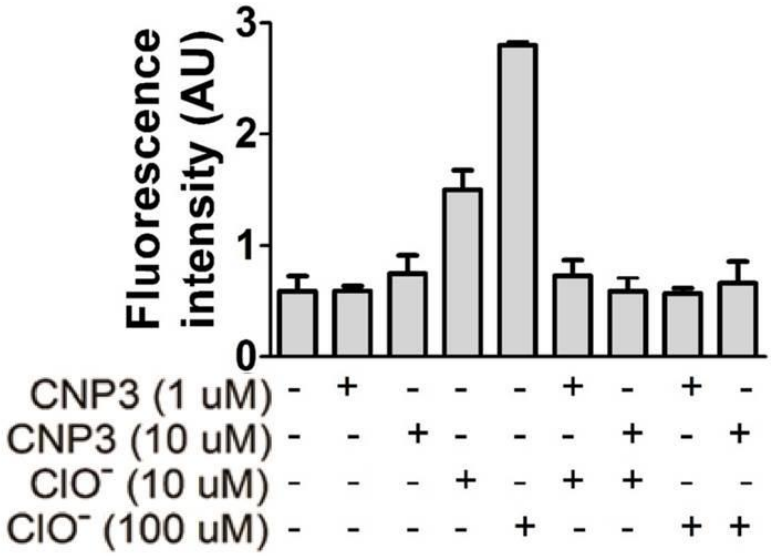

Figure S5.4.- Semi-quantitative fluorescence intensity data of ClO^-. Data indicated ClO^- in CNP3 pretreated samples were comparable to control. CNP3 itself did not induce any ClO^- generation in RAW cells.

CHAPTER 6

PHYSICOCHEMICAL AND BIOLOGICAL INTERACTIONS BETWEEN CERIUM OXIDE NANOPARTICLES AND A 1,8-NAPHTHALIMIDE DERIVATIVE

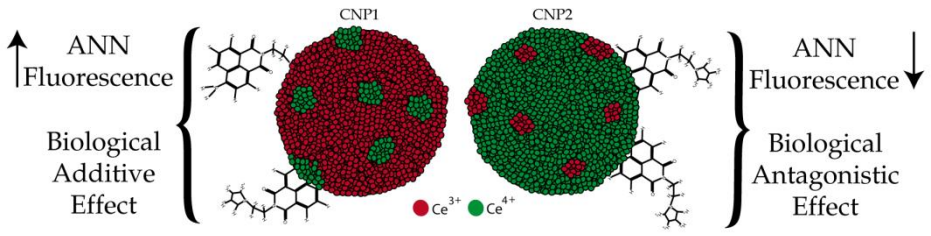

CHAPTER 6. PHYSICOCHEMICAL AND BIOLOGICAL INTERACTIONS BETWEEN CERIUM OXIDE NANOPARTICLES AND A 1,8-NAPHTHALIMIDE DERIVATIVE

6.1 Abstract

Cerium (Ce) oxide nanoparticles (CNPs) have attracted attention due to their high bioactivity and unique redox-chemistry. The oxygen vacancies at the surface of the nanoparticle explain the autocatalytic properties of CNPs in which the Ce^{3+} atoms occupy the center of the oxygen vacancies surrounded by Ce^{4+} atoms. Until now, CNPs have been associated with organic molecules at the synthesis stage to extend their applications or improve their stability. However, there is a lack of information regarding the post-synthesis interaction of CNPs and organic molecules that could enhance or induce new properties. Due to their unique optical properties and their many uses in different areas such as supramolecular chemistry or biomedicine, we have chosen a derivative from the family of naphthalimides (the 4-amino-1,8-naphthalimide-N-substituted; ANN) to study the interaction with different CNPs (CNP1-4) and their joint bioactivity compared to that of the same compounds alone. ANN-CNP complexes were formed as revealed by spectroscopic studies, but, the interaction was markedly different depending on the physicochemical properties of CNPs and their surface content of Ce^{3+} sites. The ANN adsorption on all CNPs involved the amino group in the naphthalene moiety as shown by NMR spectroscopy, while the pyrrolidine ring was mainly involved in the specific interaction between ANN and CNP1. The biological effect of each CNP and ANN individually and forming complexes

was assessed using a bioluminescent model bacterium. The results showed that ANN and CNP with the higher content of surface Ce^{3+} (CNP1) when combined acted additively towards the used model organism. In the opposite, ANN-CNP2, ANN-CNP3 and ANN-CNP4 complexes were antagonistic when the nanoparticles dominated the mixture. The results of this study contribute to expand the knowledge of the interaction between nanoparticles and organic molecules which may be useful for understanding the behavior of nanoparticles in complex matrices.

6.2 Introduction

Nowadays, nanoparticles of a huge diversity of materials, differing in their elemental composition, size, morphology and physical or chemical properties, can be synthesized through many different methods [1-3]. Cerium oxide nanoparticles are increasingly used in industrial applications such as glass polishing [4], solar cells [5] and fuel additives [6]. They have also been studied in biomedicine as anticancer agent [7, 8] and oxidative stress scavenger [9-11], among others [12]. This variety of applications is derived from their high surface activity and unique redox-chemistry. The redox/catalytic properties of cerium oxide nanoparticles (CNPs) are a consequence of the existence of two possible surface oxidation states, Ce^{3+} and Ce^{4+}, which induce a redox couple [13]. In recent years, CNPs have been synthesized and functionalized with a variety of molecules such as small ligands [14], polymers [15, 16], surfactants [17] and other organic molecules [18] using different strategies [19]. However, there are a lot of complex matrices (abiotic and biotic) where the surface of nanoparticles becomes adsorbs with external molecules that block the designed nanoparticle functionality [20, 21].

Naphthalimides (1*H*-benzo[*de*]isoquinoline-1,3-(2*H*)-diones) represent a class of compounds widely used in a variety of fields [22-24]. Among other applications, naphthalimides have been used as dyes for synthetic fibers [25], optical brighteners in detergents and polymeric materials, solar energy collectors [26], ion sensors [27-29] and biomedicine as potential anti-cancer agents [30, 31]. Chemically, 1,8-naphthalimide is a polar molecule with electron deficiency in the aromatic rings and an absorption band $n \rightarrow \pi^*$ type in the near-UV range. The introduction of substituents with electron donor character in 3- or 4-position of the naphthalene ring, such as amine ($-NH_2$) or

methoxy (–OCH_3) group, generates a new band in the visible frequency [32]. The absorption maximum of this band depends on the polarity of the solvent, due to the electronic $\pi \rightarrow \pi^*$ transition type has a charge transfer character towards the aromatic rings. It has been observed that the fluorescence quantum yield and fluorescence lifetime of these substituted compounds increase, especially in polar solvents such as acetonitrile and alcohols [23]. However, when the substituent in the imide nitrogen is an ethyl with a tertiary amino group, a fluorescence quenching is produced, a behavior associated to a Photo-induced Electron Transfer effect (PET) [33, 34]. Thus, these singular spectroscopic properties of naphthalimide molecules make relatively easy to track their possible interaction with nanoparticles.

Nanoparticles in suspension may come in contact with organic pollutants [35] or biological molecules [36] giving rise to the formation of complexes which biological effect is starting to be fully studied. The combination may produce an effect greater than the sum of their individual effects (synergism) or lower (antagonism). In this work, we have used several CNPs and a 4-amine-N-[2-(1-pyrrolidin)ethyl]-1,8-naphthalimide (ANN, hereinafter) in order to investigate whether CNPs are capable of interacting with a 1,8-naphthalimide derivative by studying their spectroscopic properties and ANN-structural changes after the interaction with CNPs. We have also studied the biological effect of CNPs and ANN using a bioluminescent model bacterium.

6.3 Material and Methods

6.3.1 Nanoparticle synthesis and characterization

Four Cerium Oxide Nanoparticles (CNPs) were synthesized using different methods with different surface Ce^{3+} contents and morphology. The physicochemical properties of the four nanoparticles were thoroughly analyzed. In particular, morphology and nominal size were assessed by High Resolution Transmission Electron Microscopy (HRTEM; FEI Tecnai F30). Ce^{3+}/Ce^{4+} ratios on the surface of nanoparticles were analyzed using X-Ray photoelectron spectroscopy (XPS) as described elsewhere (Deshpande, 2005). Hydrodynamic diameter and ζ-potential of the CNP suspensions in the different assay conditions were measured by Dynamic light scattering (DLS) and electrophoretic light scattering respectively using a Zetasizer Nano ZS particle size analyzer (Malvern Instruments Ltd; Worcestershire, UK). Further details are given elsewhere [37].

6.3.2 Synthesis and spectroscopic properties of 4-amine-N-[2-(1-pyrrolidin)ethyl]-1,8-naphthalimide

4-amine-N-[2-(1-pyrrolidin)ethyl]-1,8-naphthalimide (ANN) was synthesized according to a procedure described elsewhere [30]. Briefly, the ANN were synthesized by condensation between 4-amino-1,8-naphthalic anhydride and the 1-(2-aminoethyl)pyrrolidine. The absorption spectra were recorded in a double bean Perkin-Elmer Lambda 16 spectrophotometer (Perkin-Elmer, Massachusetts, USA). The fluorescence intensity was measured in a Schoeffel model 970 fluorimeter (Schoeffel Instrument Corp., New Jersey, USA). Fluorescence quantum yields were obtained using Norharmane solution (Sigma-Aldrich) in 0.1N sulfuric acid as standard [38]. Fluorescence lifetime measurements were performed by using time-correlated single photon counting (TCSPC) spectroscopy with a hydrogen-filled flash as the excitation

source (FWHM = 1 ns). The lifetimes were estimated from the measured fluorescence decay curves and the lamp profiles using a nonlinear least-squares iterative fitting procedure [39]. The quality of the fit was assessed by plotting the standard deviation and the chi-square values. All measurements were conducted at 10^{-5} M in three different solvents: dH_2O (pH 7), dichloromethane (DCM) and NaOH 0.01 M (pH 11). Fourier Transform InfraRed (FT-IR) spectra were obtained in KBr (1 wt %) using a Bruker model IFs 66V Fourier Transform Infrared spectrometer in transmission mode.

6.3.3 Studying the ANN-CNPs complex

The hydrodynamic diameter and ζ-potential of 10 mg/l CNP suspensions in 2.5 μM ANN in dH_2O, pH 7 were measured by Dynamic light scattering (DLS) and electrophoretic light scattering, respectively, using a Zetasizer Nano ZS particle size analyzer. The effect of the different CNPs on the absorption spectrum of ANN was measured using a Hitachi U-2000 spectrophotometer (Japan). Increasing concentrations of CNPs (8.6, 17.2, 172 mg/l) were used in order to track changes in the absorption spectrum. For it, the fluorescence emission at 560 nm of ANN with or without the presence of CNPs was analyzed during 30 min. Fluorescence readings were also taken every 10 min with a Synergy HT multi-mode microplate reader (BioTek, USA). The excitation wavelength was 360 nm.

^{1}H NMR spectra were obtained using 500 MHz Bruker Advance DRX Spectrometer equipped with a 5 mm BBOFplus 1H-19F/X Z-Grad and referenced to tetramethylsilane. The peak at 5.36 ppm and 4.80 ppm were related with dichloromethane (DCM) or water, respectively. Reference ANN

spectrum was obtained in DCM. 10 µL of CNPs (6 mg/l; final concentration) was added to the naphthalimide derivative (0.1 mM) and the corresponding spectra were recorded after 30 min of incubation. The spectra were processed using MestreNova software (version 10.0.2-15465).

6.3.4 Biological assays

As a representative biological assay, we used a high-throughput configuration of a bioluminescent whole-cell biosensor that detects metabolic toxicity based on a bacterium (*Anabaena sp.* PCC7120 CPB4337; hereinafter *A.* CPB4337) which has been used in several studies [40, 41]. *A.* CPB4337 bears in the chromosome a Tn5 derivative with *luxCDABE* from the luminescent terrestrial bacterium *Photorhabdus luminescens*. This strain shows a high constitutive self-luminescence, so the bioassays are based on the inhibition of constitutive luminescence caused by the presence of a toxic substance. *A.* CPB4337 was also chosen because it has been previously shown that it cannot internalize cerium oxide nanoparticles [42]. Accordingly, the possible effects derived from internalized particles can be excluded. The dose-response curves of ANN and all CNPs were determined after 24 h of exposure in AA/8 medium supplemented with 5 mM nitrate (AA/8+N; the composition of the bacterial growth medium is given in supplementary table S6.1). The final concentrations tested ranged from 0 (control samples) to 75 µM (for ANN) or 75 mg/l (for each CNP). The No-Observed-Effect-Concentration (NOEC) and EC_{10} (the effective concentration of ANN or CNP that caused 10% bioluminescence inhibition with respect to a non-treated control) were obtained from the dose-response curves.

The bioassays were conducted in transparent sterile 24-well plates. Each well was filled with ANN, the nanoparticle suspension or the ANN-CNP combination at different ratios based on their NOECs and EC_{10}s. Three ratios were chosen for each: ANN_{NOEC}-CNP_{NOEC} (0.75:0.25; 0.5:0.5 and 0.25:0.75) and ANN_{EC10}-CNP_{EC10} (0.75:0.25; 0.5:0.5 and 0.25:0.75). After 30 minutes, AA/8+N medium and *A.* CPB4337 were added to the wells to reach a final OD_{750nm} = 0.5. The 24-well plates were kept at 28 ºC and light ca. 65 µmol photons m^2 s^{-1} on a rotary shaker during 24 h of exposure. For luminescence measurements, 100 mL of each sample were transferred to an opaque white 96-well plate and recorded in a Centro LB 960 luminometer for 10 min.

6.3.5 Statistics

Statistical analyses were performed by using R software 3.0.2. Measurements were analyzed essentially as described elsewhere [37]. At least three independent experiments with triplicate samples were performed. A one-way ANOVA coupled with Tukey's HSD (honestly significant difference) post-hoc test was performed for comparison of means. Differences were considered statistically significant when $p < 0.05$.

6.4 Results and discussion

6.4.1 Photophysical properties of N-substituted 1,8-naphthalimide

Figure 6.1A shows the structure of the 4-amine-N-[2-(1-pyrrolidin)ethyl]-1,8-naphthalimide (ANN) used in this study. The molecule has an amino group in the 4-position of the naphthalene moiety and an aliphatic chain linked to the

pyrrolidine ring by the imide group. Figure 6.1B also shows the FT-IR spectrum of ANN in which the most characteristic bands were the carbonyl bands. Asymmetric and symmetric stretching vibration bands of the carbonyl groups of ANN appear in the 1680–1640 cm^{-1} range (the full FTIR transmission spectrum from 3600 to 1250 cm^{-1} can be found in Supplementary Figure S6.1). The C-C stretching vibration bands of naphthalimide appeared in the 1620–1550 cm^{-1} region, while the C-N stretching vibration bands in the dicarboximide appeared between 1400 and 1350 cm^{-1}. In the 3100–3000 cm^{-1} region, typical C-H stretching vibration bands of aromatic rings were observed. The region around 3350 cm^{-1} corresponds to the stretching vibration of the N-H group. The C-H asymmetric and symmetric stretching vibration bands of the methylene groups of N-substituents laid in the 3000–2850 cm^{-1} region. These assignments are all in agreement with those results

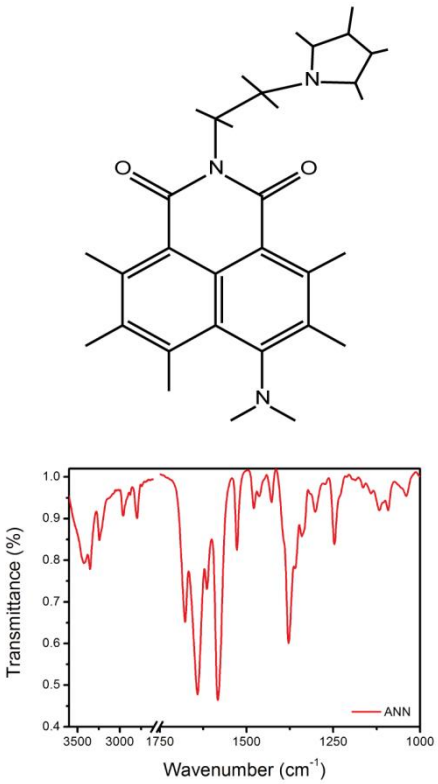

Figure 6.1.- (A) Molecular structure of ANN. (B) FTIR transmission spectrum of ANN in the 3600-2600 and 1750-1000 cm−1 regions. A break at 1750 cm−1 was used to improve the clearness of the figure. The entire FTIR spectrum can be found in Supplementary Figure S6.1.

published by Grzesiak and Brycki [43] (2012) and Philipova [44] (1995) who did a deep FTIR analysis of some derivative of N-substituted-1,8-naphtalimides.

The observed spectroscopic properties of ANN, namely absorption and fluorescence spectrum, quantum yield and fluorescence lifetime are presented in Table 6.1. The spectroscopic properties of ANN were pH and solvent polarity dependent: when ANN was diluted in DCM, there was a blue-shift from 433 nm to 407 nm in the absorption maximum and the fluorescence maximum changed to lower wavelength in comparison with the results obtained in NaOH 0.01 M and dH_2O (the complete absorption and emission spectra of ANN in dH_2O can be found in Supplementary Figure S6.2). The fluorescence quantum yields and lifetime of ANN also showed this dependence.

Table 6.1.- Spectral data of ANN in distilled water, dichloromethane and sodium hydroxide (0.01 M).

Compound	Name	Solvent	λ_{abs} (nm)	λ_{fluo} (nm)	Φ_F	τ_{flu} (ns)
4-amino-1,8-naphthalimide N-substituted	ANN	dH_2O	433	536	0.055	2.82
		DCM*	407	490	0.174	11.4
		NaOH	430	543	$1.5 \cdot 10^{-6}$	4.8

*DCM=Dichloromethane

ANN showed higher quantum yields in DCM than in dH_2O (Table 6.1). However, in NaOH solution, the fluorescence emission of ANN was strongly quenched by partial deprotonation of the amino group. The fluorescence lifetime showed that ANN in the organic solvent had the highest stabilization

in the excited state. It is known that the 4-amino-1,8-naphthalimide derivatives are highly emissive in organic solvents such as DCM and chloroform, while significant quenching is observed in water [45]. Nevertheless, the use of 4-amino-naphthalimide as detection probe in water is well established and several 1,8-naphthalimide derivatives have been used for the sensing of different cations [46, 47] and anions [33]. In these cases, upon interaction with proper chemicals, the changes may affect emission alone or both absorption and emission spectra.

Table 6.2.- Physicochemical properties of the tested Cerium Oxide Nanoparticles (CNPs) alone and mixed with ANN 2.5 µM in dH_2O (pH7).

				2.5 µM ANN	
Sample Name	**Morphology**	**ζ-potential (mV)**	**Effective Diameter (nm)**	**ζ-potential (mV)**	**Effective Diameter (nm)**
CNP1	Spheres	0.57 ± 0.7	70.2	-0.26 ± 0.7	200.2
CNP2	Spheres	12.0 ± 1.0	342.1	5.76 ± 0.3	458.7
CNP3	Rods	15.9 ± 0.4	122.4	15.0 ± 0.7	220.2
CNP4	Cubes	30.2 ± 0.7	190.1	26.3 ± 0.2	255.2

6.4.2 Physicochemical characterization of CNPs

According to HRTEM, CNP1 and CNP2 were spheres with diameters of approximately 6, and 9 nm, respectively. CNP3 had rod shape (325 nm long with a width of 22 nm) and CNP4 had cubic shape with a particle size around

50 nm. From the deconvolution of Ce (3d) XPS spectra, we determined that CNP1 had the highest amount of surface Ce^{3+} (58%) followed by CNP3 (36%), CNP2 (28%) and CNP4 (26%). Table 6.2 shows the physicochemical characteristics of the four CNPs at 10 mg/l suspended in dH_2O. Measured ζ-potential values (pH 7) of all CNPs showed that they were all positive, but CNP1 (0.57 ± 0.66 mV) had the lowest value in comparison with the other tested CNPs. According to DLS measurements, the effective diameters were in the 70-343 nm range (Table 6.2).

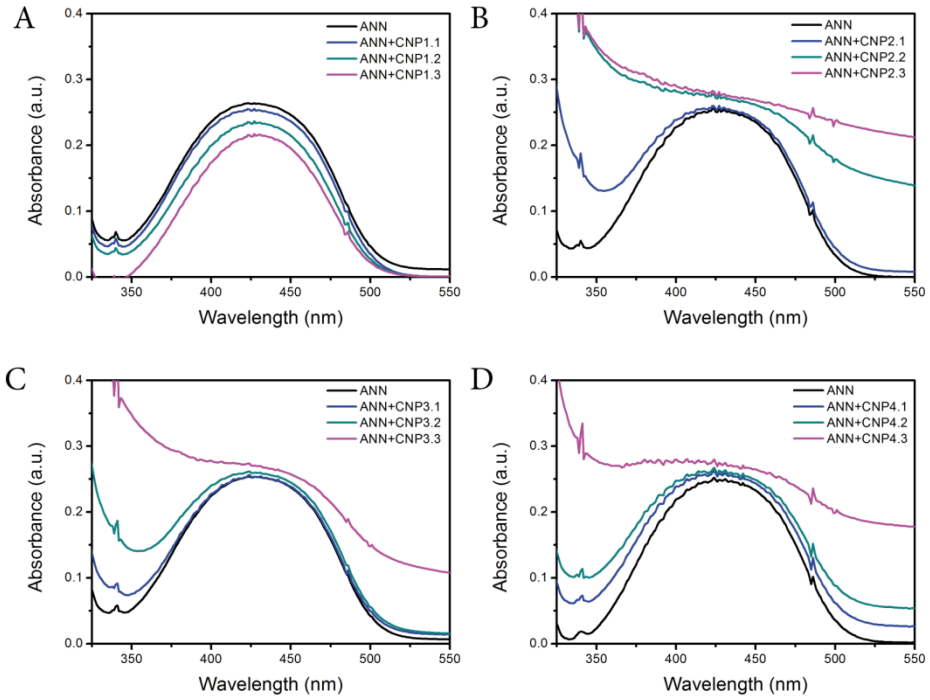

Figure 6.2.- Changes in the UV-vis spectra of ANN 0.2 mM in the presence of increasing concentration of CNPs in dH_2O. CNPs concentrations were 8.6 (CNPx.1), 17.2 (CNPx.2) and 172 mg/l (CNPx.3).

6.4.3 Characterization of the interaction between ANN and CNPs

Several experiments were conducted in order to verify the interaction of ANN with cerium oxide nanoparticles. For it, we obtained absorption spectra and stationary fluorescence maxima of the ANN-CNPs water mixtures. As shown in Figure 6.2, ANN displayed an electronic interaction with CNP1, proved by the decrease in the absorption maximum at 433 nm of ANN for increasing concentrations of CNPs from 8.6 to 172 mg/l (Figure 6.2A). A completely different behavior was observed for CNP2, CNP3 and CNP4 (Figure 6.2B, 6.2C and 6.2D, respectively) as all of them caused a light dispersion effect and the disappearance of the absorption maxima of the naphthalimide molecule. We have also recorded the whole spectrum of CNPs to prove the absence of absorption peaks due to the nanoparticles in the same region (see Supplementary Figure S6.3).

Moreover, fluorescence spectroscopy was conducted to follow changes in the fluorescence behavior of ANN derived of the exposure with CNPs. Figure 6.3 shows the fluorescence emission maximum at 530 nm of ANN and ANN-mixtures with CNP1, CNP2, CNP3 and CNP4 after 30 minutes of contact. CNP1 statistically ($p < 0.05$) increased the

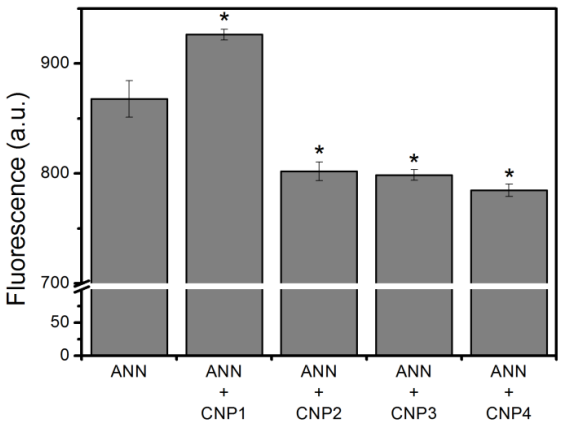

Figure 6.3.- Fluorescence emission of ANN and mixtures between ANN and CNP1, CNP2, CNP3 and CNP4 at 560 nm (the excitation wavelength was 360 nm). Mean ± standard deviation. Statistically significant differences

fluorescence emission of ANN by 6.7 % when compared to the ANN alone. Conversely, CNP2, CNP3 and CNP4 statistically ($p < 0.05$) decreased the fluorescence emission maxima of ANN by 7.6, 7.9 and 9.6 %, respectively. We also tracked the fluorescence variation over time, but the same pattern was observed (supplementary figure S6.4).

The physicochemical properties of the nanoparticles also change upon contact with ANN. ANN increased the hydrodynamic size of all CNPs, with a particularly relevant increase for CNP1 (from 70 to 200 nm; Table 6.2). Moreover, the ζ-potential of all CNPs slightly decreased when ANN was added, denoting lower stability of CNPs. Therefore, the increment in the nanoparticle hydrodynamic size suggest that ANN interacts with all the CNPs, but the higher aggregation of CNP1 after contact with ANN is probably a consequence of a preferential interaction with ANN.

We used NMR spectroscopy for determining the structural changes of the organic compound after interaction with CNPs. Figure 6.4 shows the NMR spectra of ANN and ANN-CNPs. The peaks of hydrogens in the naphthalene ring (from 8.7 to 6.7 ppm) and the primary amino group in 4-position (5.19 ppm) exhibited a left shift for all ANN-CNP complexes in comparison with the spectrum of ANN alone. This is indicative of a lower electronic density in this region (lower shielding of these hydrogens) due to the interaction with CNPs. There were no significant changes in other regions of the spectra.

Taking all these results together, we determined that ANN is able to adsorb onto the surface of CNPs. In view of NMR results, it is reasonable that all CNPs adsorb ANN through the naphthalene ring and the primary amino group. However, the main advantages of using ANN is that it has an internal charge transfer in the excited state, due to the electron donating amine and the

electron withdrawing terciary amine pyrrolidine group (PET) [33, 48]. This particularity could also be considered for determining how ANN interacts with the surface of nanoparticles. Accordingly, the formation of an ANN-CNP1 complex leading to the increment of the ANN-fluorescence (Fig. 6.3) suggests an interaction through the pyrrolidine ring and the aliphatic chain, because the PET process in this case would be inhibited by CNP1. The smallest nominal size along with the sphere morphology of CNP1 could also favor the interaction on this region of the molecule. It has been previously shown that the pyrrolidine ring of several 1,8-naphthalimide N-substituted molecules could fold to the molecular plane in certain circumstances, preventing the interaction in this region with nanoparticle with higher sizes and different morphologies [34]. Conversely, CNP2, CNP3 and CNP4 would strongly interact with the primary amino moiety of ANN, enhancing PET process and, thus, reducing the fluorescence of the chromophore as shown in Figure 6.3 and in agreement with NMR data.

The nanoparticle surface chemistry may be responsible for the different interaction of ANN with CNPs. CNP2, CNP3 and CNP4 had a relatively low surface Ce^{3+} content (between 26 to 36 %) and, therefore, their surface chemistry is governed by the Ce^{4+} form. CNP1, on the other hand, also has Ce^{4+} in its surface, but in a lower percentage. Upon ANN-CNP interaction, the surface Ce^{4+} can be reduced by the unpaired electron of the amine nitrogen as the redox potential of ANN is -1.92 V [32]. The ANN molecule has a tendency to lose electrons which could stabilize the complex formed with CNPs. Figure 6.4C illustrates how ANN interacts with CNP1 through the pyrrolidine ring and naphthalene moiety, while only the amino moiety was involved during the interaction between ANN and CNP2, CNP3 and CNP4 (CNP1 and CNP2 were chosen in Figure 6.4C to show this hypothesis).

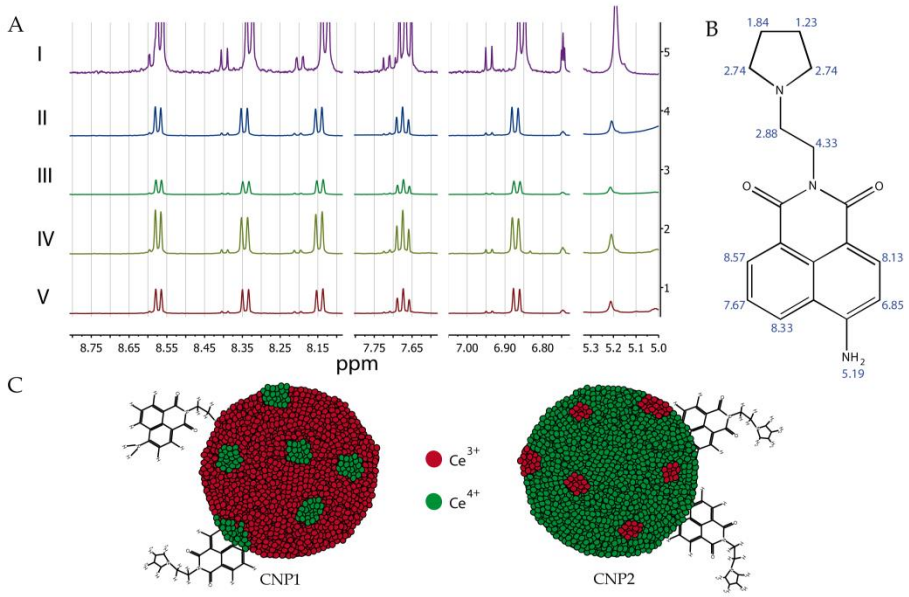

Figure 6.4.-(A) Selected ^{1}H NMR spectra of compound ANN alone (I) or with CNP1 (II), CNP2 (III), CNP3 (IV) and CNP4 (V). (B) Molecular designation of each H in order to facilitate the description of RMN results. (C) Schematic representation of the adsorption of ANN on the CNP1 or CNP2 surface depending of the Ce^{3+}/Ce^{4+} sites (the sizes are not representative).

Other factors than % surface Ce^{3+} may influence the adsorption of ANN on CNPs, such as surface facet and oxygen vacancies, but it is not clear which one is responsible for the reactivity of CNPs under a given set of conditions. Recently, Yang et al. [49] suggested that the facets of CNPs are more relevant for explaining redox activity than the % surface Ce^{3+}. In support for this hypothesis, particles with {100} facets displayed higher catalytic activity than particles with other facets but similar levels of surface Ce^{3+}. However, other authors argued that several factors would be required to explain the reactivity of CNPs. In fact, particles with higher amount of the most reactive facet towards photocatalytic oxidation of volatile organics were less effective in the

photocatalytic O_2 evolution, indicating that the surface facet itself could not fully explain the observed catalytic behavior [50]. The particles used in this work exposed different surface facet terminations. According to the existing literature, ceria nanocubes and nanorods are dominantly terminated by {100} and {110} + {100} facets, respectively [50-52]. Conversely, sphere-like CNPs expose {100} truncated {111} octahedron [53]. The similar mode of interaction found for CNP2, CNP3 and CNP4, which have different facets, with ANN suggested that the % surface of Ce^{3+} was more relevant than the surface facet composition for the interaction of ANN and CNP. Moreover, the predominance of facets on the reactivity of CNPs proposed by Yang et al [49] may be appropriate for enzymatic-mimetic reactions as they have demonstrated, but it could not be suitable for photochemical interactions such as those described here in the formation of ANN-CNP complexes.

6.4.4 Biological effect of ANN, CNPs and ANN-CNP towards A. CPB4337

The concentration-response curve for 24 h luminescence inhibition is shown in Figure 6.5 for ANN and the four CNPs over the whole concentration range studied. While ANN and CNP1 caused a 100 % bioluminescence inhibition at 50 µM and 30 mg/l, respectively; CNP2, CNP3 and CNP4 were non-toxic, with EC_{20} near the maximum concentration tested in this work (75 mg/l). Additionally, from these dose-response curves, we have calculated the NOEC and the sublethal EC_{10} of each compound, which were used as reference levels during the assessment of the biological effect of the ANN-CNP complexes (Figure 6.6). Those concentrations are relatively low, but chosen in purpose, in order to design experiments which may be closer to real world scenarios. In biomedicine, it is necessary to use efficient concentration to avoid negative

collateral effects. For concentrations higher than 75 mg/l, CNP1, for example, was very toxic, thus cells would have been severely damaged or even dead and it would have not been possible to study the biological effects.

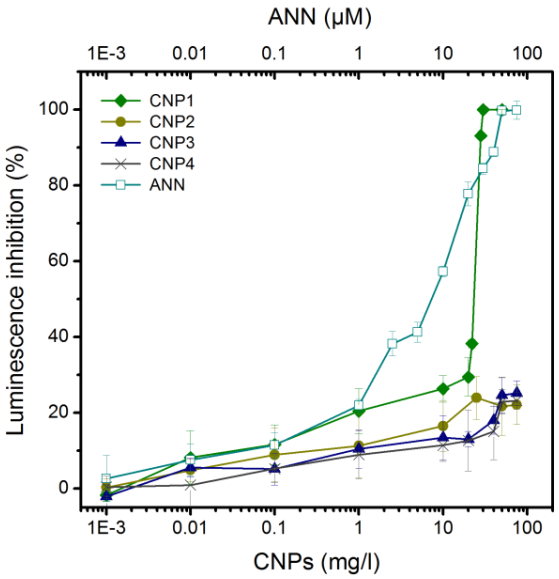

Figure 6.5.- Dose-response curve of ANN (from 0.001 to 100 µM), CNP1, CNP2, CNP3 and CNP4 (nanoparticle concentrations from 0.001 to 100 mg/l) for *A.* CPB4337. At least three independent experiments with three replicates were used (n = 9).

Different ratios were chosen in order to evaluate the possible additive, antagonistic or synergistic effect of the ANN-CNP complexes. As shown in Figure 6.6A, when ANN and CNP were mixed at the NOEC level, there were no statistical effects at any ANN-CNP ratio in comparison with ANN or CNP alone. Nevertheless, a different effect was observed when ANN and CNP were mixed at the EC_{10} level (Figure 6.6B). The 0.25:0.75 ratio of ANN-CNP2, ANN-CNP3

and ANN-CNP4 statistically ($p < 0.05$) reduced the expected adverse effect (antagonism): the luminescence inhibition of these samples was less than the sum of the known effects of the individual substances. This effect was not observed for the other ratios (0.5:0.5 and 0.75:0.25) or ANN-CNP1 complex whose mixture showed an additive effect. As mentioned before, it has been shown that CNPs have several mimetic antioxidant properties derived from their surface redox chemistry. The adsorption of ANN onto the surface of these nanoparticles could enhance these properties for CNP2, CNP3 and CNP4 (nanoparticles with low surface % of Ce^{3+}), which would also explain lower effect of 0.25:0.75 mixtures at the EC_{10} level. In fact, at the NOEC level, a slight luminescence stimulation was observed.

The bioluminescent model bacterium *A.* CPB4337 is a quantitative high-throughput screening (QHTS) method described previously [40]. The use of this organism generates fast and accurate information about the biological effect of different compounds in a short period of time. As the bacterium used here is very different from a mammalian cell, *A.*CPB4337 could be probably more resistant, due to the cell wall envelope which covers the cell. However, several test based on bacteria (Ames test [54] and *Vibrio fischeri* test [55]) have been used as first approximation of the biological effect of toxicants and it is well stablished their use in the risk management and health and safety assessment of substances.

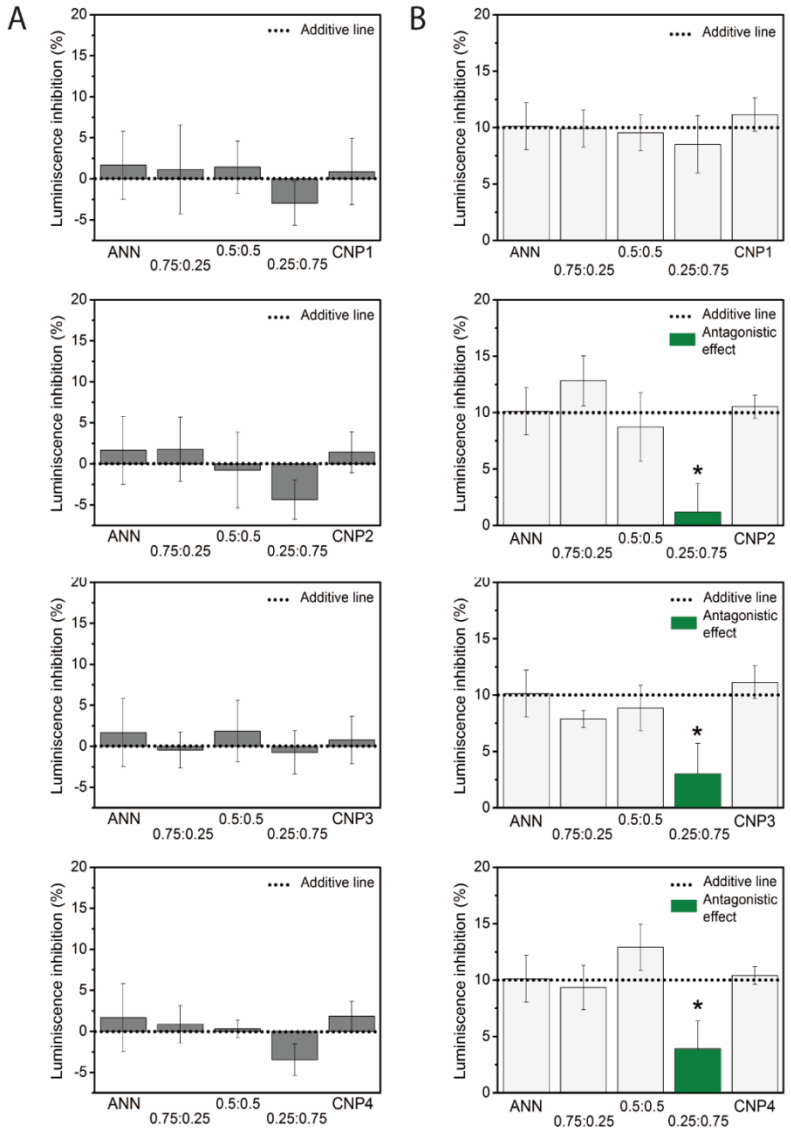

Figure 6.6.- Bioluminescence Inhibition of *A.* CPB4337 in response to ANN-CNPs complexes after 24 h. A) Effect of the ANN-CNPs complex using different ratios at the No-Observed-Effect-Concentration (NOEC). B) Effect of the ANN-CNPs complexes using different ratios at the effective concentration of ANN or CNPs that caused 10% bioluminescence inhibition with respect to a non-treated control (EC_{10}). The green bars indicate antagonism and the dotted line additivity. In all figures the response of *A.* CPB4337 to ANN and CNPs applied singly is also shown for comparison. Mean ± standard deviation. Statistically significant differences ($p < 0.05$) are marked by asterisks.

It has been previously described that naphthalimide derivatives can enter inside different cell types [56] and depending on the derivative and their substituents, it has been evidenced that some could interact with nucleic acids by intercalation [57] and others may directly break the cellular membrane [58], exerting their toxic effect in mammalian and bacterial cells, respectively. Although the ANN mode of action is beyond the aims of this study, we consider that the negative biological effect could be mediated both by direct membrane interaction (due to the non-polar nature of the molecule) and by intracellular impact on nucleic acid. We did not observe any CNP internalization in our previous study using *A.* CPB4337 and ceria-based nanoparticles [42], so this organism was chosen to avoid the possible effects derived from internalized particles. The direct contact between cell envelope and nanoparticles, resulting in cell wall and membrane disruption and cell lysis, was proposed as the mechanism underlying CNP toxicity. Moreover, the hydrodynamic size of ANN-CNPs complex is higher than the diameter of 20 nm suggested for the pores of envelope of *Anabaena sp.* PCC 7120 [59], and therefore neither CNP alone or CNP-formed complex could be internalized. The observed antagonistic effect for ANN-CNP2, ANN-CNP3 and ANN-CNP4 could be due to several causes: On the one hand, the formation of the ANN-CNP complex could reduce the bioavailability of ANN avoiding its entry into the cells and the production of its toxic effect. On the other hand, the ANN-CNP complex could also interfere in the interaction between CNP and the cell wall, as it has been shown that the formation of a corona on the surface of nanoparticles could reduce the observed toxicity of the nanoparticle alone [60].

The aggregation of CNPs and CNPs forming complexes with ANN was clear as stated in Table 6.2. However, the formation of aggregates did not influence

the adsorption of ANN on the surface of CNP. It could be argued that the lower degree of aggregation of CNP1 could favor the interaction with ANN due to its higher surface to volume ratio in comparison with the other CNPs. However, this different aggregation degree did not have a relevant effect on the biological experiments with the tested model organism, since ANN-CNP2, ANN-CNP3 and ANN-CNP4, which formed the largest aggregates, showed protective/antagonistic effect. In a previous publication, several factors were evaluated as possible drivers of the toxicity of various cerium oxide nanoparticles, including size/surface aggregation [37]. Among them, the % surface Ce^{3+} was the dominant factor as demonstrated by the fact that phosphate blocked Ce^{3+} sites and totally reverted the toxicity of CNP with the highest % surface Ce^{3+}, as a consequence of the affinity of surface Ce^{3+} to phosphate.

To the best of our knowledge, there were found no articles evaluating the toxicity of naphthalimide derivatives and only few articles studying their interaction with nanomaterials. Aguilera-Sigalat et al. [61] synthesized quantum dots (QDs) capped with ligands that possess a naphthalimide as chromophore unit with the objective of controlling the emission properties of CdSe/ZnS QDs through naphthalimide derivatives [61]. Moreover, dendrimers with amino-1,8-naphthalimide molecules in their structures were proposed as tunable organic light-emitting diodes [62]. Bekere et al. [63] evaluated the possibility of using 4-substituted 1,8-naphthalimides as sensitive molecular probes for ZnO nanoparticles. In this case, the nature of the interaction and how the molecule was adsorbed onto the nanoparticle were not studied. Huang et al. [64] showed that nanoparticle surface characteristics were key parameters during protein adsorption, since they might be able to modulate the protein conformation onto nanoparticle surface [64]. In this work, we

showed that the surface Ce^{3+} content strongly affect the adsorption of 1,8-Naphthalimide onto CNPs. Furthermore, the fact that the ANN could increase its fluorescence emission in presence of CNP with high surface Ce^{3+} suggests their use of N-substituted 1,8-naphthalimides as specific selective probes to detect nanoparticles in water and in biological samples. In this respect, 1,8-naphthalimides are able to cross the cell membrane, so it would be possible to track nanoparticles inside the cells and show their exact location.

Nanotechnology is growing quickly and it is expected that many products will have some kind of nanomaterial. The exponential increment of the number of potential applications is also probable. However, there is a lack of methodologies for the detection and characterization of engineered nanomaterials in complex matrices. It is necessary to develop new methods to solve this problem. In this regard, studies such as those provided by Othman et al. [65] and Chatterjee et al. [66] shed light on this issue when assessing the detection of nanoparticle by using specific organic dyes. Othman et al. (2016) described a method that was selectively optimized for the detection of CNP rather than any other metal oxide nanoparticles also in real water samples. In this regard, our results shown here provide a deeper insight on the interaction between an organic dye and nanoparticles, which could result in the direct detection of CNP in biological samples.

On the other hand, the use of combined molecules to fight against cancer is a standard clinical practice in the treatment of different tumors [67]. As stated above, several studies support the idea of using CNPs or 1,8-naphthalimide derivatives as anti-cancer agents. However, the biological results shown here reveal that, depending on the chosen CNP, their expected effect could be reduced if used in mixture.

6.5 Conclusions

In conclusion, in this work we demonstrated that cerium oxide nanoparticles can alter the spectroscopic properties of the 4-amine-N-[2-(1-pyrrolidin)ethyl]-1,8-naphthalimide and that the nanoparticle interaction with the organic molecule depends on their physicochemical characteristics. CNPs with high content of surface Ce^{3+} increased the fluorescence of ANN by interaction through the pyrrolidine ring; this complex caused an additive effect towards the bioluminescent model bacterium *A.* CPB4337. Conversely, CNPs with high content of surface Ce^{4+} decreased the ANN-fluorescence by enhancing PET process in the amino group and caused an antagonistic effect towards *A.* CPB4337. This study reveals a complex interaction between CNPs and 1,8-naphthalmide derivative which might cause an inefficiency use of these compounds even at low concentrations if they are used jointly as anticancer agents. The use of different mammalian and tumor cell lines will be needed to confirm the effects observed here. Besides, the results shown also contribute to untangle the unpredictable behavior of nanoparticles when they are suspended in complex matrices and open up a research line in the use of organic molecules to detect nanoparticle in liquid and biological samples.

6.6 References

[1] M. Stefaniuk, P. Oleszczuk, Y.S. Ok, Review on nano zerovalent iron (nZVI): From synthesis to environmental applications, Chemical Engineering Journal, 287 (2016) 618-632.

[2] X. Chen, S.S. Mao, Titanium dioxide nanomaterials: synthesis, properties, modifications, and applications, Chem. Rev, 107 (2007) 2891-2959.

[3] A.H. Lu, E.e.L. Salabas, F. Schüth, Magnetic nanoparticles: synthesis, protection, functionalization, and application, Angewandte Chemie International Edition, 46 (2007) 1222-1244.

[4] P.V. Dandu, B. Peethala, S. Babu, Role of different additives on silicon dioxide film removal rate during chemical mechanical polishing using ceria-based dispersions, Journal of The Electrochemical Society, 157 (2010) H869-H874.

[5] A. Corma, P. Atienzar, H. García, J.-Y. Chane-Ching, Hierarchically mesostructured doped CeO2 with potential for solar-cell use, Nature materials, 3 (2004) 394-397.

[6] D. Mei, X. Li, Q. Wu, P. Sun, Role of Cerium Oxide Nanoparticles as Diesel Additives in Combustion Efficiency Improvements and Emission Reduction, Journal of Energy Engineering, 142 (2015) 04015050.

[7] L. Alili, M. Sack, A.S. Karakoti, S. Teuber, K. Puschmann, S.M. Hirst, C.M. Reilly, K. Zanger, W. Stahl, S. Das, Combined cytotoxic and anti-invasive properties of redox-active nanoparticles in tumor–stroma interactions, Biomaterials, 32 (2011) 2918-2929.

[8] M.S. Wason, J. Colon, S. Das, S. Seal, J. Turkson, J. Zhao, C.H. Baker, Sensitization of pancreatic cancer cells to radiation by cerium oxide nanoparticle-induced ROS production, Nanomedicine : nanotechnology, biology, and medicine, 9 (2013) 558-569.

[9] E.G. Heckert, A.S. Karakoti, S. Seal, W.T. Self, The role of cerium redox state in the SOD mimetic activity of nanoceria, Biomaterials, 29 (2008) 2705-2709.

[10] T. Pirmohamed, J.M. Dowding, S. Singh, B. Wasserman, E. Heckert, A.S. Karakoti, J.E. King, S. Seal, W.T. Self, Nanoceria exhibit redox state-dependent catalase mimetic activity, Chemical communications, 46 (2010) 2736-2738.

[11] G. Pulido-Reyes, S. Das, F. Leganés, S. Silva, S. Wu, W. Self, F. Fernández-Piñas, R. Rosal, S. Seal, Hypochlorite scavenging activity of cerium oxide nanoparticles, RSC Advances, 6 (2016) 62911-62915.

[12] K. Reed, A. Cormack, A. Kulkarni, M. Mayton, D. Sayle, F. Klaessig, B. Stadler, Exploring the properties and applications of nanoceria: is there still plenty of room at the bottom?, Environmental Science: Nano, 1 (2014) 390-405.

[13] F. Esch, S. Fabris, L. Zhou, T. Montini, C. Africh, P. Fornasiero, G. Comelli, R. Rosei, Electron Localization Determines Defect Formation on Ceria Substrates, Science, 309 (2005) 752-755.

[14] L. Qi, A. Sehgal, J.-C. Castaing, J.-P. Chapel, J. Fresnais, J.-F. Berret, F. Cousin, Redispersible hybrid nanopowders: cerium oxide nanoparticle complexes with phosphonated-PEG oligomers, ACS nano, 2 (2008) 879-888.

[15] A. Asati, S. Santra, C. Kaittanis, S. Nath, J.M. Perez, Oxidase-like activity of polymer-coated cerium oxide nanoparticles, Angewandte Chemie, 48 (2009) 2308-2312.

[16] A.S. Karakoti, S. Singh, A. Kumar, M. Malinska, S.V. Kuchibhatla, K. Wozniak, W.T. Self, S. Seal, PEGylated nanoceria as radical scavenger with tunable redox chemistry, Journal of the American Chemical Society, 131 (2009) 14144-14145.

[17] Z. Wu, J. Zhang, R.E. Benfield, Y. Ding, D. Grandjean, Z. Zhang, X. Ju, Structure and chemical transformation in cerium oxide nanoparticles coated by surfactant cetyltrimethylammonium bromide (CTAB): an X-ray absorption spectroscopic study, The Journal of Physical Chemistry B, 106 (2002) 4569-4577.

[18] M. Hijaz, S. Das, I. Mert, A. Gupta, Z. Al-Wahab, C. Tebbe, S. Dar, J. Chhina, S. Giri, A. Munkarah, Folic acid tagged nanoceria as a novel therapeutic agent in ovarian cancer, BMC cancer, 16 (2016) 220.

[19] S. Das, J.M. Dowding, K.E. Klump, J.F. McGinnis, W. Self, S. Seal, Cerium oxide nanoparticles: applications and prospects in nanomedicine, Nanomedicine (London, England), 8 (2013) 1483-1508.

[20] A. Salvati, A.S. Pitek, M.P. Monopoli, K. Prapainop, F.B. Bombelli, D.R. Hristov, P.M. Kelly, C. Åberg, E. Mahon, K.A. Dawson, Transferrin-functionalized nanoparticles lose their targeting capabilities when a biomolecule corona adsorbs on the surface, Nature nanotechnology, 8 (2013) 137-143.

[21] B.S. Varnamkhasti, H. Hosseinzadeh, M. Azhdarzadeh, S.Y. Vafaei, M. Esfandyari-Manesh, Z.H. Mirzaie, M. Amini, S.N. Ostad, F. Atyabi, R. Dinarvand, Protein corona hampers targeting potential of MUC1 aptamer functionalized SN-38 core–shell nanoparticles, International journal of pharmaceutics, 494 (2015) 430-444.

[22] Q. Xuhong, Z. Zhenghua, C. Kongchang, The synthesis, application and prediction of stokes shift in fluorescent dyes derived from 1, 8-naphthalic anhydride, Dyes and Pigments, 11 (1989) 13-20.

[23] E. Martin, R. Weigand, A. Pardo, Solvent dependence of the inhibition of intramolecular charge-transfer in N-substituted 1, 8-naphthalimide derivatives as dye lasers, Journal of luminescence, 68 (1996) 157-164.

[24] S. Banerjee, E.B. Veale, C.M. Phelan, S.A. Murphy, G.M. Tocci, L.J. Gillespie, D.O. Frimannsson, J.M. Kelly, T. Gunnlaugsson, Recent advances in the development of 1, 8-naphthalimide based DNA targeting binders, anticancer and fluorescent cellular imaging agents, Chemical Society reviews, 42 (2013) 1601-1618.

[25] A. Peters, M. Bide, Amino derivatives of 1, 8-naphthalic anhydride and derived dyes for synthetic-polymer fibres, Dyes and Pigments, 6 (1985) 349-375.

[26] G.R. Bardajee, A.Y. Li, J.C. Haley, M.A. Winnik, The synthesis and spectroscopic properties of novel, functional fluorescent naphthalimide dyes, Dyes and Pigments, 79 (2008) 24-32.

[27] D. Cui, X. Qian, F. Liu, R. Zhang, Novel fluorescent pH sensors based on intramolecular hydrogen bonding ability of naphthalimide, Organic letters, 6 (2004) 2757-2760.

[28] F.M. Pfeffer, A.M. Buschgens, N.W. Barnett, T. Gunnlaugsson, P.E. Kruger, 4-Amino-1, 8-naphthalimide-based anion receptors: employing the naphthalimide N–H moiety in the cooperative binding of dihydrogenphosphate, Tetrahedron letters, 46 (2005) 6579-6584.

[29] H.-H. Lin, Y.-C. Chan, J.-W. Chen, C.-C. Chang, Aggregation-induced emission enhancement characteristics of naphthalimide derivatives and their applications in cell imaging, Journal of Materials Chemistry, 21 (2011) 3170-3177.

[30] M. Brana, J. Castellano, C. Roldan, A. Santos, D. Vazquez, A. Jimenez, Synthesis and mode (s) of action of a new series of imide derivatives of 3-nitro-1, 8 naphthalic acid, Cancer chemotherapy and pharmacology, 4 (1980) 61-66.

[31] J. Noro, J. Maciel, D. Duarte, A. Olival, C. Baptista, A. Silva, M. Alves, P. Kong Thoo Lin, Evaluation of New Naphthalimides as potential anticancer agents against breast cancer MCF-7, pancreatic cancer BxPC-3 and colon cancer HCT-15 cell lines, (2015).

[32] E. Martın, R. Weigand, A correlation between redox potentials and photophysical behaviour of compounds with intramolecular charge transfer: application to N-substituted 1, 8-naphthalimide derivatives, Chemical physics letters, 288 (1998) 52-58.

[33] T. Gunnlaugsson, P.E. Kruger, T.C. Lee, R. Parkesh, F.M. Pfeffer, G.M. Hussey, Dual responsive chemosensors for anions: the combination of fluorescent PET (Photoinduced Electron Transfer) and colorimetric chemosensors in a single molecule, Tetrahedron letters, 44 (2003) 6575-6578.

[34] E. Martín, J.L.G. Coronado, J.J. Camacho, A. Pardo, Experimental and theoretical study of the intramolecular charge transfer on the derivatives 4-methoxy and 4-acetamide 1,8-naphthalimide N-substituted, Journal of Photochemistry and Photobiology A: Chemistry, 175 (2005) 1-7.

[35] J.R. Lead, K.J. Wilkinson, Aquatic colloids and nanoparticles: current knowledge and future trends, Environmental Chemistry, 3 (2006) 159-171.

[36] I. Lynch, K.A. Dawson, Protein-nanoparticle interactions, Nano today, 3 (2008) 40-47.

[37] G. Pulido-Reyes, I. Rodea-Palomares, S. Das, T.S. Sakthivel, F. Leganes, R. Rosal, S. Seal, F. Fernández-Piñas, Untangling the biological effects of cerium oxide nanoparticles: the role of surface valence states, Scientific Reports, 5 (2015) 15613.

[38] A. Pardo, D. Reyman, J. Poyato, F. Medina, Some β-carboline derivatives as fluorescence standards, Journal of luminescence, 51 (1992) 269-274.

[39] D. O'Connor, Time-correlated single photon counting, Academic Press, 2012.

[40] I. Rodea-Palomares, M. Gonzalez-Pleiter, S. Gonzalo, R. Rosal, F. Leganes, S. Sabater, M. Casellas, R. Muñoz-Carpena, F. Fernández-Piñas, Hidden drivers of low-dose pharmaceutical pollutant mixtures revealed by the novel GSA-QHTS screening method, Science Advances, 2 (2016) e1601272.

[41] M. González-Pleiter, S. Gonzalo, I. Rodea-Palomares, F. Leganés, R. Rosal, K. Boltes, E. Marco, F. Fernández-Piñas, Toxicity of five antibiotics and their mixtures towards photosynthetic aquatic organisms: implications for environmental risk assessment, Water research, 47 (2013) 2050-2064.

[42] I. Rodea-Palomares, K. Boltes, F. Fernandez-Pinas, F. Leganes, E. Garcia-Calvo, J. Santiago, R. Rosal, Physicochemical characterization and ecotoxicological assessment of CeO2 nanoparticles using two aquatic microorganisms, Toxicological sciences : an official journal of the Society of Toxicology, 119 (2011) 135-145.

[43] W. Grzesiak, B. Brycki, Synthesis, FTIR, 13C-NMR and Temperature-Dependent 1H‑NMR Characteristics of Bis-naphthalimide Derivatives, Molecules, 17 (2012) 12427-12448.

[44] T. Philipova, I. Karamancheva, I. Grabchev, Absorption spectra of some N-substituted-1, 8-naphthalimides, Dyes and pigments, 28 (1995) 91-99.

[45] X. Poteau, A.I. Brown, R.G. Brown, C. Holmes, D. Matthew, Fluorescence switching in 4-amino-1, 8-naphthalimides:“on–off–on” operation controlled by solvent and cations, Dyes and Pigments, 47 (2000) 91-105.

[46] R. Parkesh, T.C. Lee, T. Gunnlaugsson, Highly selective 4-amino-1, 8-naphthalimide based fluorescent photoinduced electron transfer (PET) chemosensors for Zn (II) under physiological pH conditions, Organic & biomolecular chemistry, 5 (2007) 310-317.

[47] H. Mu, R. Gong, Q. Ma, Y. Sun, E. Fu, A novel colorimetric and fluorescent chemosensor: synthesis and selective detection for Cu 2+ and Hg 2+, Tetrahedron letters, 48 (2007) 5525-5529.

[48] L.K. Limbach, Y. Li, R.N. Grass, T.J. Brunner, M.A. Hintermann, M. Muller, D. Gunther, W.J. Stark, Oxide Nanoparticle Uptake in Human Lung Fibroblasts: Effects of Particle Size, Agglomeration, and Diffusion at Low Concentrations, Environmental science & technology, 39 (2005) 9370-9376.

[49] Y. Yang, Z. Mao, W. Huang, L. Liu, J. Li, J. Li, Q. Wu, Redox enzyme-mimicking activities of CeO(2) nanostructures: Intrinsic influence of exposed facets, Scientific Reports, 6 (2016) 35344.

[50] D. Jiang, W. Wang, L. Zhang, Y. Zheng, Z. Wang, Insights into the surface-defect dependence of photoreactivity over CeO2 nanocrystals with well-defined crystal facets, ACS Catalysis, 5 (2015) 4851-4858.

[51] H.-X. Mai, L.-D. Sun, Y.-W. Zhang, R. Si, W. Feng, H.-P. Zhang, H.-C. Liu, C.-H. Yan, Shape-selective synthesis and oxygen storage behavior of ceria nanopolyhedra, nanorods, and nanocubes, The Journal of Physical Chemistry B, 109 (2005) 24380-24385.

[52] X. Liu, K. Zhou, L. Wang, B. Wang, Y. Li, Oxygen vacancy clusters promoting reducibility and activity of ceria nanorods, Journal of the American Chemical Society, 131 (2009) 3140-3141.

[53] S. Das, S. Singh, J.M. Dowding, S. Oommen, A. Kumar, T.X. Sayle, S. Saraf, C.R. Patra, N.E. Vlahakis, D.C. Sayle, W.T. Self, S. Seal, The induction of angiogenesis by cerium oxide nanoparticles through the modulation of oxygen in intracellular environments, Biomaterials, 33 (2012) 7746-7755.

[54] V.N. Kouvelis, C. Wang, A. Skrobek, K.M. Pappas, M.A. Typas, T.M. Butt, Assessing the cytotoxic and mutagenic effects of secondary metabolites produced by several fungal biological control agents with the Ames assay and the VITOTOX® test, Mutation Research/Genetic Toxicology and Environmental Mutagenesis, 722 (2011) 1-6.

[55] M. Hernando, S. De Vettori, M.M. Bueno, A. Fernández-Alba, Toxicity evaluation with Vibrio fischeri test of organic chemicals used in aquaculture, Chemosphere, 68 (2007) 724-730.

[56] S.-A. Choi, C.S. Park, O.S. Kwon, H.-K. Giong, J.-S. Lee, T.H. Ha, C.-S. Lee, Structural effects of naphthalimide-based fluorescent sensor for hydrogen sulfide and imaging in live zebrafish, Scientific reports, 6 (2016).

[57] M. Brana, M. Cacho, A. Gradillas, B.d. Pascual-Teresa, A. Ramos, Intercalators as anticancer drugs, Current pharmaceutical design, 7 (2001) 1745-1780.

[58] C.T. Miller, R. Weragoda, E. Izbicka, B.L. Iverson, The synthesis and screening of 1, 4, 5, 8-naphthalenetetracarboxylic diimide–peptide conjugates with antibacterial activity, Bioorganic & medicinal chemistry, 9 (2001) 2015-2024.

[59] Z. Zheng, A. Omairi-Nasser, X. Li, C. Dong, Y. Lin, R. Haselkorn, J. Zhao, An amidase is required for proper intercellular communication in the filamentous cyanobacterium Anabaena sp. PCC 7120, Proceedings of the National Academy of Sciences, (2017) 201621424.

[60] C. Ge, J. Du, L. Zhao, L. Wang, Y. Liu, D. Li, Y. Yang, R. Zhou, Y. Zhao, Z. Chai, Binding of blood proteins to carbon nanotubes reduces cytotoxicity, Proceedings of the National Academy of Sciences, 108 (2011) 16968-16973.

[61] J. Aguilera-Sigalat, V.n.F. Pais, A. Doménech-Carbó, U. Pischel, R.E. Galian, J. Pérez-Prieto, Unconventional fluorescence quenching in naphthalimide-capped CdSe/ZnS nanoparticles, The Journal of Physical Chemistry C, 117 (2013) 7365-7375.

[62] P. Du, W.-H. Zhu, Y.-Q. Xie, F. Zhao, C.-F. Ku, Y. Cao, C.-P. Chang, H. Tian, Dendron-functionalized macromolecules: enhancing core luminescence and tuning carrier injection, Macromolecules, 37 (2004) 4387-4398.

[63] L. Bekere, D. Gachet, V. Lokshin, W. Marine, V. Khodorkovsky, Synthesis and spectroscopic properties of 4-amino-1, 8-naphthalimide derivatives involving the carboxylic group: a new molecular probe for ZnO nanoparticles with unusual fluorescence features, Beilstein journal of organic chemistry, 9 (2013) 1311-1318.

[64] R. Huang, R.P. Carney, K. Ikuma, F. Stellacci, B.L. Lau, Effects of surface compositional and structural heterogeneity on nanoparticle–protein interactions: different protein configurations, ACS nano, 8 (2014) 5402-5412.

[65] A. Othman, K. Bear, S. Andreescu, Quantitative assay for the detection, screening and reactivity evaluation of nanoceria particles, Talanta, 164 (2017) 668-676.

[66] A. Chatterjee, M. Santra, N. Won, S. Kim, J.K. Kim, S.B. Kim, K.H. Ahn, Selective fluorogenic and chromogenic probe for detection of silver ions and silver nanoparticles in aqueous media, Journal of the American Chemical Society, 131 (2009) 2040-2041.

[67] P.G. Corrie, Cytotoxic chemotherapy: clinical aspects, Medicine, 36 (2008) 24-28.

6.7 Suplemmentary information

Supplementary table S6.1: Composition of the cyanobacterial growth medium AA/8 (Gonzalez-Pleiter, 2013)

Component	Final concentration (mM)
KH_2SO_4	0.25
$MgSO_4$	0.125
$CaCl_2$	0.0625
NO_3	5
NaCl	0.5
Na_2-EDTA	0.009625
$FeSO_4$	0.08375
B	0.00053125
Co	0.00002125
Cu	0.00004
Mn	0.00093
Mo	0.00015625
Zn	0.000095
V	0.000025

González-Pleiter, M., Gonzalo, S., Rodea-Palomares, I., Leganés, F., Rosal, R., Boltes, K., ... & Fernández-Piñas, F. (2013). Toxicity of five antibiotics and their mixtures towards photosynthetic aquatic organisms: implications for environmental risk assessment. *water research*, *47*(6), 2050-2064.

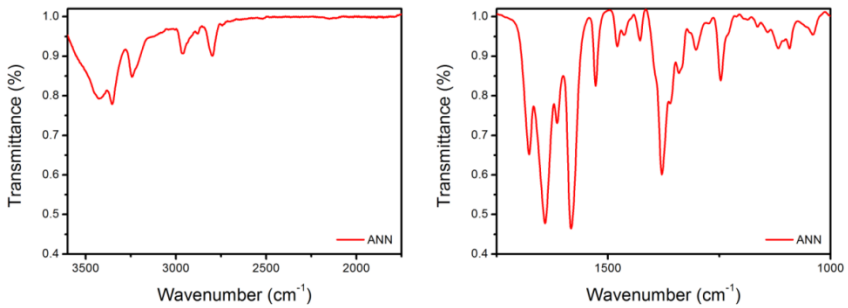

Supplementary Figure S6.1.- FTIR transmission spectrum of ANN in the 3600-1750 cm^{-1} range (left) and 1750-1000 cm^{-1} range (right).

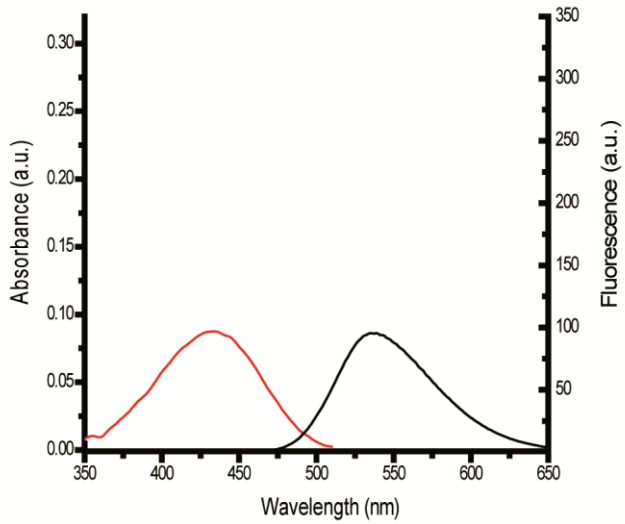

Supplementary Figure S6.2.- The absorption (red line) and emission spectra (black line) of ANN in dH_2O at pH 7.0.

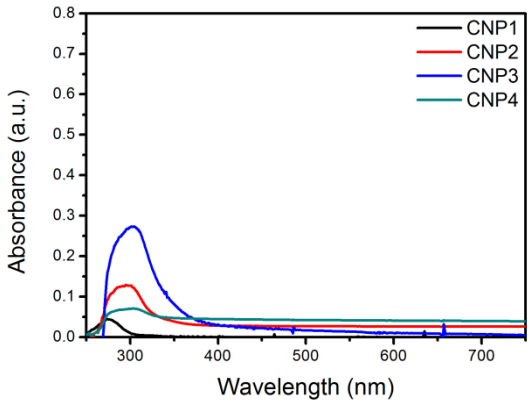

Supplementary Figure S6.3.- The absorption absorption spectra of CNPs in dH_2O from 250 to 750 nm.

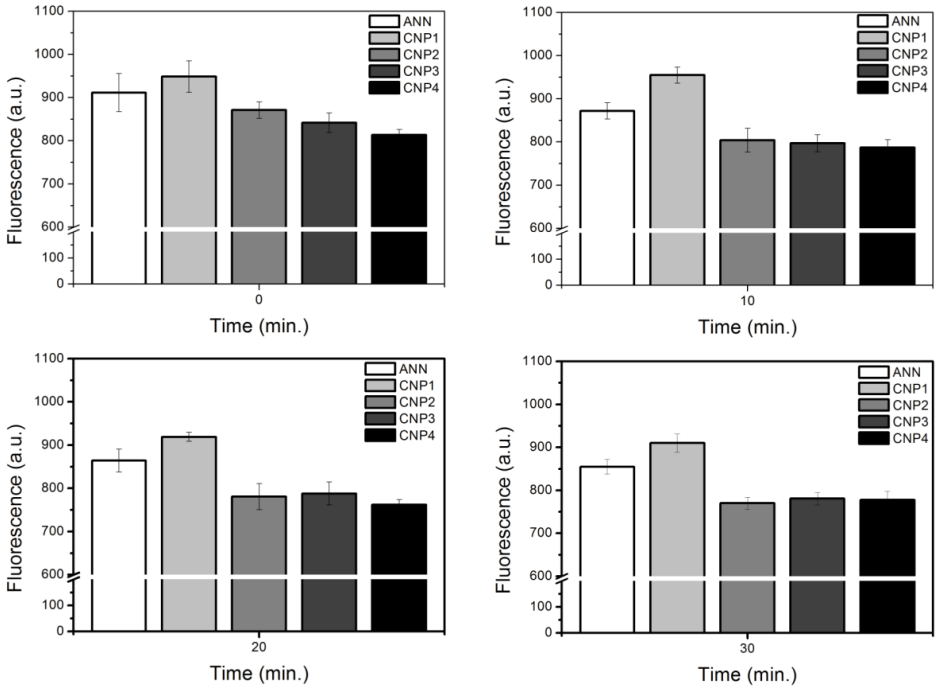

Supplementary Figure S6.4.- Fluorescence emission (Ex/Em 360/560 nm) of ANN and mixtures with CNPs at 1, 10, 20 and 30 min after CNP addition. Mean ± standard deviation.

CHAPTER 7

GENERAL DISCUSSION

CHAPTER 7. GENERAL DISCUSSION

The impact of nanomaterials on the environment is not completely understood yet. Until now, most of the available information refers to the biological effects of some nanomaterials in selected species under laboratory conditions [1-3]. Although some advances have been done regarding the consequences of nanotechnology in the environment, much more efforts are needed to clarify the uncertainties that this new technology generates. In Chapter 1, it has been recognized that when manufactured nanomaterials enter the environment (intentionally or otherwise), they have a great potential to move, transform and interact with other naturally-occurring substances, directly affecting the so-called Bio-Nano interface. The contribution of the adsorption of environmentally relevant molecules onto the surfaces of nanomaterials (the eco-corona) remains essentially unexplored, while solid progress has been performed in the biomedical field regarding the formation, behavior and evolution of the nanomaterial protein corona [4, 5].

Nanomaterials can undergo dramatic changes in the environment, including physical, chemical, and biological transformations. Therefore, ecotoxicity tests using pristine or as-manufactured nanomaterials may not exactly predict the toxicity of these materials once transformed under the influence of environmental factors. Knowing what form a nanomaterial takes in the environment is important to understand

exposure, uptake into organisms and likely ecotoxicological impacts. In waters and soils, for example, both synthetic and environmental coatings have been found to play a significant role in persistence of the nanomaterials [6, 7]. The presence of either a polymer coating or a natural organic coating on the nanomaterial surface increases its stability and slows down particle aggregation, suggesting that the material coating is likely to affect its behavior and transport.

The surface chemistry of cerium oxide nanoparticles (CNPs) is rich and intriguing. This is one of the reasons why the interface of these nanoparticles with living cells (Bio-Nano interface) has been chosen to be thoroughly analyzed. Along this Thesis, it has been emphasized the duality of CNPs to display both therapeutic/non-toxic and harmful effects. The importance of surface oxidation state as driver of their bioactivity and responsible for their ability to interact with other bio/molecules has been exposed as well. As stated before, the behavior of CNPs is dependent on and also a consequence of their exceptional reduction-oxidation properties enabled by the capacity of redox-cycling between their surface Ce^{3+}/Ce^{4+} oxidation states.

The most common definitions of nanoparticles and nanomaterials are based on the size and/or surface area of the particles. Nevertheless, when reporting toxicological parameters of nanoparticles, the more appropriate metrics may not necessarily be those ones. The metric considered the most suitable and the one that should be considered for reporting toxicological effects will be the one that correlates better

with the observed effects. In Chapter 3, it is stated that the observed toxicity of CNPs correlated well with the nanoparticle ζ-potential as well as surface content of Ce^{3+}/Ce^{4+}. However, the modification of surface chemistry and colloidal stability experiments showed that the main biological descriptor was the latter. Therefore, this parameter should be taken into account when assessing the biological effects of these nanoparticles. Although the different biological models and endpoints investigated as well as different range of doses play an important role, the reported discrepancies on the effects of CNPs could be related to the fact that surface content of Ce^{3+}/Ce^{4+} was not generally considered or measured [2, 8, 9]. Moreover, the use of coatings to enhance the nanoparticle suspension stability has been undertaken in different toxicological studies without considering that this modification could have great consequences to the Bio-Nano interface. As described in Chapter 4, different molecular weights of the same coating result in different biological effects.

The identification of hazardous nanomaterial properties presents a considerable challenge because of the large number of materials being produced and the proven fact that more than a dozen physicochemical properties could potentially contribute to hazardous interactions at the Bio-Nano interface. However, the results shown in this Thesis together with those shown by Thomas et al [10], where ZnO nanoparticles were doped with iron in order to reduce their toxicity derived from dissolution, could be useful for synthesizing and developing safer nanomaterials to lessen their environmental impacts.

The antioxidant properties of CNPs have been examined with the results derived from Chapter 5. Recently, it has been shown that CNPs have multi-enzyme mimetic properties: They are able to scavenge superoxide [11], hydrogen peroxide [12], hydroxyl radical [13] and nitric oxide radical [14]. The work done in this Thesis has provided another oxidative agent to the list by proving that CNPs can also scavenge hypochlorite anion. Oxidative stress in biological systems results from an imbalance between Reactive Oxygen/Nitrogen Species (RO/NS) production and antioxidant levels. These reactive species are consequence of regular metabolism and have dual roles in living cells, causing toxicity or acting as signaling molecules, depending on concentration, location and intracellular conditions [15]. Due to the fact that oxidative stress has a role in aging and in a variety of human pathologies, the use of CNPs in the biomedical field has been attracting significant attention during the last years [16]. CNPs have proved to be a better antioxidant agent because the traditional enzymes or molecules often scavenge only a single type of free radical before being inactivated, whereas CNPs show a great range of antioxidant-enzyme-like activities and could potentially be used several times due to the auto-regenerative capability.

Along Chapter 6, the interaction of CNPs with the an organic molecule derived from 1,8-naphthalimide and the biological effects of the complex formed were assessed. There are no reports in the scientific literature showing that CNPs could modulate the spectroscopic properties of the molecule by adsorption onto the particle surface, so

opening a new research line. There is a huge concern in the nanoscience field regarding the detection of nanoparticles inside tissues and organisms. The tiny size of nanoparticles hinders their direct observation even with Transmission Electron Microscopy. Therefore, the use of the 1,8-naphthalimide derivative, which can pass through the cellular membrane and differently adsorb onto the nanoparticle surface depending on the surface properties of CNPs, could be used to detect internalization of CNPs inside cells. Moreover, the additive or antagonistic effect of the formed complex revealed that the biological effects could be more complex than it could be expected. Both compounds are expected to be used to fight against cancer, so if a combined therapy is applied, their expected effect could be reduced.

Overall, this Thesis shows that CNPs are a great nanomaterial with multiple applications and potentialities whose biological effects essentially depend on their exceptional surface chemistry. The adsorption of molecules on their surface could also modulate their surface properties and therefore, alter the Bio-Nano interface with the consequence of a decreased toxicity. As stated before, the nanoparticle surface content of Ce^{3+}/Ce^{4+} and the type of coating should be taken into account in the next studies. By studying the harmful effects of CNPs towards several environmentally relevant microorganisms, this Thesis aimed at improving our understanding of the toxicity of this nanomaterial and contributing to the sustainable development of nanotechnology.

7.1 References

[1] von Moos N, Maillard L, Slaveykova VI. 2015. Dynamics of sub-lethal effects of nano-CuO on the microalga Chlamydomonas reinhardtii during short-term exposure. *Aquatic toxicology* 161:267-275.

[2] Auffan M, Bertin D, Chaurand P, Pailles C, Dominici C, Rose J, Bottero JY, Thiery A. 2013. Role of molting on the biodistribution of CeO2 nanoparticles within Daphnia pulex. *Water research* 47:3921-3930.

[3] Van Hoecke K, De Schamphelaere KA, Ramirez-Garcia S, Van der Meeren P, Smagghe G, Janssen CR. 2011. Influence of alumina coating on characteristics and effects of SiO2 nanoparticles in algal growth inhibition assays at various pH and organic matter contents. *Environment international* 37:1118-1125.

[4] Hadjidemetriou M, Al-Ahmady Z, Kostarelos K. 2016. Time-evolution of in vivo protein corona onto blood-circulating PEGylated liposomal doxorubicin (DOXIL) nanoparticles. *Nanoscale* 8:6948-6957.

[5] Docter D, Strieth S, Westmeier D, Hayden O, Gao M, Knauer SK, Stauber RH. 2015. No king without a crown–impact of the nanomaterial-protein corona on nanobiomedicine. *Nanomedicine : nanotechnology, biology, and medicine* 10:503-519.

[6] Whitley AR, Levard C, Oostveen E, Bertsch PM, Matocha CJ, von der Kammer F, Unrine JM. 2013. Behavior of Ag nanoparticles in soil: Effects of particle surface coating, aging and sewage sludge amendment. *Environmental pollution* 182:141-149.

[7] Barton LE, Auffan M, Bertrand M, Barakat M, Santaella C, Masion A, Borschneck D, Olivi L, Roche N, Wiesner MR. 2014. Transformation of pristine and citrate-functionalized CeO2 nanoparticles in a laboratory-scale activated sludge reactor. *Environmental science & technology* 48:7289-7296.

[8] Pelletier DA, Suresh AK, Holton GA, McKeown CK, Wang W, Gu B, Mortensen NP, Allison DP, Joy DC, Allison MR. 2010. Effects of engineered cerium oxide nanoparticles on bacterial growth and viability. *Applied and environmental microbiology* 76:7981-7989.

[9] Van Hoecke K, De Schamphelaere KA, Van der Meeren P, Smagghe G, Janssen CR. 2011. Aggregation and ecotoxicity of CeO(2) nanoparticles in synthetic and natural waters with variable pH, organic matter concentration and ionic strength. *Environmental pollution* 159:970-976.

[10] Thomas CR, George S, Horst AM, Ji Z, Miller RJ, Peralta-Videa JR, Xia T, Pokhrel S, Madler L, Gardea-Torresdey JL, Holden PA, Keller AA, Lenihan HS, Nel AE, Zink JI. 2011. Nanomaterials in the environment: from materials to high-throughput screening to organisms. *ACS nano* 5:13-20.

[11] Korsvik C, Patil S, Seal S, Self WT. 2007. Superoxide dismutase mimetic properties exhibited by vacancy engineered ceria nanoparticles. *Chemical communications*:1056-1058.

[12] Pirmohamed T, Dowding JM, Singh S, Wasserman B, Heckert E, Karakoti AS, King JE, Seal S, Self WT. 2010. Nanoceria exhibit redox state-dependent catalase mimetic activity. *Chemical communications* 46:2736-2738.

[13] Xue Y, Luan Q, Yang D, Yao X, Zhou K. 2011. Direct evidence for hydroxyl radical scavenging activity of cerium oxide nanoparticles. *The Journal of Physical Chemistry C* 115:4433-4438.

[14] Dowding JM, Dosani T, Kumar A, Seal S, Self WT. 2012. Cerium oxide nanoparticles scavenge nitric oxide radical (NO). *Chemical communications* 48:4896-4898.

[15] Apel K, Hirt H. 2004. Reactive oxygen species: metabolism, oxidative stress, and signal transduction. *Annu Rev Plant Biol* 55:373-399.

[16] Xu C, Qu X. 2014. Cerium oxide nanoparticle: a remarkably versatile rare earth nanomaterial for biological applications. *NPG Asia Materials* 6:e90.

GENERAL CONCLUSIONS
CONCLUSIONES GENERALES

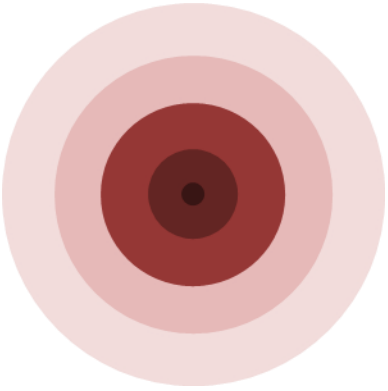

GENERAL CONCLUSIONS

1. The environmental Bio-Nano interface was recognized as an important element in the interaction between Engineered NanoMaterials (ENM) and living organisms. Once in the environment, ENM may suffer a battery of different physicochemical and biological transformations, which may change their synthetic identity to an environmental identity. The formation of an eco-corona on the surface of ENM has also been revealed as a key factor to assess their biological effects under realistic conditions. The techniques applied to characterize the bio-corona derived from the biomedical field could be useful in the study of environmental samples as well.

2. The biological activity of cerium oxide nanoparticle (CNPs) was governed by the ratio of Ce^{3+}/Ce^{4+} at the nanoparticle surface, displaying markedly different characteristics derived by their unique surface chemistry. The way that they interacted with other molecules such as hypochlorite anion and a 1,8-naphthalimide derivative also depended on this specific factor.

3. The abiotic ROS formation and the attachment to the cell walls were shown as the main toxicity mechanisms of CNPs. However, different mechanisms and different degree of biological effects were observed when CNPs were coated with various types of the organic molecule polyvinylpyrrolidone (PVP). PVP coated-CNPs significantly increased intracellular ROS formation, affecting different physiological

parameters without damaging the cellular envelopes. The internalization of coated and uncoated CNPs in *Chlamydomonas reinhardtii* was demonstrated and followed a time-dependent relationship.

4. As several toxicological mechanisms have been observed depending on the surface ratio of Ce^{3+}/Ce^{4+} and the type of coating, both characteristics should be taken into account by safer-by-design strategies, in Environmental Health and Safety (EHS) assessment of CNPs, but also in specific applications where these features are needed to display their intended function.

CONCLUSIONES GENERALES

1. La Bio-Nano interfaz ambiental se ha mostrado como un elemento importante en la interacción entre los Nanomateriales (ENM) y los seres vivos. Una vez llegan al medio ambiente, los ENM pueden sufrir una batería de transformaciones fisicoquímicas y biológicas, las cuales pueden cambiar su identidad sintética de partida por una identidad ambiental. Se ha destacado la formación de una corona ambiental sobre la superficie de los ENM (eco-corona) como factor clave en la evaluación de sus efectos biológicos bajo condiciones más realistas. Las técnicas aplicadas para caracterizar la biocorona derivadas del campo biomédico podrían ser útiles de igual forma en el estudio de las eco-coronas en muestras ambientales.

2. La actividad biológica de las nanopartículas de óxido de Cerio (CNPs) está fundamentalmente gobernada por la relación Ce^{3+}/Ce^{4+} en su superficie, mostrando efectos muy diferentes como consecuencia de su química de superficie única. La manera en la que las CNPs interactúan con otras moléculas, como el anión hipoclorito o un derivado de la 1,8-naftalimida, también depende de este factor específico.

3. La formación abiótica de especies reactivas y la adsorción a las envueltas celulares fueron los principales mecanismos de acción tóxica de las CNPs. Sin embargo, se observó un mecanismo distinto (y diferente grado de efecto biológico) cuando las CNPs se recubrieron

con la molécula orgánica polivinilpirrolidona (PVP). Las CNPs recubiertas con PVP significativamente incrementaron la formación de especies reactivas de oxigeno intracelulares, afectando a varios parámetros fisiológicos sin dañar directamente a las envueltas celulares. Asimismo, la internalización de CNPs en células de *Chlamydomonas reinhardtii* fue independiente de la presencia de recubrimiento, pero sí siguió una relación dependiente del tiempo.

4. Debido a que se han detectado diversos mecanismos toxicológicos dependiendo de la relación Ce^{3+}/Ce^{4+} en la superficie de las CNPs y el tipo de recubrimiento, ambas características deben ser tomadas en consideración al abordar el diseño seguro de nanomateriales, durante la evaluación de la contaminación ambiental y los riesgos potenciales para la salud humana, pero también en aplicaciones específicas donde es preciso conocer en exactitud su química superficial.

ACKNOWLEDGEMENTS

ACKNOWLEDGEMENTS / AGRADECIMIENTOS

This has been a great journey, a journey which would not have been possible without the help and support of many people. First of all, I would like to thank my remarkable supervisors: Francisca Fernández-Piñas and Roberto Rosal. I could not have wished for a better group for doing my PhD. You two have outstanding knowledge and skills to work in this field we called research and thanks to that, I have learnt a lot form both of you during the achievement of this thesis. I am the first experiment of a jointly supervised thesis and I deeply hope that both of you are satisfied with the work I present here. Thank you Roberto for accepting me without even knowing me and helping me to gain the FPU grant. Hopefully our taxes sometimes go for good purposes, this is the reason why I would also like to thank the Ministry of Education for letting me the chance to do this work through the FPU grant. Furthermore, I would like to thank Dr. Sudipta Seal from the University of Central Florida and his entire research group for doing of my short stay in their lab a pleasant, productive and memorable experience. This thesis would not have been the same whether you wouldn't have provided us so kindly with the cerium oxide nanoparticles, I deeply thank you for that. Moreover, I am very grateful to my international reviewers for taking the time to evaluate this thesis in such a short time.

And now, I would like to switch to Spanish to continue these acknowledgements. Estaré eternamente agradecido por haber tenido la posibilidad de realizar esta Tesis doctoral en la Comisión de Fisiología Vegetal. La estructura y eficiencia lograda en el pasado da como fruto que se pueda trabajar perfectamente en estos pasillos. Pero, lo que la hace más grande aún

es la gente que trabaja en ellos. Muchísimas gracias a todos los profesores y becarios que me han acompañado durante este período, desde los que ya estaban cuando llegué hasta los nuevos que están ahora. No sería justo nombrar a unos y no a otros, así que mi agradecimiento infinito va para todos vosotros.

A mi grupo de investigación, liderado por los extraordinarios jefes que he tenido y seguido por los enormes compañeros que me han acompañado. Gracias Paqui, Paco y Roberto por todo vuestro apoyo y dedicación. Gracias por confiar en mí y ofrecerme la libertad en muchos casos de continuar nuestras investigaciones por donde consideraba oportuno. Espero no haber defraudado la confianza que depositasteis en mí. A Isma, que aún lejos, sigue estando presente en nuestro día a día, por ayudarme y, fundamentalmente, guiarme durante mis dos primeros años de Tesis. A Maiki, Keyla, Jara, Idoia, Tamayo y todos los integrantes del binomio UAM-UAH, gracias por tantos momentos de risas y por el buenísimo clima que hemos generado durante todos estos años. Vuestra ayuda ha sido inestimable.

A todos mis amigos: los del Colegio Mayor, los ambientólogos, los del voley y a todos los que me han seguido en la distancia desde Canarias. Esta tesis tiene un pedacito de todos vosotros.

A mi familia, por estar ahí siempre. Por hacer de mí la persona en la que me he convertido, por aportarme todo vuestro amor, cariño y comprensión toda la vida. Por trabajar duro tantos años para que podamos ser y tener todo lo que nos habéis ofrecido. Y a mi hermana, gracias por tu apoyo incondicional, nada sería igual sin ti. Este trabajo está dedicado especialmente a ustedes tres.

APPENDIX I

ABBREVIATIONS

AA	Allen and Arnon medium
AFM	Atomic Force Microscopy
ANN	4-amino-1,8-naphthalimide-N-substituted
ANOVA	Analysis of variance
BSA	Bovine serum albumin
CNM	Carbon based nanomaterial
CNPs	Cerium oxide nanoparticles
CPI	Nanotechnology consumer product inventory
CT	Control
DCM	Dichloromethane
dd	Double distilled
DHR	Dihydrorhodamine
DiBAC	Bis-(1,3-Dibutylbarbituric Acid)Trimethine Oxonol
DLS	Dynamic light scattering
DMSO	Dimethyl sulfoxide
EC	Effective concentration
ED	Effective diamater
EDTA	Ethylenediaminetetraacetic acid
EHS	Environment, health and safety
EIPA	5-(N-ethyl-N-isopropyl)-amiloride
ENM	Engineered nanomaterials
ENP	Engineered nanoparticles
EPS	Extracellular polymeric substances
FCM	Flow cytometric analyses
FDA	Fluorescein Diacetate
FFF	Field-flow fractionation
FS	Forward scatter
FTIR	Fourier Transformed Infrared
H_2DCFDA	Dichlorodihydrofluorescein diacetate
HCS	Boron dipyrromethene-based fluorometric probe
HE	Hydroethidine
HPLC	High-performance liquid chromatography
HRP	Horseradish peroxidase
HRTEM	High resolution Transmission electron microscopy

HSD	Honestly significant difference
MDC	Monodansylcadaverine
MWCNT	Multiwalled carbon nanotubes
NMP	Nanotechnologies, Materials and Production Technologies
NMR	Nuclear Magnetic Resonance
NOEC	No-observed-effect-concentration
NOM	Natural organic matter
NP	Nanoparticles
NTA	Nanoparticle tracking analysis
OECD	Organization for economic cooperation and development
PAGE	Polyacrylamide gel electrophoresis
PC	Protein corona
PDI	Polydispersity index
PET	Photo-induced electron transfer effect
PI	Propidium iodide
PSNP	Polystyrene nanoparticles
PVP	Polyvinylpyrrolidone
QD	Quantum dots
QHTS	Quantitative high-throughput screening
RNS	Reactive nitrogen species
ROS	**Reactive oxygen species**
SAED	Selected area electron diffraction
SEM	Scanning electron microscope
spICP-MS	Single particle inductively coupled plasma mass spectrometry
SS	Side scatter
TCSPC	Time-correlated single photon counting
TEM	Transmission electron microscopy
XEDS	X-Ray Energy Dispersive Spectroscopy
XPS	X-ray Photoelectron Spectroscopy
ZVI	Zero valent iron nanoparticles

APPENDIX II